DISSERTATION

METHODOLOGY AND APPLICATIONS FOR INTEGRATING EARTHQUAKE AFTERSHOCK RISK INTO PERFORMANCE-BASED SEISMIC DESIGN

Submitted by

Negar Nazari Khanmiri

Department of Civil and Environmental Engineering

In partial fulfillment of the requirements

For the Degree of Doctor of Philosophy

Colorado State University

Fort Collins, Colorado

Spring 2015

Doctoral Committee:

Advisor: John van de Lindt

Paul Heyliger
Hussam Mahmoud
Bolivar Senior

ABSTRACT

METHODOLOGY AND APPLICATIONS FOR INTEGRATING EARTHQUAKE AFTERSHOCK RISK INTO PERFORMANCE-BASED SEISMIC DESIGN

Aftershocks have the potential to cause severe damage to buildings and contribute to threaten life safety following a major earthquake. However, their effect on seismic hazard is not explicitly accounted for in modern building design codes, nor in emerging methodologies such as performance-based seismic design. In this dissertation a methodology was developed to systematically integrate aftershock seismic hazard into performance-based earthquake engineering (PBEE). This is achieved through a combination of analytical studies with structural degradation models derived from existing publicly available Network for Earthquake Engineering Simulation (NEES) data as well as numerical models. The design adjustments due to aftershock seismic hazard were calculated for the Direct Displacement Design (DDD) approach for a building portfolio. A comprehensive sensitivity analysis was performed to investigate the effect of different factors such as the location and number of stories of the building and magnitudes of mainshocks and aftershocks on the design adjustments needed. The results of this research will have multiple applications such as allowing code developers to investigate different options for change in structural design to account for aftershock hazard. Aftershock consideration can be an option for stake holders in selection of their design criteria to minimize life-cycle cost. Since aftershock hazard is a major consideration when safety tagging a building following an earthquake, the results of this project will provide insight into quantitatively investigating risk for damaged buildings.

ACKNOWLEDGEMENTS

I would like to express my special appreciation and thanks to my advisor Professor John van de Lindt. I would like to thank you for encouraging my research and for allowing me to grow as a researcher. Your advice on both research as well as on my career have been priceless. I would also like to thank my committee members, Professor Paul Heyliger, Professor Hussam Mahmoud and Professor Bolivar Senior for serving as my committee members. I also want to thank you for your brilliant comments and suggestions. I would also like to thank my husband, Mehdi Hemmati who supported me in writing, and incented me to strive towards my goal.

Funding for this study was provided through National Science Foundation (NSF) grant CMMI-1100423 through a subcontract from Michigan Technological University to Colorado State University. That support is gratefully acknowledged. The opinions contained herein represent the opinions of the authors and not necessarily NSF.

TABLE OF CONTENTS

LIST OF TABLES

LIST OF FIGURES

CHAPTER ONE: INTRODUCTION AND LITERATURE REVIEW

Although aftershocks have the potential to cause severe damage to buildings and threaten life safety, their effect in seismic risk analysis is not explicitly accounted for in modern building design codes, nor in emerging methodologies such as performance-based seismic design. As indicated by the title of this dissertation, the general purpose of this study is to develop procedures and a method to systematically integrate aftershock seismic hazard into Performance-Based Earthquake Engineering (PBEE). This is achieved through a combination of analytical studies with structural degradation models derived from existing publicly available Network for Earthquake Engineering Simulation (NEES) data as well as numerical modeling.

In order to accomplish this objective the following steps must be completed as part of this research: (1) Developing a portfolio of representative structural models (2) Calibration of global-level hysteresis damage models, (3) Fragility generation for different limit states for degraded systems (4) Integration of aftershock seismic hazard with fragility curves, and (5) Illustration and integration into existing PBEE methodologies. Items 4 and 5 represent fundamental contributions to structural seismic earthquake engineering and have not been accomplished previously in earthquake engineering.

1.1. Overview and Problem Statement

Different structures are vulnerable to multiple earthquake ground motions. Multiple earthquakes include foreshocks, mainshock and aftershocks. Aftershock is defined as the smaller

earthquake following large earthquakes significantly increasing the seismic activity near the mainshock rupture. The sequences of fore-, main- and aftershocks are shown in Fig. 1.1.

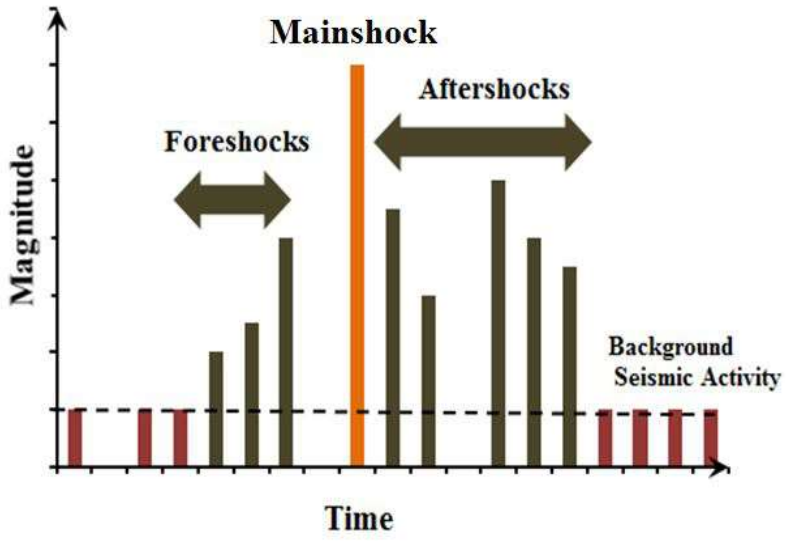

Figure 1.1 Magnitude versus time of foreshocks, mainshock and aftershock

There is a high chance that aftershocks cause severe damage to buildings and threaten life safety even in the case that only minor damage is present from the mainshock. This high damage potential of aftershocks has several reasons. First, the aftershocks cannot be predicted in terms of their location (distance from the site to source), time of occurrence and energy content. Second, the structures are damaged under the previous mainshock which results in lower stiffness and strength capacity.

Fig. 1.2 shows the earthquake hypocenters of earthquakes greater than greater than magnitude M5.0 in the period 1964-2007 including the 11-March-2011 M9.0 Tohoku (Japan) earthquake and its aftershocks. The main earthquake was preceded by a number of large foreshocks hundreds of aftershocks were reported. A M7.0 aftershock succeeded by a M7.4

and a M7.2 were reported following the main earthquake. Over eight hundred aftershocks of magnitude M4.5 or greater have including one on 26-October-2013 of M7.3 occurred since the initial earthquake.

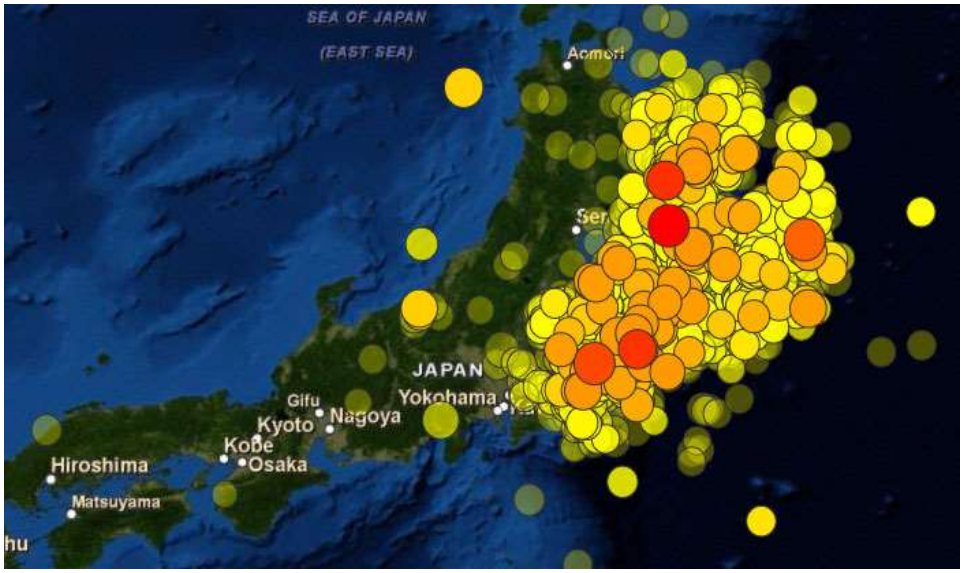

Figure 1.2 Mainshock and aftershocks epicenter locations in 2011 Tokoho earthquake, Japan (USGS, 2014)

In 1960 Chile earthquake, the time gap between the mainshock of M9.5 and an aftershock of M7.2, was 12 days. Landslides were generated by the earthquake and subsequent aftershocks which killed many people. The time gap between the M6.3 aftershock and the M7.1 mainshock was more than four months in the case of the 2010 New Zealand earthquake. There was a widespread damage due to the mainshock but, the aftershock was much more destructive particularly in the city of Christchurch, New Zealand's second largest city because of the proximity of the center of the aftershock to Christchurch. Magnitude and frequency of the 2010 New Zealand earthquake sequence is presented in Fig. 1.3.

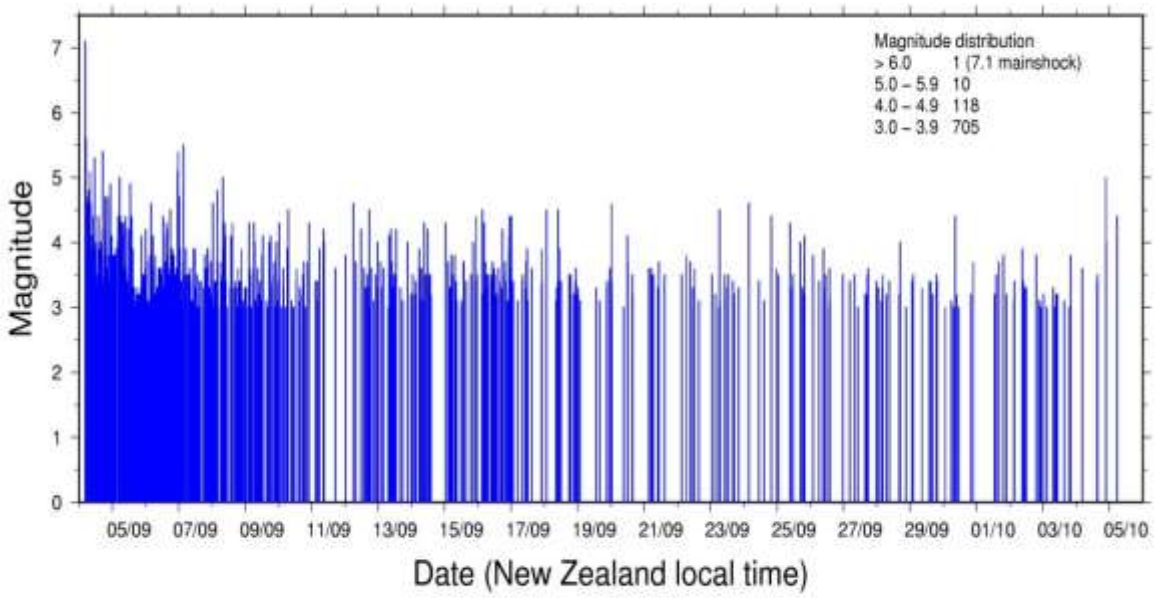

Figure 1.3 Magnitude and frequency of the 2010 New Zealand earthquake sequence; URL: (http://info.geonet.org.nz/display/quake/Aftershock+Detection+and+Modelling)

New Zealand 2011 and 2012, Christchurch earthquake are the example of a vast damage and collapses of the mainshock-damaged buildings and structures due to the occurrence of the aftershocks. New Zeland's second largest city, Christchurch was hit by a M7.1 magnitude earthquake on September 4, 2010. The 29 aftershocks ranging in strength from M3.7 to M5.4 occurred during the 14 hour after the mainshock. Fig. 1.4 shows distribution of the M6.3 Christchurch earthquake and its aftershocks. The largest aftershocks had moment magnitudes of M4.9 and M5.7 that occurred a few minutes after the mainshock. Severe damage and casualties occurred due to the major Christchurch earthquake that was centered south of the city.

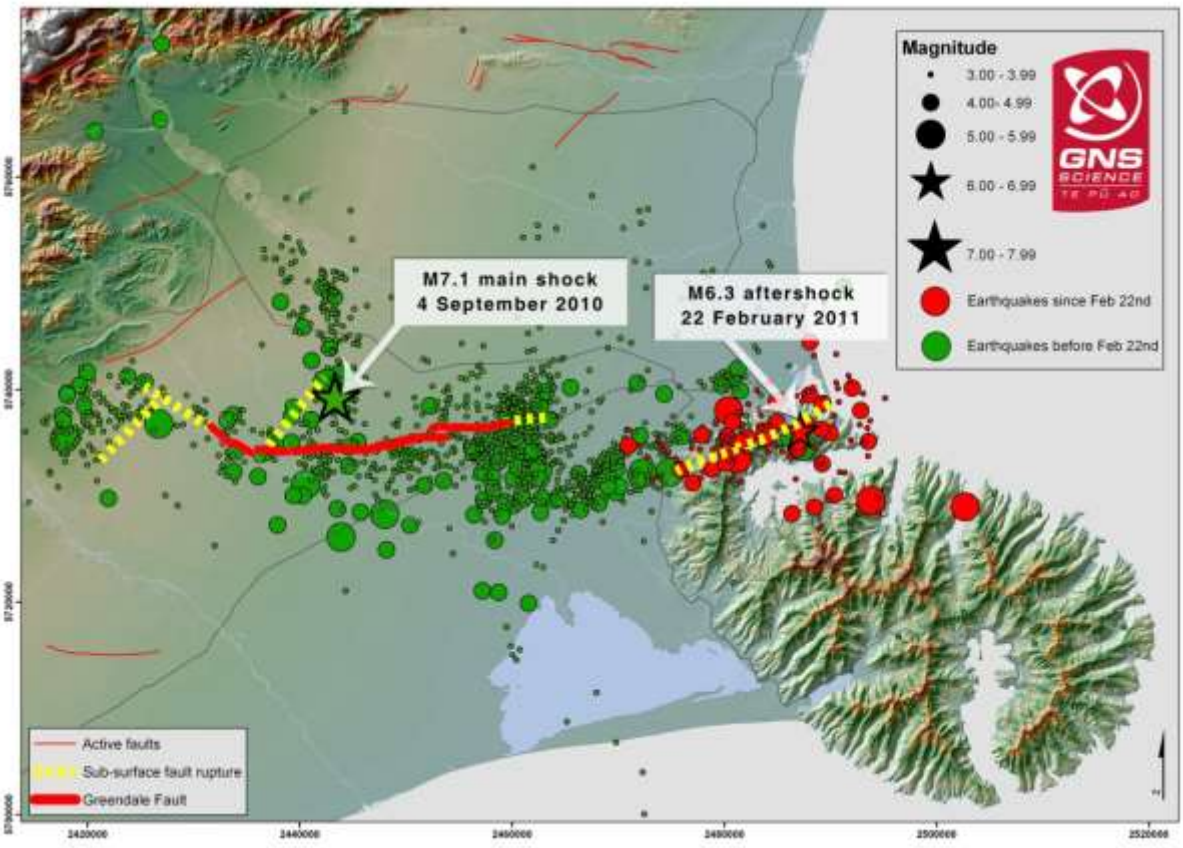

Figure 1.4 Geographical distribution of mainshock and aftershocks in 2011 Christchurch earthquake;
URL: (http://www.rebuildchristchurch.co.nz/blog/2011/2/februarys-6-3-christchurch-earthquake-explained)

Fortunately, the M7.1 Darfield (Canterbury) earthquake on 4 September 2010 was within 10 kilometers of the Christchurch city. The 2010 Darfield earthquake caused destruction, injuries and deaths approximately one year before the February Christchurch earthquake. From the seismologic perspective, the 2010 Christchurch earthquake is classed as an aftershock because of its relationship to the ongoing activity since September last year. And, the occurrence of the aftershock was always statistically possible. However, the occurrence of an aftershock seemed less likely due to the long time interval and slow decrease in general activity. Unfortunately, it has happened after all and in a location that has caused lots of casualties and damage.

Fig. 1.5 shows the damage to the Cathedral Christchurch due to the earthquake.

Figure 1.5 Damaged Christchurch Cathedral after the earthquake; URL: (http://www.odt.co.nz/news/dunedin/209566/city-councillor-explains-significance-peoples-place)

Approximately 90 aftershocks with magnitudes equal or larger than M5.0 were recorded in 24 hours following the Richter M8.8 earthquake in Chile on February 27, 2010. By September 8, 2008, totally 42,719 aftershocks occurred after the M7.9 Wenchuan earthquake that occurred on May 12, 2008. Among these aftershocks, 34 of them were from M5.0 to M5.9, and 8 of them were from M6.0 to M6.5. The collapse of many of the damaged buildings under the mainshock was the result of these strong aftershocks. And, the estimation of economic loss was $150 billion (Wen et al., 2009). Fig. 1.6 shows an example of the vast building devastation in 2008 Wenchuan earthquake.

Figure 1.6 Building devastation from the 2008 Wenchuan earthquake in China; URL: (http://www.iris.edu/gallery3/research/lrsp/SB5b)

There also have been several large earthquakes which seem to be related but they are not necessarily aftershocks. For instance, an extensive damage was a result of the New Madrid Earthquakes of 1811-1812 which consisted of three earthquakes between M8.1-M8.3. It is often assumed that the aftershocks are smaller events compared to mainshocks. However, they normally have somewhat smaller magnitudes and they do not always have a smaller ground motion intensity measure than the mainshocks. For example, there were some cases that Peak Ground Motion (PGA) of aftershock records was as high as the PGA in the mainshock.

The 1983 California Coalinga earthquake is a good example of this case which had an aftershock of moment magnitude 5.9. Two months later, the aftershock resulted in a 0.43g PGA at Pleasant Valley pump plant which exceeded the PGA of 0.31g caused by the moment magnitude 6.5 mainshock at the same site (USGS, 1986). Another example for larger PGA caused by the aftershock is the 2004 Japan Niigata earthquake. In this earthquake the M6.6 mainshock caused a PGA of 0.1g while half an hour later, the M6.3 aftershock resulted in 0.15g PGA (PGA values obtained from the COSMOS Virtual Data Center). Also, the aftershocks may

contain different energy content than the mainshock usually due to a longer duration (Alliard and Leger 2008). Since the building is damaged under the mainshock, the change in energy, i.e. at different frequencies, can be dangerous. The earthquake record consisted of a sequence of mainshock and aftershock results in a very long duration earthquake. Therefore, the structure has to dissipate even more energy.

Due to the potential larger ground motions caused by aftershocks and their different energy content, it is possible that the undamaged buildings after the mainshock sustain more incremental damage after the occurrence of the aftershock. Since, the mainshock-damaged structures have reduced stiffness and strength resulting in reduced structural capacity that is less than the structure's ground motion intensity measure needed to cause more damage after the mainshock. The 1999 Turkey Kocaeli earthquake is an instance of further damage or even collapses due to the aftershocks. Geographical distribution of this earthquake is presented in Fig. 1.7. The epicenter of the earthquake was in Izmit (Kocaeli) and, the most severely affected locations were Izmit, Adapazari (Sakarya) and Gölcük. A severe aftershock on September 13th damaged Yalova and, a new M 7.2 earthquake struck Duzce on November 12th. Two examples of buildings that collapsed during the 1999 Kocaeli earthquake are presented in Fig. 1.8.

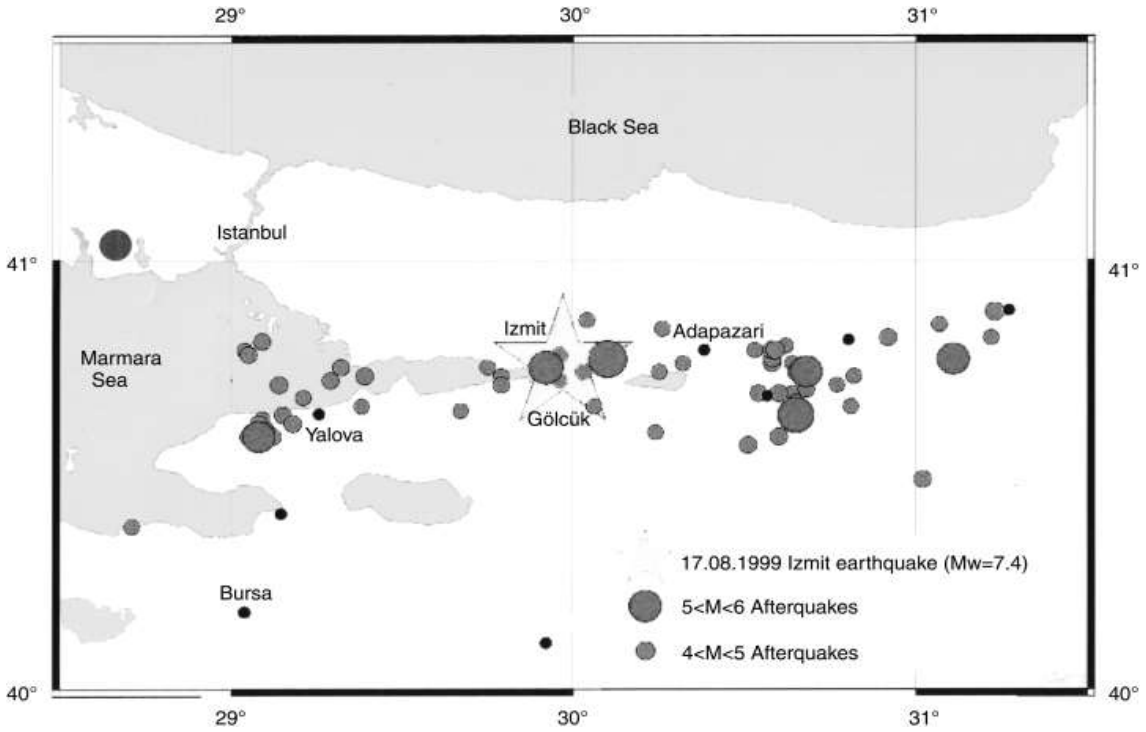

Figure 1.7 Geographical distribution of the 1999 Turkey Kocaeli earthquake (Information was obtained with the help of Dr. Sahin Akkargan, Istanbul University);
URL: (http://www.nature.com/ki/journal/v59/n2/fig_tab/4492083f1.html#figure-title)

(a) **(b)**

Figure 1.8 Building collapses during the Turkey Kocaeli earthquake (a) Collapse of the first story and damage due to pounding between adjacent buildings (b) Total collapse of a building because of inadequate design at the beam-column joints;
URL: (http://whatiscivilengineering.csce.ca/structural_earthquakes2.htm)

The widespread damage is shown in Fig. 1.9 in the Izmit bay in the East-West direction over the 100-150 kilometers length which is concentrated in several areas including Izmit, Golcuk, Avcilar, Yalova, Adapazari, and Karamursel after 1999 Kocaeli earthquake.

Figure 1.9 Location of main damage areas and casualties in 1999 Turkey Kocaeli earthquake; URL: (http://nisee.berkeley.edu/turkey/report.html)

The hazard posed by aftershocks to the buildings is also demonstrated in 1999 Kocaeli earthquake. Fig. 1.10 presents an example of a multistory building severely damaged in the 1999 Kocaeli mainshock which totally collapsed due to an aftershock of M5.9 that occurred one month later. This large aftershock killed seven people and injured about 239 people in the cities near the epicenter.

(a) **(b)**

Figure 1.10 Multistory residential building in Gölcük, Turkey (a) The survived building after the mainshock (b) The same collapsed building in the M5.9 aftershock one month after the mainshock (photos are excerpted from USGS, 2000)

In 1999 Kocaeli earthquake, the different performance of similar buildings that survived or were severely damaged illustrates that using the modern building codes can help prevent or limit disaster. Another example of further damage and collapses due to aftershock is the M5.7 Italy Molise earthquake on October 31 2002 followed by an aftershock of a similar moment magnitude of M5.7 the next day. Also, a mainshock-damaged nine-story building in 1995 Japan Kobe earthquake overturned during an aftershock (Whittaker et al., 1997). Moreover, a gasoline service station which was damaged in the mainshock collapsed due to an aftershock in 1999 Taiwan Chi-Chi earthquake (Lew et al., 2000). A high-rise building collapsed due to the failure of the columns in the first story and, another high-rise building overturned during the Taiwan Chi-Chi earthquake. These building collapses are presented in Fig. 1.11.

(a) **(b)**

Figure 1.11 Building collapse examples during the Taiwan Chi-Chi earthquake
(a) Collapse of a high-rise building due to the failure of the columns at the first story
(b) Overturning collapse of a high-rise building;
URL: (http://whatiscivilengineering.csce.ca/structural_earthquakes2.htm)

The Bakersfield, California in the 1952 Kern County event sequence (Dreger and Savage, 1998) and the Big Bear, California in the 1992 Landers event sequence (Hauksson et al., 1993) are the cases that the aftershock magnitude was significantly smaller than the mainshock however, the aftershock epicenter was much closer to the built-up community and resulted in a progressive softening and collapse of the mainshock-damaged buildings. On January 20, 2010, a strong M6.1 earthquake aftershock hit Haiti 8 days after the occurrence of M7.0 earthquake. The earthquakes with large aftershocks are not limited to the ground motions mentioned in this section.

1.2. Motivation

Based on the evidence and observations discussed previously, it is obvious that the accumulated damage and the collapse of these structures are due to the subsequent earthquakes. Although, the importance of multiple earthquakes in the progressive damage to the structures is observed, current design codes for buildings do not take into account the effect of multiple earthquakes in the assessment and design of structures. Therefore, the multiple earthquakes effect should be included in new design codes.

To date, the probability of aftershocks has not been included in Performance-Based Engineering (PBE). The National Earthquake Hazard Reduction Programs new goal is that new buildings will have only a 1% probability of collapse in 50 years (BSSC 2009) which is reflected in ASCE 7-10. This logic is used for updating the seismic maps used in civil engineering design while the aftershock implications are not still explicitly accounted for in the new maps. However, the evidence by China Wenchuan earthquake collapses and several other major earthquakes with aftershocks that were discussed previously clearly show that considering the aftershocks could have a significant impact on the design of safe structures.

1.3. Current State of Knowledge in Aftershock Research

This section provides a comprehensive literature review in the subjects that will be used throughout this dissertation. These subjects include Performance-Based Engineering (PBE), Performance-Based Seismic Design (PBSD) and Direct Displacement Design (DDD). Fragility curves for mainshock plus aftershock (MS+AS) sequences, collapse criteria for structural systems and damage modeling for different types of structures are included in this section. Other related subjects are ground motion aleatoric and epistemic uncertainties, Next Generation

Attenuation (NGA) relationships, aftershock models and Aftershock Probabilistic Seismic Hazard Analysis (APSHA). The literature review also goes through quantifying the collapse probability of structural systems and convolution of collapse fragility curves with seismic hazard curves.

Codes and standards for structural design have served the profession well since, they are prescriptive, quantitative, and detailed in most instances. These building codes contain prescriptive criteria to ensure the safety of the building in extreme events (Ellingwood, 2004). The Force-Based Design (FBD) procedure which is commonly used for seismic design requires the designer to apply a set of forces to the structure and detail it to have adequate strength. Then, the structure should be checked and its components should have adequate deformation capacity (Deam, 2005). The FBD codes, to an arguable degree, intrinsically account for the effect of multiple earthquakes on constructed facilities since these codes such as the International Building Code (IBC, 2009) are calibrated and adjusted over time based on the observation of structural performance during earthquakes and other loading. However, a number of advances and significant changes have occurred in building design and construction during the past decade. A displacement-Focused, Force-Based structural design procedure was introduced by Deam (2005) which focuses on deformations resulting from ground movement beneath the structure. First, the deformation capacity of the structure and its components are checked. Once the deformations are acceptable, the equivalent-static design forces are applied to the structure and the components are detailed in order to have adequate strength (Deam, 2005).

Recently, a new design paradigm was introduced that focuses on the performance needed to satisfy the increased owner and public expectations. Definition of the Performance-Based

Engineering (PBE) is a seismic engineering approach based on specific performance objectives and safety goals of building occupants, owners and the public (ASCE 41, 2007). PBE is mostly based on probabilistic or deterministic evaluation of seismic hazard. Basically, quantitative evaluation of design alternatives are utilized against the performance objectives in PBE. It should be noted that a specific technical solution should not be prescribed by PBE (Ellingwood, 1998). Performance-based design helps to implement risk analysis tools directly in the structural design of new buildings and evaluation of existing facilities (Ellingwood, 2000). The performance capability of a building is the inherent part of design process which guides the design decisions that must be made. Design criteria selection is the first step of the process. Design criteria are presented in the form of one or more performance objectives.

The acceptable risk of incurring damage of different amounts and the consequential losses that occur as a result of this damage are presented in a statement for each performance objective. Fig. 1.12 presents a flowchart that contains the key steps in the performance-based design process (ATC-58, 2005). After selecting the performance objectives for the project, a preliminary design should be developed by design professionals. Then, analysis of the building response to ground shaking is performed to estimate the probable performance of the building under different design scenarios. The design can then be completed and the project can be constructed if the predicted performance matches or exceeds the performance objectives. Otherwise, the design must be revised in an iterative process until the building's performance capability adequately matches the desired objectives. Although in some cases meeting the stated objectives at a reasonable cost is not possible. In some other cases, the building is inherently capable of a performance which is superior to that required by the performance objectives. The superior performance capability is documented and accepted in such cases. Relaxation of the

design objective is another option for cases with superior performance capability (ATC-58, 2005). In performance-based design, the performance metrics and the design criteria for different occupancy classifications and construction categories must reflect the uncertainties that govern the performance of the structure for example, the inherent uncertainties and modeling uncertainties (Ellingwood, 2000).

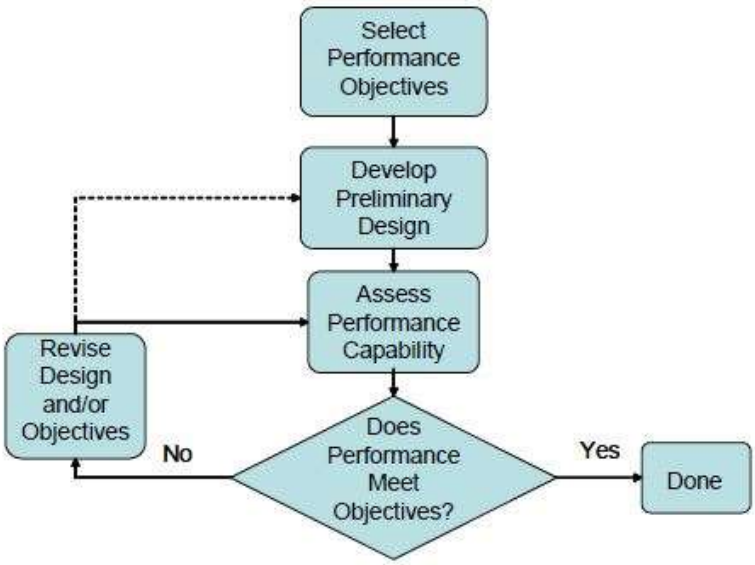

Figure 1.12 Performance-based design Flowchart (Excerpted from ATC-58, 2005)

A theoretical framework for performance-based earthquake engineering was developed by the Pacific Earthquake Engineering Research Center (PEER). The uncertainties and the reliability at each stage of the process are recognized explicitly in the PEER methodology, although it is not the only approach. The following framework Eq. 1.1 (Moehle, 2003 and Deierlein, 2004) tracks the uncertainties in the assessment process based on the total probability theorem (Benjamin, 1970):

$$\lambda(\mathrm{DV}) = \iiint \mathrm{G}\langle \mathrm{DV}|\mathrm{DM}\rangle \mathrm{dG}\langle \mathrm{DM}|\mathrm{EDP}\rangle \mathrm{dG}\langle \mathrm{EDP}|\mathrm{IM}\rangle \mathrm{d}\,\lambda(\mathrm{IM}) \qquad (1.1)$$

where IM is the intensity measure or intensity. EDP is the Engineering Demand Parameter or demand. DM is the Damage Measure or damage state. DV is the Decision Variable or projected loss. The term $\lambda(\mathrm{IM})$ is the probability of experiencing ground shaking of a given intensity, obtained from the site-specific seismic hazard curve. The term $\langle \mathrm{EDP}|\mathrm{IM} \rangle$ states the relationship between the intensity and the demand, the term $\langle \mathrm{DM}|\mathrm{EDP} \rangle$ presents the conversion of demand to damage and, the term $\langle \mathrm{DV}|\mathrm{DM} \rangle$ generates loss from damage.

In the past decade, the understanding of, the ability to predict, the seismic behavior of woodframe structures has improved significantly. There were several notable projects focusing on woodframe structures such as the Consortium of Universities for Research in Earthquake Engineering (CUREE) - California Institute of Technology (Caltech) CUREE-Caltech Woodframe Project and the Network for Earthquake Engineering Simulation (NEES) NEESWood Project. Specifically, the NEESWood project resulted in the development of PBSD procedures for mid-rise woodframe buildings (Pang et al., 2010). The foundation for the development of Performance-Based Seismic Design (PBSD) of woodframe buildings was provided by several key papers. Allowable mass charts based on the desired peak inter-story drift were developed by Rosowsky (2002). These charts were developed using a numerical model provided within the CUREE-Caltech Woodframe Project entitled Seismic Analysis of Woodframe Structures (SAWS) (Folz and Filiatrault, 2004).

One of the PBSD methods is Direct Displacement-Based Design (DDD) which falls into the broad family of displacement-based methods. The performance level of a structure is defined in terms of inter-story drift which is the key parameter in most displacement-based design approaches. Although displacement is not explicitly performance, it is considered as an

engineering demand parameter that correlates well with both structural and non-structural damage. Damage or lack of damage is, of course, a measure of performance. Priestley and Kowalsky (1998) proposed direct displacement design (DDD) as an alternative to full nonlinear time-history analysis (NLTHA) for concrete structures. Since most woodframe structures are developed to meet the strength requirements, the implementation of PBSD philosophy will require more advanced analysis of complete structures (Pang et al., 2010). Pang et al. (2010) presented a DDD procedure that can be used for PBSD of multi-story woodframe structures. In that method, the NLTHA of the complete structure is not required for their DDD procedure and obtaining a resulting design. Filiatrault and Folz (2002) adapted the DDD approach and presented a possible displacement-based design procedure for light-frame wood structures which addresses many of the deficiencies of the force-based procedure. Their proposed DDD procedure is tailored specifically for multi-story woodframe structures with the purpose of addressing the drawbacks of current force-based procedures. A simplified DDD procedure was then developed by Pang et al. (2010). The simplified DDD procedure was used to design the shear walls for a six-story woodframe structure. As an example application, of which there have been many, and the method validated at full-scale in Japan (van de Lindt et al., 2010). Malekpour and Dashti (2013) the DDD approach for different types of reinforced concrete structural systems including single moment-resisting, dual wall-frame and dual steel-braced systems.

Comparison of the analysis results with NLTHA results show that the DDD approach is sufficient for different reinforced concrete structural systems. There were also a series of fragility-based analysis and design methods which considered drift as the performance indicator for woodframe buildings (e.g. Ellingwood et al., 2004; Rosowsky and Ellingwood, 2002; van de Lindt and Walz, 2003). Van de Lindt (2005) introduced a damage-based concept for wood shear

walls. This concept was applied at the wall level (van de Lindt and Gupta, 2006) and system level (Liang et al., 2011). In the NEESWood Project, the performance expectations are a combination of inter-story drift limits and prescribed seismic hazard levels associated with predefined non-exceedance probabilities (Pang et al., 2010).

The NEESWood Project's (van de Lindt, et al., 2006) objective was to develop a PBSD philosophy for mid-rise woodframe buildings. To achieve this, extensive numerical simulations and full-scale system-level experiments were performed (Filiatrault et al., 2010; van de Lindt et al., 2010) as well as numerical modeling (Chrisovasilis at al., 2007; Pei and van de Lindt, 2009). The DDD concept introduced by Folz and Filiatrault (2004) was extended as part of the NEESWood Project to become a viable PBSD procedure. This procedure was applied to shear wall section (Pang et al., 2010) of a full-scale six-story woodframe building tested in Miki City, Japan (van de Lindt et al., 2010). Additionally, other less direct procedures such as the use of NLTHA to develop design charts for low-rise woodframe buildings have been investigated (e.g. Liu and van de Lindt, 2011). Van de Lindt, et al. (2010) provided a technical documentation on the comprehensive procedure used to perform a PBSD of a mid-rise woodframe building located in a high seismic zone. All of these DDD procedures are incapable of handling irregular structures such as buildings with significant torsion. Bahmani et al. (2013) developed a displacement-based method that accounted for both torsional and rotational displacements in the design process.

As mentioned previously, aftershocks have not been considered in determination of seismic hazard. There was some preliminary effort to include the aftershock effect and integrate aftershocks into PBE. For instance, a conceptual analytical framework in order to incorporate the

aftershock effect in PBEE was proposed by Yeo and Cornell (2005). However, they mentioned that "the investigation of aftershocks on performance-based earthquake engineering is still in its infancy at every stage". Little progress was made between 2006 and 2012. Earthquakes cluster in space and time. Aftershock models need to be able to include aftershocks in seismic hazard. Aftershocks triggered by the mainshock can be very far away from the center of the mainshock (Alliard and Leger, 2008; Yeo and Cornell, 2009). The time between the occurrence of the mainshock and the largest aftershock is difficult to predict and can range between several minutes to months. Nevertheless, the magnitude of the aftershocks is relatively easy to predict (Scholtz, 2002). Generally, the aftershocks have an occurrence rate which decreases with the elapsed time from the mainshock. Also, magnitude of the aftershock is usually less than the mainshock based on Bath's law (Bath, 1965). Eq. 1.2 presents of the empirical laws that has been used to successfully model the short term clustering of earthquakes is Omori's law which describes the decay of earthquake activity with time as:

$$\frac{dN}{dt} = \frac{K}{(t + t_c)^p} \qquad (1.2)$$

where dN is the number of earthquakes in the time interval dt; K is the a parameter that is proportional to the aftershock productivity; p describes the decay and takes values around 1; and c stands for a small time interval just after the mainshock (see e.g. Utsu et al., 1995). Kagan and Houston (2004) investigated the relation between mainshock rupture process and Omori's law for aftershock moment release rate. Omori's law is one of the few time-predictable patterns which are evident in the global occurrence of earthquakes (Parsons, 2002). Parsons (2002) also states that if large triggered earthquakes habitually obey Omori's law, then, their hazard can be more readily assessed. Eq. 1.3 presents the Gutenberg-Richter relation which describes the magnitude-frequency distribution as:

$$\log_{10} N(M) = a - b\,M \qquad (1.3)$$

where N(M) is the number of earthquakes of magnitude M, a and b are parameters (see e.g. Gutenberg and Richter, 1949). The occurrence rate of the aftershock hazards in California was described by Reasenberg and Jones (1989, 1994). However, they did not explicitly consider the aftershock intensity. Also, aftershock ground motion at a site is dependent on the location and magnitude of the mainshock. Reasenberg and Jones combined equations 1.2 and 1.3 to determine the rate of aftershocks of magnitude m and above, at time t following the mainshock of magnitude m_m as presented in Eq. 1.4:

$$R(t, m_m) = \frac{10^{a+b(m_m-m)}}{(t+c)^p} \qquad (1.4)$$

Reasenberg and Jones analyzed 62 California earthquake sequences and derived the parameters a = -1.67, p = 1.08, b = 0.91 and c = 0.05. These parameters have become known as the generic Californian aftershock model parameters (see e.g. Gerstenberger et al., 2007). The rate of aftershocks with moment magnitude m or larger at time t following the mainshock of moment magnitude m_m can be calculated using Eq. 1.4. Fig. 1.13 was developed by assuming t=30 days and using the parameters of a, b, c and p derived by Reasenberg and Jones (1994). It is observed in Fig. 1.13 that the number of aftershocks shows a decreasing trend with increasing the aftershock magnitude. For example, assuming a M7 mainshock the number of aftershocks decreases with increasing the magnitude of the aftershock. This means that, for a specific mainshock magnitude, the number of expected aftershocks with smaller magnitudes is more than the number of aftershocks with larger magnitudes.

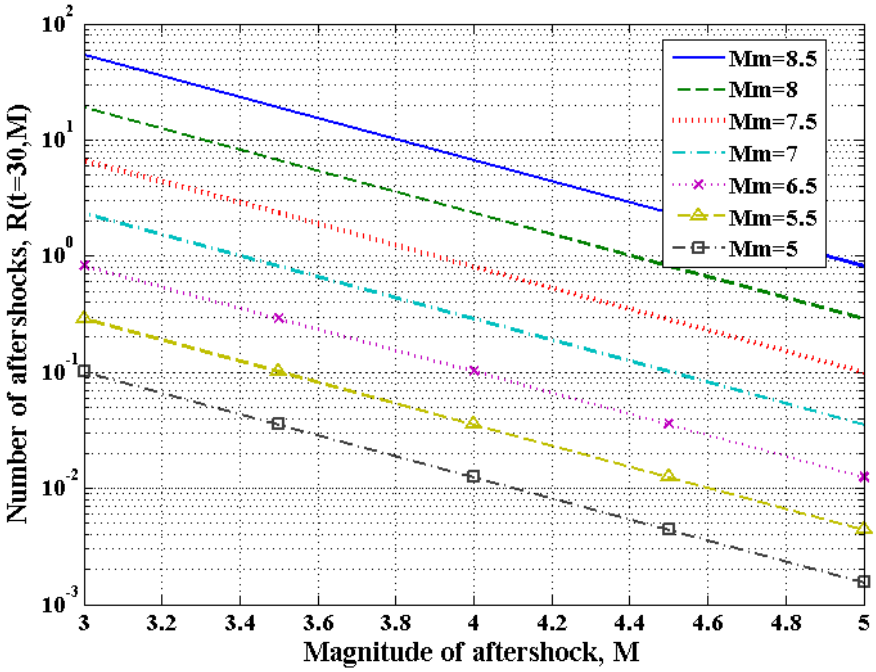

Figure 1.13 Relationship between number of aftershocks and magnitude as a function of mainshock magnitude

The rate computed in Eq. 1.4 can be used to calculate the probability of occurrence of at least one earthquake of magnitude M or above in the time interval $[t_1, t_2]$ (see Eq. 1.5. by Yamanaka 1990).

$$P = 1 - \exp \int R(t, m_m)dt \qquad (1.5)$$

Utsu (1969) defined the rate of aftershock occurrence to be:

$$R(t, M_m) = \frac{10^{a+b(M_m - M_0)-a}}{(t+c)^p} \qquad (1.6)$$

Smith and Christophersen (2005) developed a new type of model for the recurrence time between earthquakes greater than some (large) reference magnitude. The sensitivity of a number of large aftershocks to changes in model parameters was investigated for three aftershock models

of Short-Term Earthquake Probability (STEP) and two implementations of Epidemic Type Aftershock (ETAS) models (Christophersen and Rhoades, 2013).

Between 1940 and 1992, the 1519 earthquakes with magnitude M3 or greater that occurred near Eureka, CA were analyzed by Sunasaka and Kiremidjian (1993). The time-variant aftershock collapse frequency was represented by equivalent constant rates (Yeo and Cornell, 2009b). Markov and semi-Markov loss models were used in order to include both homogeneous and non-homogeneous models (Yeo and Cornell, 2009a). A Markov process was used by Al-Hajjar et al. (1997) for modeling the aftershock earthquakes. Also, a probabilistic framework was introduced for quantifying aftershock hazard in California (Yeo and Cornell, 2009c). Allameh Zadeh (2004) predicted the aftershock pattern distribution using self-organizing feature maps.

Aftershock Probabilistic Seismic Hazard Analysis (APSHA) and the transformation of time-varying aftershock hazard into an equivalent constant rate were achieved by Yeo and Cornell, (2005). The conventional Probabilistic Seismic Hazard Analysis (PSHA) was illustrated by Kramer (1996). In PSHA, it is assumed that the mainshock occurrence is homogeneous and therefore, it can be modeled by a Poisson process. One of the applications of ASPSHA is post-earthquake safety evaluations where quantifying the occurrence rates of ground motions caused by aftershocks is required (Yeo and Cornell et al., 2005). In PSHA, the annual exceedance probability of a given ground motion intensity measure such as PGA or the first mode spectral acceleration (S_a) is computed for a given structural period and damping ratio. A homogeneous Poisson earthquake occurrence model is used for mainshock occurrence rates since they are time-invariant constant values. Conventional PSHA uses a truncated exponential magnitude model or a characteristic magnitude model or both. PSHA is well explained in a relatively recent

literature review (see e.g. Kramer, 1996). First, the geometry of the neighboring faults with respect to the site of concern is considered in the mainshock PSHA process. Then, the annual earthquake rate on these faults is determined. In order to address the randomness in occurrence time, earthquake magnitudes and site-to-source distances, development of an earthquake model is required for basic formulation of PSHA. However, in the aftershock environment, the occurrence rates are time-variant. Therefore, the aftershock occurrence is non-homogeneous and it is at its maximum rate immediately following the mainshock and decreases as time passes. Additionally, the aftershock ground motion hazard at a site is dependent on the magnitude and location of the mainshock. The aftershock locations are limited to the aftershock zone which also depends on the magnitude and location of the initial mainshock. The method proposed by Yeo and Cornell (2005) enables estimation of the aftershock likelihood at a site by treating the uncertainty in the magnitude, site-to-source distance and ground motion intensity in a similar way to the conventional PSHA. The interested reader is referred to Yeo and Cornell (2005) for additional details.

Fig. 1.14 is excerpted from Yeo and Cornell (2005) and, it presents the two cases for ASPSHA versus the mainshock hazard curve. In case one, the aftershock analysis is based on the assumption that the aftershock events are equally likely and they have equal probability of occurrence. However, the second case assumes that the aftershock events concentrated at the end of fault rupture zones are more probable. Using the ASPSHA approach, the aftershock hazard curves are computed for both cases. As it is shown in Fig. 1.14, the aftershock hazard curve is more for case one where the aftershock events are assumed to be equally likely. The hazard curves are presented in terms of annual rates of exceeding site PGA versus the intensity measure of PGA in Fig. 1.14.

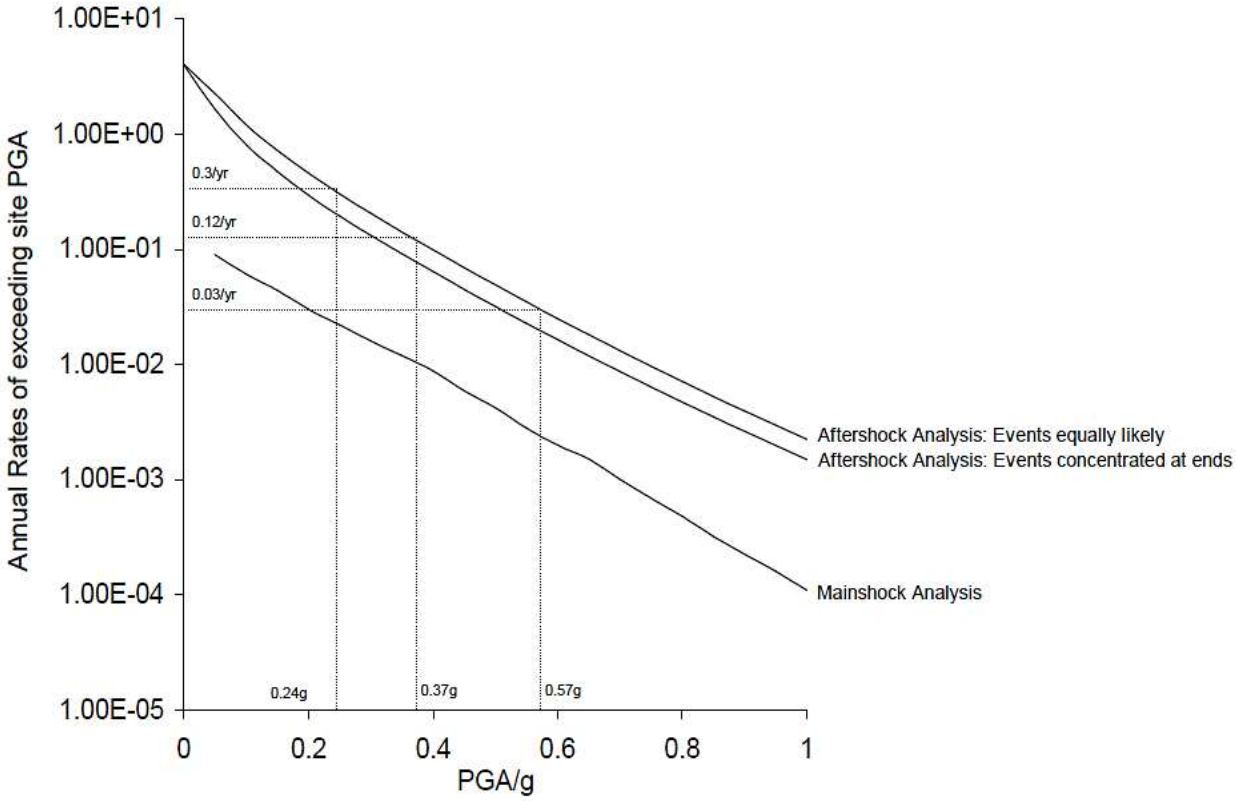

Figure 1.14 Comparison of mainshock and aftershock site hazard curves
(Note: The aftershock hazard curves were calculated at t = 7 days after the mainshock with duration of interest of T = 365 days. Also, the mainshock magnitude is assumed to be M7)
(Excerpted from Yeo and Cornell, 2005)

From Fig.1.14 it is observed that the base case aftershock ground motion hazard (i.e. case one) is approximately a scalar multiple of the mainshock hazard for all of the PGA levels. Yeo and Cornell (2005) proposed that an estimate of the aftershock hazard curve can be obtained by multiplying the mainshock hazard curve at the site for all PGA's by a constant value of mean number of aftershocks with magnitudes between m_l and m_m in the time interval [t, t+T], (denoted as $\mu^*(t, T, m_m)$). This value is defined by Eq. 1.7 as:

$$\mu^*(t, T; m_m) = \int_t^{t+T} \mu(\tau; m_m) d\tau = \frac{10^{a+b(m_m - m_l)} - 10^a}{p-1} [(t+c)^{t-p} - (t+T+c)^{1-p}] \qquad (1.7)$$

where a, b, c and p are parameters of the generic California model that was mentioned earlier in Eq. 1.4. Time t is the elapsed time following the mainshock of magnitude $m_{m,}$ and T is the duration being considered after time t following the original rupture. The terms m_l and m_m are the minimum and maximum aftershock magnitude of engineering interest, respectively; m_l is typically assumed to be 5.0 and m_m is usually set equal to the magnitude of the mainshock.

Definition of the aftershock zone is complicated and, it has been observed that the aftershock occurrence is more frequent in the ends of the rupture zones of the initial mainshock (Hough and Dreger, 1995). However, the ASPSHA can consider such complexity in the aftershock zone definition. Christophersen et al. (2011) applied different declustering methods to the New Zealand earthquake catalogue to prepare a range of seismicity data for Probabilistic Seismic Hazard modelling. Gerstenberger et al. (2007) investigated short-term post-mainshock earthquake probability.

Probabilistic aftershock hazard mapping was introduced by Weimer (2000) and it is being developed by USGS and others. A 2% exceedance probability spectral acceleration (S_a) in 50 years is currently used in seismic design maps. The design spectral acceleration is assumed to be 2/3 of the stipulated intensity (ASCE 7-05, 2006). There was a shift in ground motion maps of ASCE 7-10 (2010) from uniform-hazard philosophy to one of uniform risk with risk-targeted Maximum Considered Earthquake (MCE) ground motions where the probability of collapse in 50 years is 1% instead of 2%. Also, time dependent maps (USGS-STEP) were developed at USGS which are under continuing development in collaboration with scientists in New Zealand.

For the purpose of simulation of mainshock plus aftershock (MS+AS) scenarios an attenuation relationship is needed in order to scale the mainshock and aftershock earthquake

records. Abrahamson and Silva (2008) derived an empirical ground motion model for the rotation-independent average horizontal component from shallow crustal earthquakes using the PEER Next Generation Attenuation (NGA) database. This model is applicable to magnitudes of M5-M8.5, distances of 0-200 kilometers, and spectral periods of 0-10 seconds. The site is parametrized by average shear-wave velocity in the top 30 meters (V_{s30}) and the depth to engineering rock (depth to $V_s = 1000\ \mathrm{m/s}$). The source term is dependent on the depth-to-top-of-rupture in addition to magnitude and style-of-faulting. The effect of a hanging wall is included with an improved model which varies smoothly as a function of the source properties and the site location. The range of applicability of previous empirical ground motion models was based on the range covered by the available empirical data set; however, the ground motion must be computed for all relevant earthquakes. Therefore, the limit on the range of applicability was often neglected. The NGA project addressed this issue. The developers of the models extrapolated their models such that they are applicable to all crustal earthquakes relevant for seismic hazard analysis in California: M5-M8.5 for strike-slip, M5-M8.0 for dip-slip, distance 0-200 kilometers, and spectral periods up to 10 seconds.

The next generation of PBE relies completely on the fragility concept. This generation of PBE uses fragilities where the drift is a function of seismic intensity. The PBE approach de-conditions the drift and seismic intensity to damage and eventually represents them in terms of loss (ATC, 2008). In a fragility curve, the probability of exceeding one or more engineering demand parameter (EDP) is presented as a function of hazard intensity. Back-to-back dynamic structural analysis simulations were performed by Luco et al. (2004) and the fragilities of damaged buildings were developed. Van de Lindt (2008) demonstrated that damage from a mainshock results in the softening and near-collapse of a wood shear wall in an aftershock. It

was also demonstrated experimentally by van de Lindt et al. (2012) that the effect of previous intense earthquakes on the performance or integrity of a woodframe garage wall is also quite significant. The seismic loss of woodframe buildings subjected to sequences of mainshocks and aftershocks was estimated by Yin and Li (2011). The result was that the mainshock-damaged buildings had a significantly higher seismic loss. The seismic collapse risk of woodframe construction was investigated by Yin and Li (2010) over a period of time. They also considered both aleotoric and epistemic uncertainties. Bernal (1992) investigated instability of buildings subjected to earthquakes. He presented a method to check the safety against dynamic instability of two-dimensional buildings by reduction of the multi-story structure to an equivalent Single Degree of Freedom (SDOF) system. It was concluded that the minimum strength (base shear capacity) needed to withstand a given ground motion without collapse is strongly dependent on the shape of the controlling mechanism but it is insensitive to the initial elastic stiffness. Ibarra (2003) investigated global collapse of frame structures under seismic excitations.

Ryu et al. (2011) presented a methodology for developing fragilities for mainshock-damaged structures. Li et al. (2010) determined the seismic capacities of woodframe residential construction using incremental dynamic analyses (IDA) for typical lateral force resisting systems and the collapse fragilities determined were based on story drifts. Other types of buildings have also been studied. Abdelnaby et al. (2012) investigated the behavior of reinforced concrete frame systems under multiple successive earthquakes. The damage features were modeled at the material level by using a plastic energy-based degrading concrete model and a steel model that considered the reinforcing bars deterioration under large cyclic amplitude plastic excursions. The potential for aftershocks to cause additional damage to steel moment frame buildings was investigated by Li and Ellingwood, (2007a). Their study also provides a probabilistic description

of structural damage states prior to and following the aftershocks. Liel et al. (2011) investigated the seismic collapse safety of reinforced concrete frame buildings and non-ductile moment frames that are representative of those built before the mid-1970s in California. In their study, the probabilistic assessment relies on nonlinear dynamic simulation of structural response to calculate the collapse risk, accounting for uncertainties in ground motion characteristics and structural modeling. Luco et al. (2004) investigated the residual capacity against collapse for MS-damaged buildings and recommended a new approach to determine the residual capacity, which could enable the development of fragility curves for mainshock-damaged buildings. Steel frame buildings were investigated under the mainshock plus aftershock earthquake sequences and it was found that the damage level from the mainshock, the amplitude and the frequency of the aftershock significantly affects the damage pattern due to the aftershocks (Li and Ellingwood, 2007a). Luco et al. (2004) linked the post-mainshock capacity to residual drift after the mainshock. Alliard and Leger (2008) developed a methodology to perform seismic response analysis of concrete gravity dams considering aftershocks. Methods of bridge fragility curve development was presented by Shinozuka et al. (2000) based on statistical analysis in which the emprirical fragility curves were developed by using bridge damage data obtained from past earthquakes. Li et al. (2014) presented approaches for assessment of wood and steel structures subjected to earthquake mainshock+aftershock.

The parameter that has been used mostly as a metric for earthquake damage due to mainshock or aftershock is the inter-story drift. A damage-based index has been proposed to be considered in order to improve design for the new and existing structures (Cosenza and Manfredi, 1997). An energy-based linear damage model was used for high intensity seismic loading (Chai et al., 1995). Cumulative damage in steel structures subjected to earthquake

ground motions was investigated by Krawinkler and Zhorei (1983). A damage index based on ductility and stiffness degradation was introduced (Khashaee, 2005). The proposed index is strongly linked to the dissipated energy by inelastic action. A damage model for woodframe shearwalls was proposed by van de Lindt (2005). The introduced model was later used by van de Lindt and Gupta (2006) and Park and van de Lindt (2009).

Ibarra and Krawinkler (2005) presents the description, calibration and application of relatively simple hysteretic models that include strength and stiffness deterioration properties. The hysteretic energy capacity and the related exhaustion of the energy capacity to system collapse were investigated by Ibarra and Krawnkler (2005). A model was proposed by Benavent-Climent (2007) in order to quantify the damage in structural steel components caused by earthquakes. This model was validated using shake table tests. The ultimate energy dissipation capacity of the steel component which is path-dependent was included in their model. Similarly, the hysteretic energy dissipation capacity was investigated for concrete columns (Poljansek et al., 2009). It was observed that both maximum displacements and the number of large-amplitude displacement response cycles are dependent on the energy dissipation capacity in a way that it significantly increases when the energy dissipation capacity decreases resulting in more damage.

Sucuoglu and Erberik (2004) presented an energy-based hysteresis and damage models for deteriorating systems. The hysteresis model performs strength reduction at a current displacement cycle by evaluating the loss in the energy dissipation capacity along the completed displacement path. Therefore, it is completely memory dependent. Pinching is also accounted for implicitly by a reduced energy dissipation capacity in a displacement cycle (Sucuoglu and Erberik, 2004). Park and Ang (1985) presented a mechanistic seismic damage model for

evaluating structural damage in reinforced concrete structures under earthquake ground motions. They expressed damage as a linear function of the maximum deformation and the effect of repeated cycling loading. Seismic reliability of damaged concrete beams was investigated by Shinozuka and Tan (1983). Whitman et al. (1975) proposed an interesting characterization of the probabilistic nature of the state of structural damage in terms of the damage probability matrix for dealing with building structures. These matrices describe the general correlation between building damage and earthquake intensity.

Luco et al. (2007) calculated the collapse probability of the structure in Y years assuming there was no uncertainty in the collapse capacity. The collapse probability in Y years would be equal to the probability of the ground motion spectral acceleration (S_a) or demand at the structure's location exceeding the capacity value in Y years. This probability of exceeding a certain spectral acceleration value also can be obtained from hazard curves. The hazard curves could be produced using the application provided in USGS website or computed via site specific probabilistic seismic hazard analysis (PSHA; Cornell, 1968; McGuire, 2005). Therefore, the collapse probability can be easily read from a corresponding (i.e. for the same number of years and spectral acceleration vibration period) hazard curve (Luco et al., 2007). In Luco et al. (2007), the PDF form of the fragility curve was developed and with the seismic hazard curve known, the fragility can be convolved with the site-specific seismic hazard curve to determine the probability of collapse when the structure is subjected to a mainshock. The annual probability of collapse provides a metric for evaluation of risk, and it includes the site specific seismic hazard. The fragility curve shows the probability of exceedance ($P[S_a>c]$) versus collapse capacity (c) parameter which was selected as spectral acceleration ($S_a[g]$). This risk integral can be expressed

generally by using the total probability theorem. By taking into account the uncertainty in the collapse capacity of a given model, the collapse probability can be calculated as:

$$\mathrm{P[Collapse]} = \int_0^{\infty} \mathrm{P[SA > c]} \,.\, \mathrm{f_{Capacity}(c)dc} \qquad (1.8)$$

(See Luco et al., 2007).

Eq. 1.8 couples the probability distribution for the collapse capacity with a corresponding ground motion hazard curve. This collapse probability is equal to the probability that the ground motion demand exceeds the particular capacity value, multiplied by the probability of the capacity value. Eq. 1.9 is then used to obtain the uniform collapse probability in Y years or a uniform annual probability and vice versa (Luco et al., 2007).

$$\mathrm{P[Collapse\ in\ Y\ years]} = 1 - (1 - \mathrm{P[Collapse]})^{\mathrm{Y}} \qquad (1.9)$$

Zareian and Krawinkler (2007) illustrated a probabilistic-based methodology for quantifying the collapse potential of structural systems. The assessment of collapse probability results in more accurate estimates of losses induced by earthquakes. The collapse potential is represented by the probability of collapse at discrete hazard levels and annualized basis. In their methodology a 'collapse fragility curve' which expresses the probability of collapse as a function of the selected ground motion intensity level plays an important role. In the proposed methodology and the design processes, the effect of aleatoric and epistemic uncertainties is incorporated. It has been shown that the effect of aleatoric and epistemic uncertainties is significant on the conceptual design for collapse safety. A Monte Carlo simulation is required to convolve the uncertainties in hazard estimation with uncertainties in collapse fragility (Zareian and Krawinkler, 2007).

Shi et al. (2012) presented a fundamental concept of uniform-risk-targeted seismic design for collapse safety of building structures and its relevant assessment process. Shi et al. (2012) mentions that seismic design should evaluate and control the risk of earthquake-induced collapse that a building structure may experience during its design service life. Therefore, both of the collapse resistant capacity and the earthquake ground motion demand of the building structure should be taken into account.

Alessandri et al. (2013) stated that using a pure analytical tool to assess the aftershock risk of a structure can be contrasted with the limited time available to make a decision about the usability of the structure after the mainshock. Therefore, they presented a method for evaluating post-earthquake bridge practicality which is based on a combination of the information from the numerical analysis and the in situ inspections. Specifically, they proposed an effective tool to speed up the decision-making process which contains evaluation of the seismic risk of mainshock-damaged bridges in aftershock context. The aftershock hazard provided by using the Omori's law is combined with fragility curves of the structure (Alessandri et al., 2013).

The majority of uncertainty in performance-based seismic engineering and seismic reliability is due to the uncertainty that rests in ground motion. Considering the probability of aftershocks seems necessary in order to achieve a more accurate seismic hazard at a site. This is likely more critical for structures which are not able to dissipate energy as well as the modern engineered structures i.e. older non-ductile buildings.

1.4. Objectives and Scope of Research

The objective of this dissertation is to integrate aftershock seismic hazard into PBE in a systematic manner. This will be reached through a combination of analytical studies with

structural degradation models. Initially a portfolio of representative structural building models will be developed from the existing plan views for the two-story and six-story model for engineered light-frame wood buildings. A numerical model of a four-story building which was developed in software SAPWood is also used in the building portfolio. Each building is designed based on the direct displacement design (DDD) approach. These woodframe building models with a degrading model fitted to each story of the building will be used to develop Multi Degree of Freedom (MDOF) phenomenological degrading global level models known as Degraded System Hysteresis (DSH) models. In order to provide the system level behavior, the detailed nonlinear models will be calibrated to the DSH models. Providing a mechanism to calibrate detailed nonlinear mechanistic models is particularly important since, system-level measurements are not often available. Fragilities for the collapse limit state will be provided using the detailed nonlinear models for structures under degradation. Finally, the undamaged fragilities and the conditional (damaged) fragilities can be combined with the developed aftershock hazard curves in order to quantify the effect of aftershock seismic hazard in PBE. In order to integrate aftershock seismic hazard into PBE a methodology is developed to quantify the change that would be needed in design drift limit of a building to account for aftershock hazard in simplified DDD. In other words, what change to the design drift limit would be needed such that the building has the same collapse probability for the combined mainshock plus aftershock hazard as the collapse probability for the original building subjected to the mainshock-only? A transformative change in design might be achieved due to the effect that aftershock seismic hazard has on PBE resulting in less damage-susceptible and safer buildings.

Specifically, the proposed dissertation has the following main objective: Quantify how a performance-based evaluation and structural design would need to be altered if the aftershock

hazard taken into account. It is envisioned that the results of this research will have widespread applications including (but not necessarily limited to the following:

Application 1: Allow code developers to investigate different options for change in structural design such as modifying the nail patterns, use of base isolation, dampers or shape memory alloys, to account for aftershock hazard.

Application 2: Aftershock consideration can be an option for stake holders in selection of their design criteria to minimize life-cycle cost.

Application 3: Aftershocks are a major consideration when safety tagging a building following an earthquake. However, existing aftershock consideration is purely qualitative. The results of this project will provide insight into quantitatively investigating risk for damaged buildings.

1.5. Challenges in Mainshock + Aftershock Analysis

There are several conceptual challenges about aftershock environment that are different from mainshock environment. For example, the aftershock ground motion hazard is non-homogeneous in time which means they are at their maximum right after occurrence of the mainshock and decreases gradually after that. Moreover, the magnitude of the aftershock is not dependent on the elapsed time after the mainshock which results in the potential large magnitudes of aftershocks a long time after the mainshock. Meanwhile, the distribution of aftershocks and the mean occurrence rate is strongly correlated with mainshock magnitude (Reasenberg and Jones, 1989, 1994; Yeo and Cornell, 2005). Also, the probability distribution of aftershock locations is dependent on the geometry of mainshock rupture zone. The increased mean rate of the aftershocks, the uncertainty and variability in ground motions and the damaged structure results in a possible larger ground motion intensity measure than the mainshock. It is found that the parameter of epsilon (ε) which is associated with an earthquake ground motion is

able to predict the seismic responses (Baker and Cornell, 2005). This is significantly important since the fundamental period of a system changes due to the degradation of the structure. Additionally, Luco and Bazzarro (2007) found that scaling the amplitude of ground motion records might cause a biased nonlinear structural drift response. Some of the other challenges for inclusion of aftershocks in PBE are the variability in non-homogeneous aftershock ground motions and uncertainty in capacity of the building after the mainshock.

1.6. Organization of Dissertation

This dissertation is organized into six chapters. Chapter One is an introduction illustrating the overview and statement of the problem, motivation, objectives of the research and the challenges in the post-earthquake aftershock environment. This chapter is also about the background and literature review in the scope of performance-based engineering (PBE), aftershock probabilistic seismic hazard analysis (APSHA), mainshock plus aftershock fragilities, mainshock-damaged models. Chapter Two is the methodology for integrating earthquake aftershock risk into seismic design. Chapter Three illustrates the methodology for quantifying the design changes needed due to integrating the aftershock hazard. The first section of Chapter Three investigates the needed changes in the hysteretic model parameters such as the stiffness and strength. Quantification of the design changes is presented using the Direct Displacement Design (DDD) method in section two of Chapter Three. Chapter Four presents a comprehensive sensitivity analysis about the effect of different factors on the design changes needed. Examples of these factors are the number of stories of the building, location of the building and the magnitudes of the mainshock and aftershock earthquake records. The effect of aftershock hazard on the collapse probabilities of different damage states is also investigated in Chapter Four. Chapter Five presents the effect of aftershock intensity on collapse probabilities where different

aftershock intensities were generated by variation of either moment magnitude or site-to-source distances of earthquake records. And, Chapter Six provides a summary, conclusions and recommendations for future research.

CHAPTER TWO: METHODOLOGY TO INTEGRATE AFTERSHOCK HAZARD INTO SEISMIC DESIGN

In this chapter a framework was developed for integration of earthquake aftershock risk into Performance-Based Engineering (PBE). This solution framework will be illustrated on the Direct Displacement Design (DDD) approach in this dissertation. The steps proposed for the solution framework are outlined in the flowchart presented in Fig. 2.1. The nonlinear time-history analysis (NLTHA) with 10% damping ratio and 0.0002 seconds time steps was used in this study. Damping ratio of 5% and initial natural period of the building was used in scaling the earthquakes. These values were also used in simulation of mainshock plus aftershock (MS+AS) scenarios. In this dissertation, it is assumed that the building has the same natural period in all possible post-mainshock damage states as that of the intact building. Since, using the damaged building's natural period did not have a considerable effect on the results. This is due to the short natural periods of 0.2 seconds for the two-story building and 0.5 seconds for the four- and six-story buildings. However, the natural period of the damaged building can be longer as compared to that of the impact building (See e.g. Bazzurro et al., 2004).

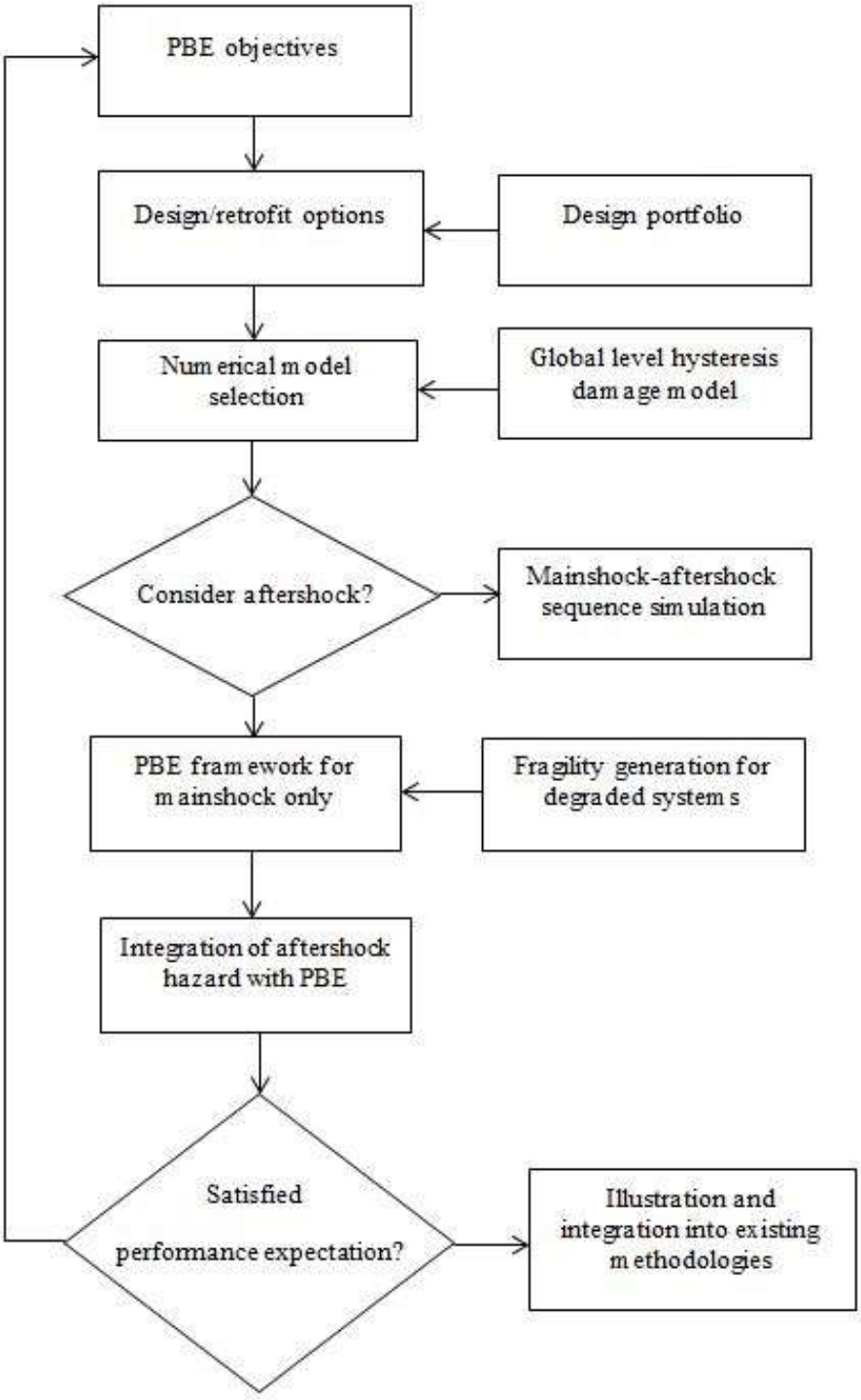

Figure 2.1 Flowchart for the plan of work

2.1. Developing the Portfolio of Representative Structures

In this study a systematic approach is explained which was developed to include the effects of aftershock (AS) hazard into Performance-Based Engineering (PBE). The "portfolio approach" which is a technique used in reliability analysis and design code calibration is utilized. Table 2.1 provides the proposed building variants which will make up the portfolio for this project.

Table 2.1 Proposed structures for base portfolio

Building No.	Building Type	No. of Stories	Location	Data type used
1	LFW	Two-story woodframe building	High seismic hazard	Experimental
2			Moderate seismic hazard	
3	LFW	Four-story woodframe building	High seismic hazard	Numerical
4			Moderate seismic hazard	
5	LFW	Six-story woodframe building	High seismic hazard	Experimental
6			Moderate seismic hazard	

LWF: Light-frame Wood Building

Each of the three building types will have two variants which will alter the design bringing the portfolio to a total of six buildings. These variants will include the number of stories and, two locations – one with moderate seismic hazard and one with high seismic hazard. The two past NEES projects for the two-story and six-story buildings were used. Since, these two projects were felt to provide acceptable data for calibration of global models in this study. The application of the two NEES projects in this study was calibration of the two-story and six-story light-frame wood buildings and their variants. The ability to calibrate the system as it softens to successive earthquakes and match natural periods at each step provided very good calibration information. The first building in the portfolio is the two-story full scale townhouse building used in the NEESWood Benchmark test. Fig. 2.2 shows the full-scale benchmark structure.

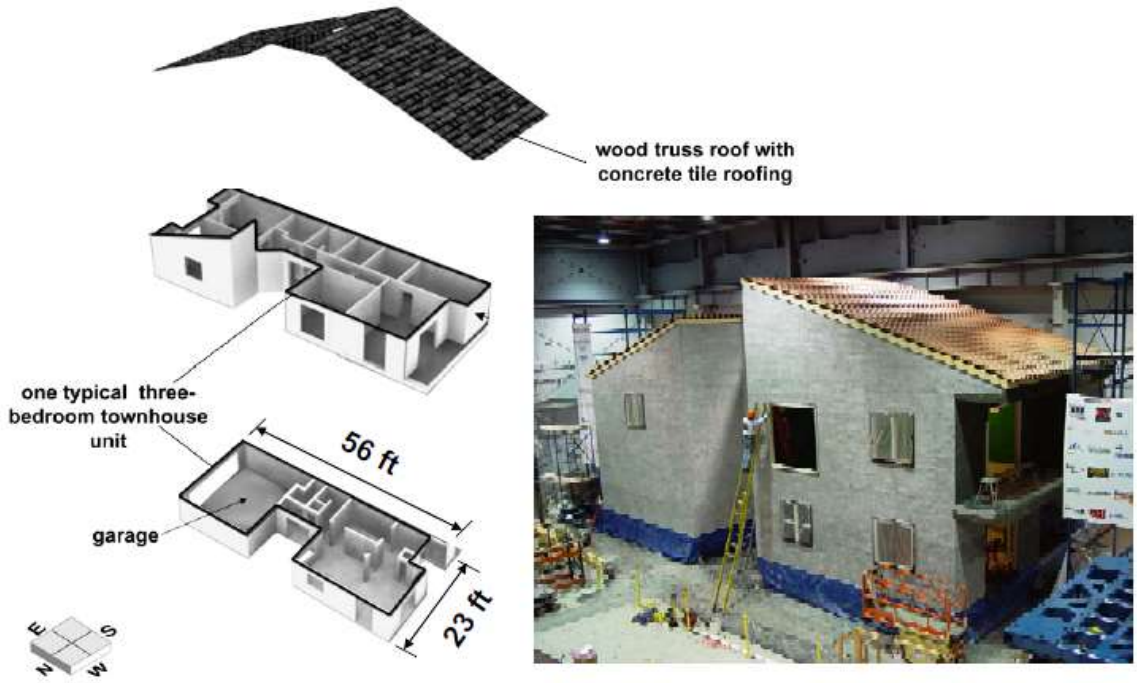

Figure 2.2 Full scale townhouse building (Excerpted from Christovasilis et al., 2009)

The NEES project for the two-story building was entitled "Seismic Testing of a Full-Scale Two-Story Light-Frame Wood Building: NEESWood Benchmark Test". The structure was a two-story woodframe residential building which was tested as part of the U.S. National Science Foundation-funded NEESWood project (Filiatrault et al., 2010). The test facility at SUNY-Buffalo was able to accommodate the full scale building by using a steel frame to link two adjoining shake tables. At that time, this test represented the largest woodframe shake table test ever conducted in the United States. The total weight of the building was 359 KN (80 kips) but was modeled as approximately 90% of the total weight at 320 KN (36 kips) in this dissertation. The weight of the first and second floor is 134 KN and 186 KN, respectively. The first floor slab to the roof eave is 5.49 m (18 ft). The two-story building was a one unit townhouse with three units. The living space was approximately 1800 ft^2 with the lower level of 17.7 m by 6.7 m and the upper level of 18.6 m by 6.7 m. The building was built in 1980's or 1990's in California

according to the seismic provisions of the 1988 edition of the Uniform Building Code (Christovasilis et al., 2009). Fig. 2.3 presents the floor plans and the elevation view of the two-story woodframe building. In this project, the two-story townhouse was tested to five levels of earthquakes ranging from a small scaling of the Canoga Park record to 100% of the Rinaldi record (Christovasilis et al., 2010). The building did not collapse but was badly damaged following the final Maximum Credible earthquake (MCE) level test. System identification tests were performed following each level of seismic testing and the building was softening following each test.

Initially, existing experimental data is obtained in order to accurately model the seismic behavior of the structure. However, it is equally possible to utilize a comprehensive analytical model without the use of experimental data. In this study, resources such as NEEShub (Network for Earthquake Engineering Simulation) (www.nees.org) were used to obtain the data. The hysteresis data used in this dissertation was generated by the response of the completed two-story building with drywall and stucco to the Northridge Rinaldi record. This is primarily because this is the way the finished building would be expected to behave; other stages of construction, while interesting from a wall layering and stiffness contribution standpoint, were not used.

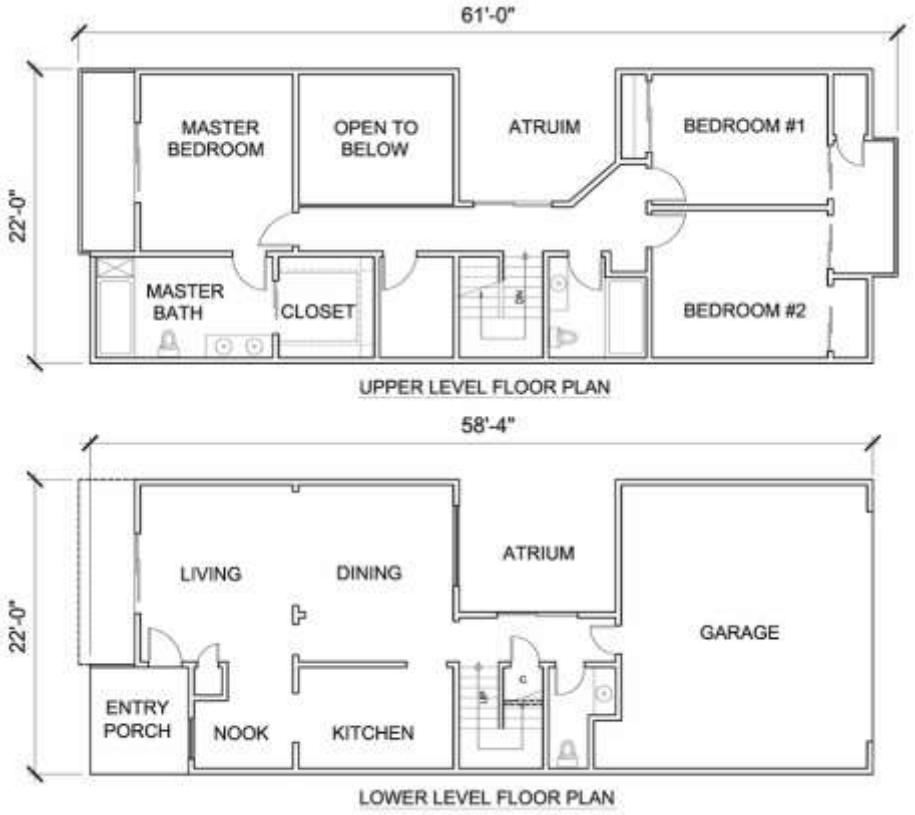

(a)

(b)

Figure 2.3 Floor plans and elevation view of the two-story building (a) Floor plans, (b) elevation view (Excerpted from Filiatrault et al, 2010)

The second building in the design portfolio was a four-story building which was designed based on the ASCE7-10 (ASCE, 2010) seismic provisions. The equivalent lateral force procedure was used for the design of the building hypothetically located in Los Angeles, CA (Jennings and van de Lindt, 2014). This building was an apartment building with four apartments at each level and the weight of each story was 780 KN (179 kips) resulting in total building weight of 3120 KN (7.17 kips). And, clear height of each story was 2.4m (8ft). Jennings and van de Lindt (2014) designed this four story building using the calculated shear capacities of 479 KN (107.7 kips), 429 KN (96.4 kips), 329 KN (73.9 kips), and 178 KN (40.1 kips), for stories 1, 2, 3, and 4, respectively. Fig. 2.4 shows the floor plans and shear walls of the four-story woodframe building where the shearwalls are shown with bold lines.

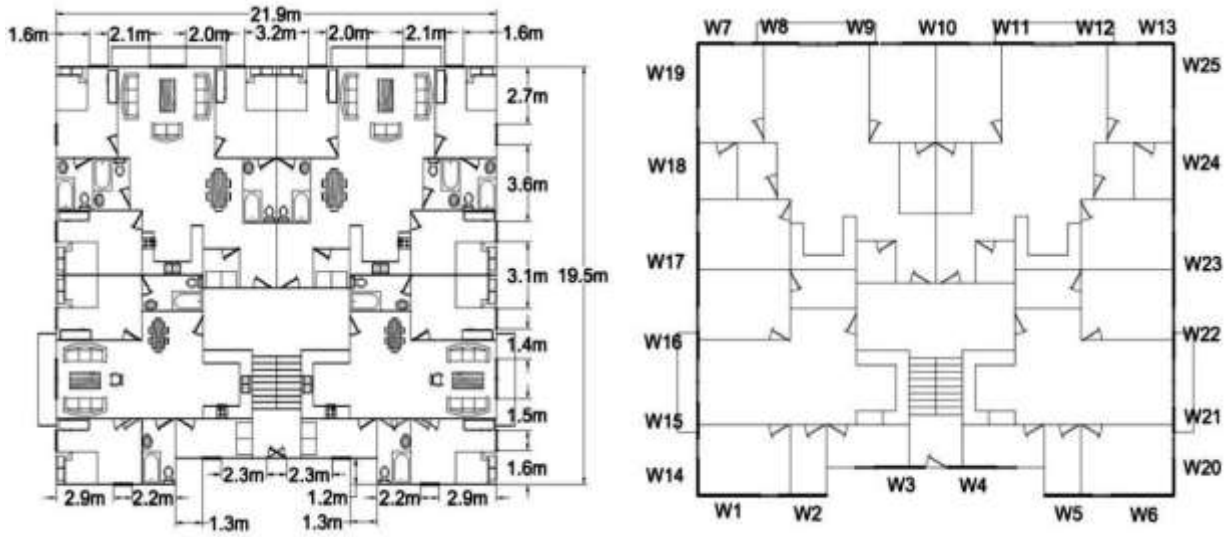

Figure 2.4 Four-story apartment building floor plan (Note: Interior walls are not selected as shear walls) (Excerpted from Jennings and van de Lindt, 2014)

Since the introduced four-story building has not been tested, the data from numerical analysis of the building was used for model calibration in this study. More details about this procedure will be presented in the next section. The full-scale NEESWood six-story Capstone

building was used as the third building in the portfolio. Fig. 2.5 shows the full scale view and the elevation view of this building.

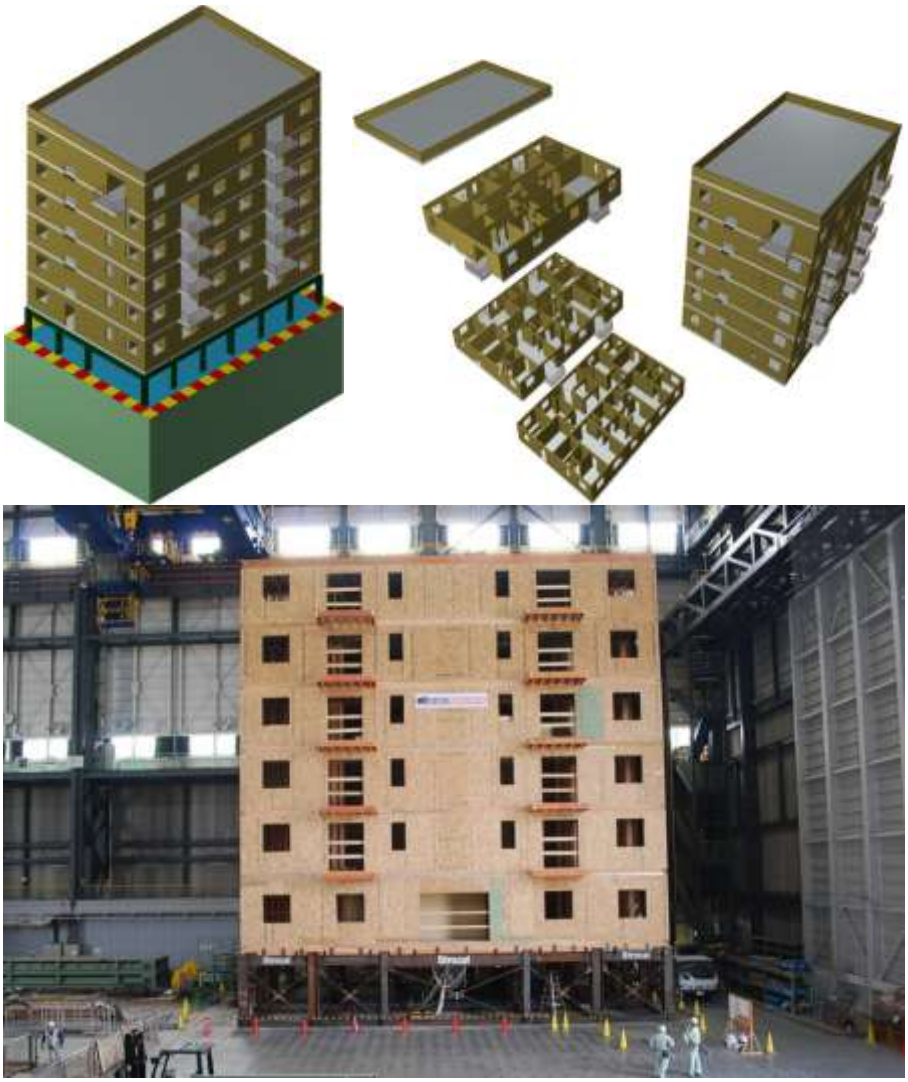

Figure 2.5 Full scale NEESWood six-story Capstone test building and the elevation view (Excerpted from Pei et al., 2010)

The NEES project for the six-story building was entitled "Seismic Testing of a Full-Scale Mid-Rise Building: The NEESWood Capstone Test: Development of a Performance-Based Seismic Design Philosophy for Mid-Rise Woodframe Construction". A six-story 14400 ft^2 wood frame apartment building was tested in this project. Multiple seismic tests were conducted for the

two configurations of the Capstone test building. A total of five seismic tests were included in the test program. One set of tri-axial historical ground motions were used for all seismic tests: an ordinary ground motion recorded during the Northridge earthquake at the Canoga Park recording station. The ground motion was scaled to Design Basis Earthquake (DBE), MCE and an intensity level between DBE and MCE. The Capstone building was an apartment building with one additional Steel Moment Frame (SMF) story at the bottom. The floor plans of the building were of a typical residential multi-story condominium in California (see Fig. 2.6 and Fig. 2.7).

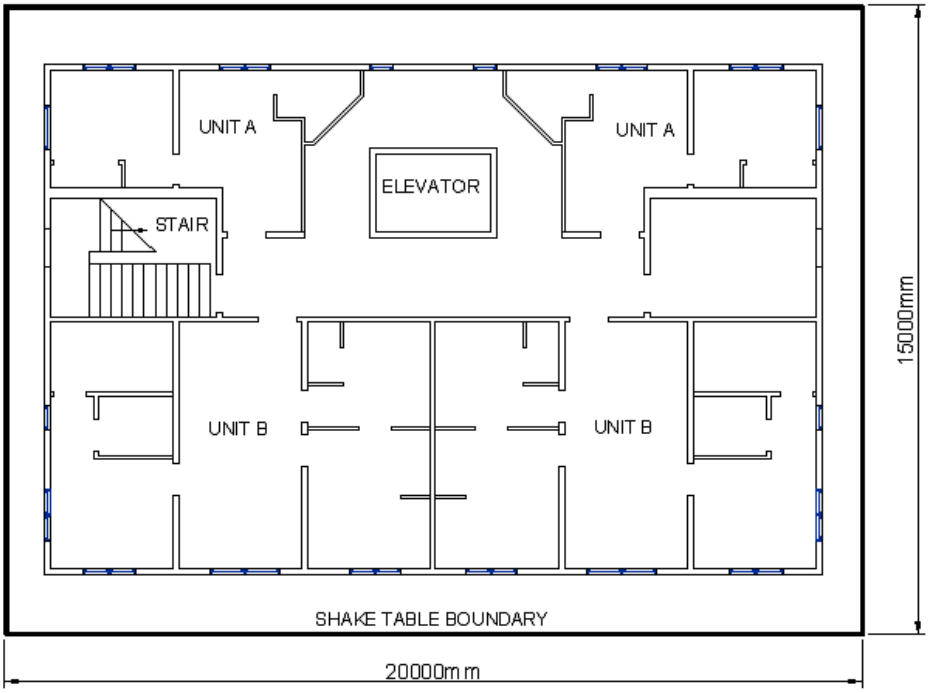

Figure 2.6 Floor plan for second story of the Capstone building (Excerpted from Pei et al., 2010

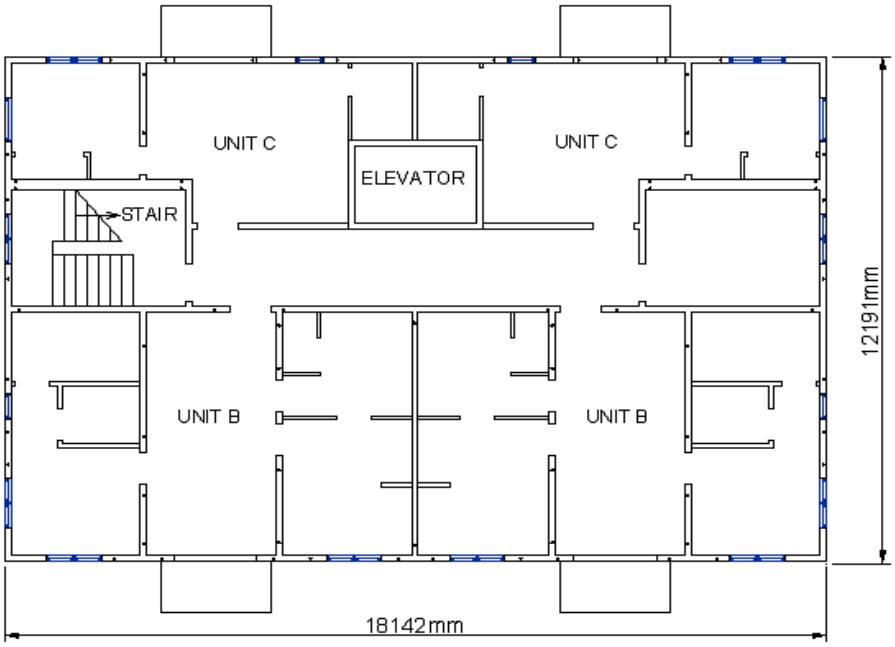

(a)

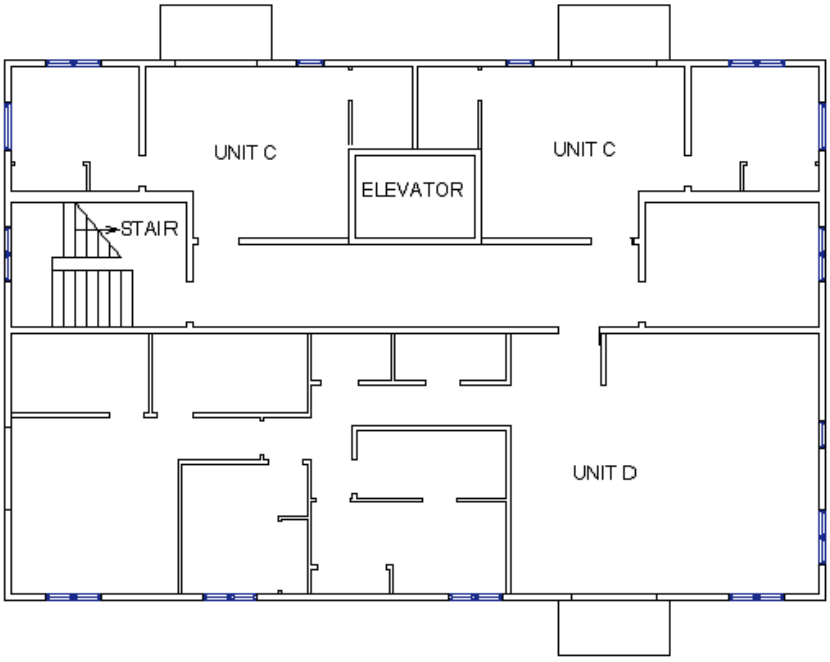

(b)

Figure 2.7 Floor plan of the Capstone building (a) for story 3-6, (b) for story 7 (Excerpted from Pei et al., 2010)

A full-scale test structure was constructed with twenty-three living units (see Pei et al., 2010 for more details). A Force-Based Design (FBD) of the building based on International

Building Code (IBC) (2006) was followed to determine the dead load of the building. However, the actual design of the building was based on a (Performance-Based Seismic Design) PBSD procedure. The floor slab to roof eave of the six-story building was 17 m (55.7 ft). The height of story 1 was 3.35 m (11 ft) and the height of story 2 through 6 was 2.7 m (9 ft), respectively. The total weight of the wood only building was 285 tons (628 kip). More details about this building can be found in Pei et al. (2010) or van de Lindt et al (2010). The 1994 Northridge Earthquake ground motions in California were used in the seismic test of the structure by van de Lindt et al (2010). The response of the building to the Canoga Park earthquake record scaled to an amplitude scaling factor of 1.8g was used in this study. This amplitude scaling factor was considered by Pei et al. (2010) to represent a Maximum Credible Earthquake (MCE) which has a 2% probability of exceedance in 50 years (2475 year return period).

2.2. Calibration of Global-Level Hysteretic Damage Models

The numerical model employed in the present study was a Multi-Degree-of-Freedom (MDOF) phenomenological degrading global level model with one DOF at each story level in the N-S direction that implicitly accounted for sliding of the sill plate, splitting of the plate, uplift, and shear deformation all lumped together by fitting the global hysteresis. It should be noted that the hysteretic fit is to the centroid of each floor level since this dissertation examines story collapse and not a single wall line. When simplifying to one DOF at each story, some portion of the weight gets numerically assigned to the shake table (in a real building this would be the slab-on-grade foundation) – for example, consider the tributary weight of the lowest walls. The half attached to shake table becomes assigned to the bottom while the lumped mass at the second floor diaphragm is assigned the upper half of those walls along with the floor system and upper half of the next walls. The weight of the lower half of the first story walls is

approximately 10% of the building weight. Therefore, the seismic weight that was considered in calibration of the model was approximately 90% of the total weight of the structure.

Fig. 2.8 shows the concept of an n-DOF model used to represent an n-story building by fitting a spring model to the global hysteresis loops at each story. It was assumed that weight of each story was lumped at each DOF of the n-story model. It should be noted that the hysteretic fit was to the centroid of each floor level since this study examines story collapse and not a single wall line as noted above. Although there is some torsion observed in several cases, this is not modeled in the present study since one DOF at each story was utilized in a single direction.

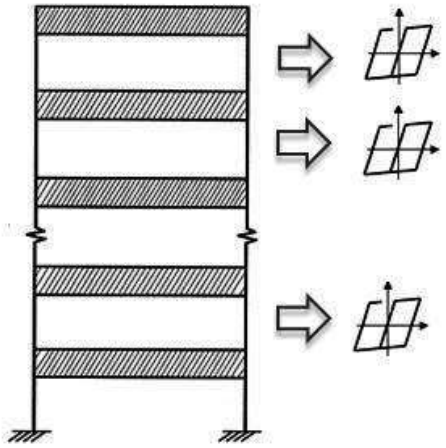

Figure 2.8 Model calibration for the n-story building

A 10-parameter CUREE (Consortium of Universities for Research in Earthquake Engineering) spring model was fit to the global hysteresis data measured during the test (Filliatrault et al., 2010). Loading paths and parameters in the CUREE hysteretic model are presented in Fig. 2.9 and Table 2.2, respectively.

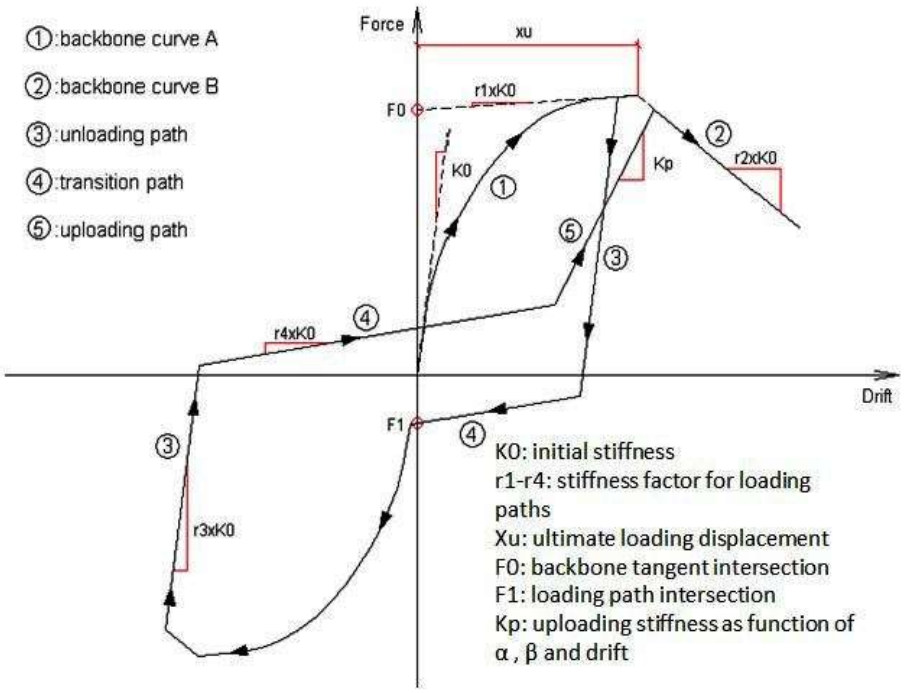

Figure 2.9 Loading paths and parameters in SAWS hysteresis model (adopted from User's Manual for SAPWood by Pei and van de Lindt, 2010)

Table 2.2 Descriptions of the CUREE model parameters

Parameters	Description
K_0	Initial Stiffness
F_0	The resistance force parameter of the backbone
F_1	Pinching residual resistance force
R_1	The stiffness ratio parameter of the backbone, typically be a small positive value
R_2	The ratio of the degrading backbone stiffness to K0, typically be a negative value
R_3	The ratio of the unloading path stiffness to K0, typically close to 1
R_4	The ratio of the pinching load path stiffness to K0, typically under 0.1
X_u	The drift corresponding to the maximum restoring force of the backbone curve
α	Stiffness degradation parameter, usually takes a value between 0.5~0.9
β	Strength degradation parameter, usually takes a value between 1.01~1.5

Past studies have calibrated component or sub-assembly-level hysteresis and then assumed the behavior of the components could be combined to predict system behavior. This is

true for many models at low deformation levels where nonlinearity is limited to material behavior, but when geometric nonlinearity is present these models no longer provide accurate prediction. Ibarra and Krawinkler (2005) pointed out that some hysteretic models that have been calibrated as damage models are component-based, but calibrated system models are needed to accurately represent the system (global) performance. Furthermore, very few studies have taken into account the deterioration of strength and stiffness in the nonlinear range (Ibarra and Krawinkler, 2005). When buildings are subjected to multiple earthquakes, the damaged building model following the first earthquake (e.g. mainshock) should be used in the subsequent analysis and the cumulative damage from the mainshock accounted for throughout the subsequent analyses. This is typically done when comparing numerical predictions to test results if numerous tests are performed on the same un-repaired specimen (Pei and van de Lindt 2010). The use of experimental data for model calibration will allow incorporation of cumulative damage including any low-cycle fatigue phenomena. It should be noted that this will be captured phenomenologically within the model and not constitutively. Large-scale test specimens are very expensive to construct and test and therefore are often tested multiple times even after they are (slightly) damaged during the earlier tests. This type of data is exactly what is needed for calibration of this type of degrading numerical model. This is similar to the numerical concept in that the data computed at the last step of the mainshock analysis of the calibrated model is used to generate the degraded model for the aftershock analysis.

Fig. 2.10 shows an example of the hysteresis fitted to the original model (shown by solid line) versus the hysteresis for the degraded model (shown by dashed line). As expected, the hysteresis fitted to the degraded model has degraded stiffness and strength compared to that of

the original model. Therefore, the fitted hysteretic model is can be used to take into account the degradation that occurs during the mainshock earthquake.

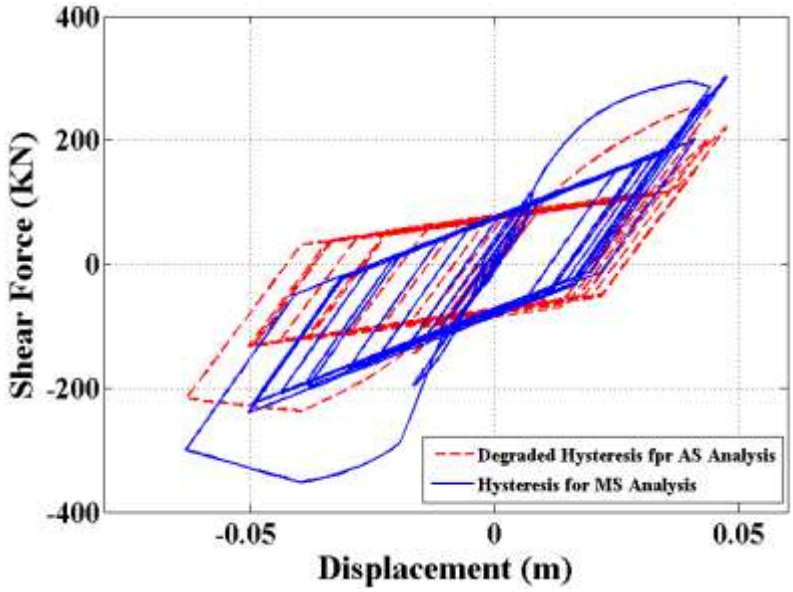

Figure 2.10 Hysteresis and backbone curves for undamaged and degraded systems

2.3. Mainshock + aftershock Sequence Simulation

The earthquake ground motion records used in this study were from the Applied Technology Council Project 63 which resulted in the development of FEMA P-695 (FEMA, 2009) and consists of a suite of 22 far field (ordinary) ground motions (FEMA, 2009). Table 2.3 presents the list of 22 earthquake records. Specifically, these were used as MS records and the record-to-record variation represents the total earthquake variability for the MS. That project focused on collapse and determination of R-factor acceptability and is therefore felt to provide a good representation of large crustal earthquakes. Although each earthquake in the suite of 22 records has its own magnitude (between M6.5 and M7.6), associated with the historical event, a different procedure was used herein to develop MS+AS scenarios. The aftershock records were selected on a random basis among the 22 suite of earthquakes (see Table 2.3).

The mainshock and aftershocks of specified moment magnitude and site-to-source-distance was used in the Next Generation Attenuation (NGA) relationship at the natural period of the building. The reason that the mainshocks and aftershocks were scaled to the spectral acceleration calculated from attenuation relationships was to be able to show the lower intensity level of aftershocks compared to the mainshocks. Since, the aftershocks usually have smaller moment magnitude than the mainshock and their energy content can be different from the mainshock. This effect is taken into account by using the aftershock parameter in the NGA relationship presented by Abrahamson and Silva (2008) where the aftershock parameter of zero and unity was used for the mainshock and aftershock, respectively.

Table 2.3. 22 Far-Field earthquake suite, ATC-63 Project

	Earthquake			Recording Station	
ID No.	Magnitude	Year	Name	Name	Owner
1	6.7	1994	Northridge	Beverly Hills - 14145 Mulhol	USC
2	6.7	1994	Northridge	Canyon Country-W Lost Cany	USC
3	7.1	1999	Duzce-Turkey	Bolu	ERD
4	7.1	1999	Hector-Mine	Hector	SCSN
5	6.5	1979	Imperial Valley	Delta	UNAMUCSD
6	6.5	1979	Imperial Valley	El Centro Array #11	El Centro Array #11
7	6.9	1995	Kobe-Japan	Nishi-Akashi	CUE
8	6.9	1995	Kobe-Japan	Shin-Osaka	CUE
9	7.5	1999	Kokaeli-Turkey	Duzce	ERD
10	7.5	1999	Kokaeli-Turkey	Arcelik	KOERI
11	7.3	1992	Landers	Yermo Fire Station	CDMG
12	7.3	1992	Landers	Coolwater	SCE
13	6.9	1989	Loma Prieta	Capitola	CDMG
14	6.9	1989	Loma Prieta	Gilroy Array #3	CDMG
15	7.4	1990	Manjil, Iran	Abbar	BHRC
16	6.5	1987	Superstition Hills	El Centro Imp. Co. Cent	CDMG
17	6.5	1987	Superstition Hills	Poe Road (temp)	USGS
18	7	1992	Cape Mendocino	Rio Dell Overpass - FF	CDMG
19	7.6	1999	Chi-Chi Taiwan	CHY101	CWB
20	7.6	1999	Chi-Chi Taiwan	TCU045	CWB
21	6.6	1971	San Fernando	LA - Hollywood Stor FF	CDMG
22	6.6	1976	Friuli, Italy	Tolmezzo	-

2.4. Fragility Generation for Different Limit States for Degraded Systems

The fragilities of the degraded/damaged building systems in the portfolio were used to develop the mainshock collapse fragilities. Then, the aftershock records were selected randomly among the same suite of ground motions presented in Table 2.3. It should be noted that only one aftershock was assumed in simulation of the mainshock plus aftershock sequence. Since, the

time, magnitude and space distribution of aftershocks have been accounted for in the aftershock hazard curve generated by Aftershock Probabilistic Seismic Hazard Analysis (ASPSHA).

Fragility development was performed for four limit state definitions in order to provide the necessary database (i.e. fragility curves). A drift-based limit state is defined as a lower bound on the collapse portion of the investigation since for most engineered structures these limits are felt to be conservative. Another definition of limit state will be considered an upper bound for the collapse. Table 2.4 contains damage states 1 to 4 which were used for the initial investigation of a mainshock-damaged building. Each peak inter-story drift limit state level was associated with a damage state (see Table 2.4). This table was derived with some modifications from Christovasillis et al. (2007) for a two-story building which describes the visual damage based on the Benchmark at Buffalo.

The collapse criteria for the woodframe buildings is based on a combination of observations made and documented in different projects including the Benchmark final report (Christovasilis, 2007), the ATC-63 project light-frame wood example performed by Filiatrault (FEMA, 2009), and a recent collapse test performed by van de Lindt (van de Lindt et al. 2010). During the Benchmark testing at Buffalo approximately 3.5% inter-story drift was observed without nearing collapse and in the recent tests by van de Lindt et al. (2012) a garage wall achieved to 5.5% inter-story drift with severe loss of capacity but did not collapse. It was agreed upon by the ATC-63 technical committee to use 7% inter-story drift in that project as representative of collapse for woodframe buildings, which is still likely conservative for buildings when system effects are included. For consistency, 7% inter-story drift will be used to define the collapse limit state. One advantage of this value is that the Incremental Dynamic

Analysis (IDA) curve is typically flat at that point indicating that increasing the inter-story drift limit would not provide any additional information with regard to the spectral acceleration that results in collapse.

Table 2.4. Damage states based on visual observations (Derived from Christovasilis et al., 2007)

Damage states(DS)	Corresponding Peak Inter-story Drift (%)	Wood Framing and Oriented Strand Board(OSB) Plywood Sheathing	Gypsum Wall Board (GWB)
DS1 (Immediate Occupancy)	0.1 - **1%**	Minor splitting and cracking of sill plates (some propagation) Slight sheathing nail withdraw	Slight cracking of GWB Diagonal propagation from door/window openings Partial screw withdraw Cracking at ceiling-to-wall interface
DS2 (non-structural damage)	1.0 - **2.0%**	Permanent differential movement of adjacent panels Corner sheathing pullout Cracking/splitting of sill/top plates	Crushing at corners of GWB Cracking of GWB taped/mud joints
DS3 (Life safety)	2.0 - **4.0%**	Splitting of sill plates equal to anchor bolt diameter Cracking of studs above anchor bolts Possible failure of anchor bolts	Separation of GWB corners in ceiling Buckling of GWB at openings
DS4 (Collapse prevention)	4.0-**7.0%**	Severe damage across edge nail lines, separation of sheathing Vertical posts uplifted Failure of anchor bolts	Large pieces separated from framing Entire joints separated and dislodged

When buildings are subjected to multiple earthquakes, the damaged building model after one earthquake (e.g. mainshock) should be used in the subsequent analysis and the cumulative damage that occurred in the mainshock needs to be included. The seismic fragilities for most building types can be modeled by a lognormal distribution (Li et al. 2010, Li and Ellingwood 2007b, Zareian and Krawinkler 2007, Shinozuka et al. 2000) which will be utilized in this study.

Fig. 2.10 presents the collapse fragility curves for the MS-only case using undegraded system and the mainshock plus aftershock case using the degraded system under Design Basis Earthquake (DBE) level mainshock. The fragility curves were developed for the four-story building introduced earlier which was designed for 4% design drift and 50% exceedance probability.

Collapse fragilities for the degraded and undegraded models are presented in Fig. 2.11. Inspection of this figure shows that the fragility for the degraded model has higher Cumulative Distribution Function (CDF) values compared to that of undegraded model. For example, at normalized collapse capacity of c=0.5, the collapse probability of the damaged (degraded) system is 0.9 resulting in 0.1 probability of survival, whereas the undamaged system has about 0.7 probability of survival. Note that the collapse probability here is does not take into account the effects of seismic hazard for a specific location. It should be noted that in this dissertation, the collapse capacity, c is chosen to be the spectral acceleration (S_a) at the natural period of the building.

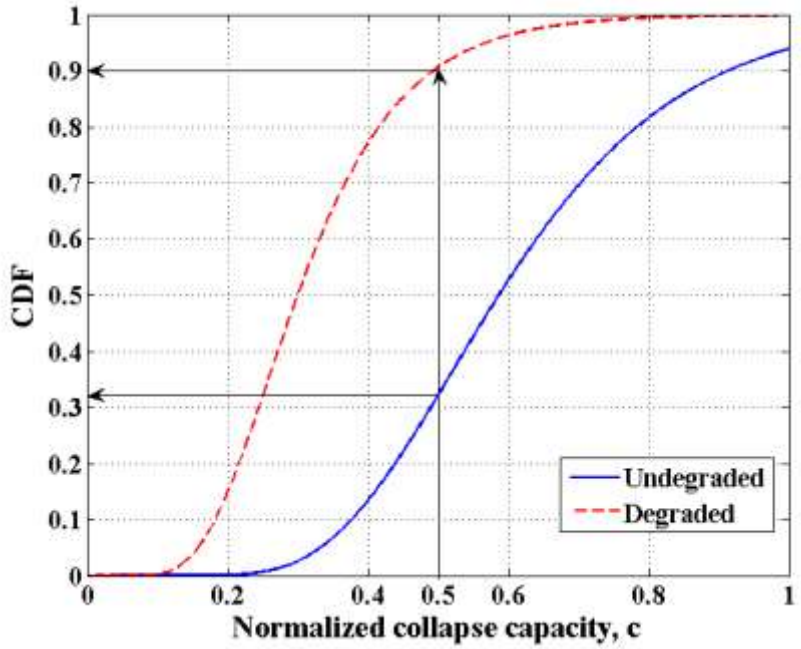

Figure 2.11 Collapse fragility for undamaged and degraded systems

The fragility curves also could be developed for limit states other than the collapse limit state. These fragilities are useful in PBSD when different levels of performance for the structure are expected. Additionally, the fragilities for damage states less than collapse are useful for the purposes of building tagging (see Luco et al. 2011). Fig. 2.12 presents the fragility curves developed for four different damage states (DS). These fragilities were developed once for the new, undamaged, system for the MS-only case (see Fig. 2.12(a)) and once for the system degraded in an Maximum Considered Earthquake (MCE) level mainshock (see Fig. 2.12(b)). As observed in Fig. 2.12(a), there is no fragility curve for DS1. In other words, the entire 22 suite of earthquake records caused the model to exceed 1% inter-story drift associated with DS1 resulting in the zero fragility curve for this damage state. This is not unexpected since the motion was scaled to MCE level.

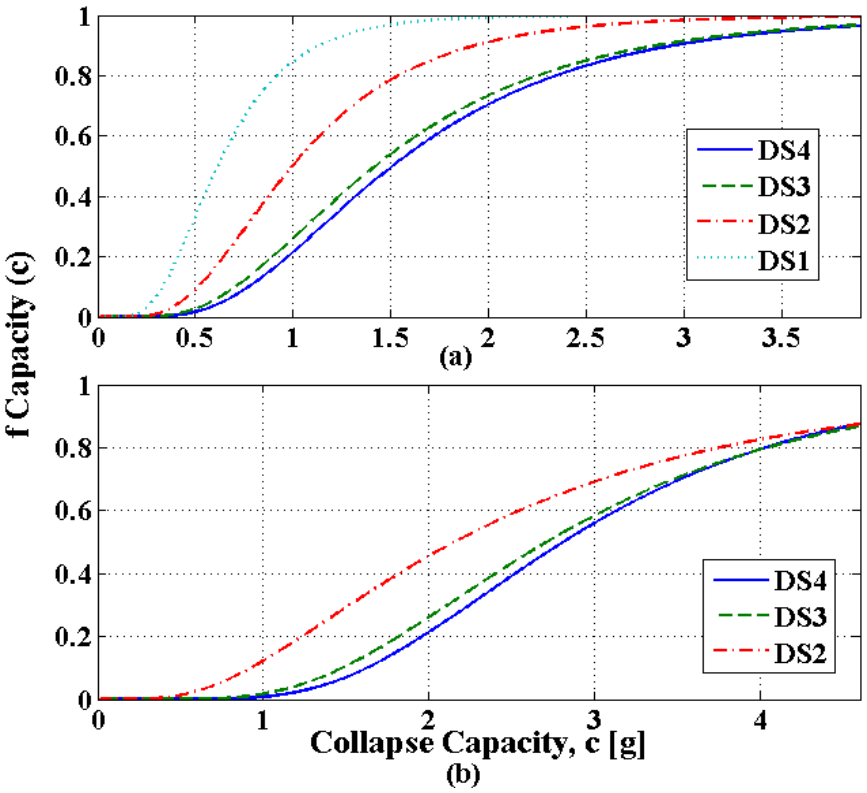

Figure 2.12. Collapse fragility curves for undegraded and degraded systems (a) undegraded system, (b) degraded system

2.5. Integration of Mainshock and Aftershock Seismic Hazard with Fragility Curves and Collapse Probability Calculation

The conditional probability of collapse (the fragility) determined using nonlinear time-history analysis (NLTHA) then be convolved with the site-specific seismic hazard curve to determine when the structure is subjected to a mainshock at the prescribed magnitude. This is a well-known procedure that has most recently been used to calibrate the seismic risk maps for design in the United States (see e.g. ASCE 7-10). The probability of exceedance of various limit states can be related to Performance-Based Earthquake Engineering (PBEE) metrics for decision making. For example, determining whether the collapse risk is acceptable, i.e. does it align with the objective of 1% in 50 year collapse probability targeted by The Building Seismic Safety Council (BSSC, 2009). Consideration of the effect of mainshock plus aftershock sequences on

the total collapse risk is important. The outcome of this convolution can be used for such calibration purposes. The annual probability of collapse provides a metric for evaluation of risk, and of course includes the site-specific seismic hazard.

The collapse probability (risk integral) can be calculated using Eq. 1.8 where the uncertainty in the collapse capacity of a given model is also taken into account. In this equation, the probability distribution for the collapse capacity is coupled with a corresponding hazard curve for the location of the model (Luco et al., 2007). Fig. 2.13 presents the calculation of the risk integral using Eq. 1.8. In this figure, the collapse capacity of the structure (c) is the S_a (at the fundamental period of the building) that it can resist without collapse; $f_{Capacity}$ (c) is the probability density function (PDF) of the estimated lognormal distribution for the collapse capacity. The first subplot shows the hazard curve with horizontal axis of S_a. This is hazard curve is convolved with the Probability Density Function (PDF) of the collapse fragility curve. In this study, the risk integral is computed numerically. The hazard curve and the PDF fragility curve are multiplied in the third subplot and the area under this curve is taken. The area under the curve in the third subplot is the result of the risk integral in Eq. 1.8 which is the collapse probability.

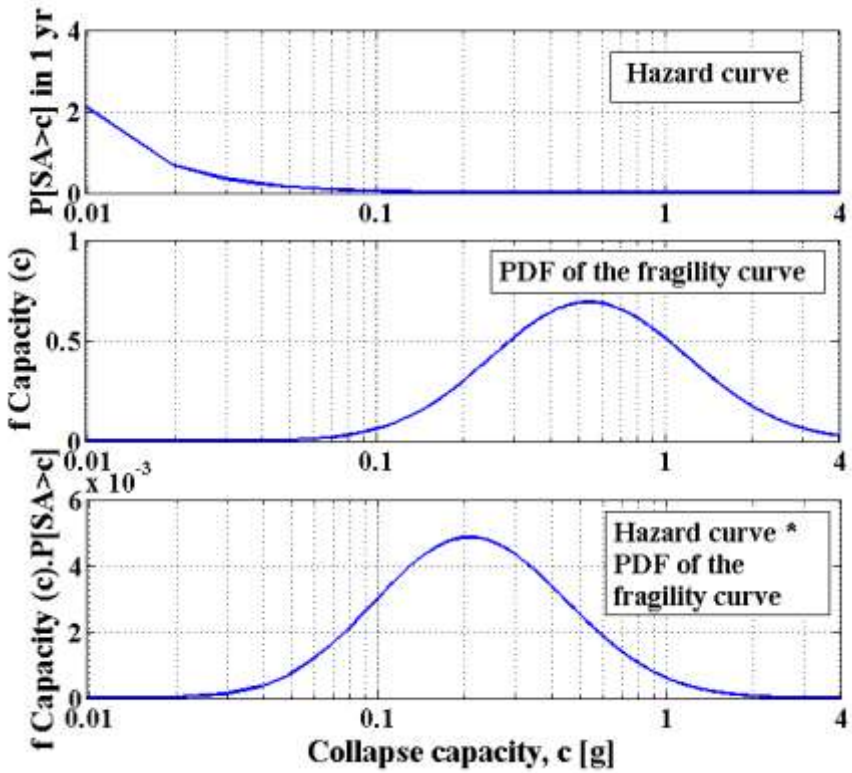

Figure 2.13. Calculation of the risk integral of the probability of collapse in 1 year

In order to be able to use Eq. 1.8 to calculate the aftershock collapse probability, the aftershock hazard curve must also be generated which is less trivial. The MS hazard curve was generated based on the National Seismic Hazard Mapping Project (NSHMP) hazard application software (USGS, 2013). The aftershock hazard can then be developed using the procedure described by Yeo and Cornell (2005). This procedure was developed with PGA horizontal axis for both MS and AS hazard curves. However, the AS hazard curve in terms of Spectral Acceleration (S_a) is needed for the purpose of convolving with the fragility curve. Therefore, the AS hazard curve with PGA horizontal axis was converted to the AS hazard curve with S_a horizontal curve by using a basic procedure. Fig. 2.14 presents the MS and AS hazard curve for Los Angeles, CA (Latitude: 34.0537, Longitude: -118.2427) with a spectral acceleration horizontal axis. Developing the aftershock hazard curve is dependent on several parameters

including the magnitudes of MS and AS. The aftershock hazard curve also depends on the time span that is investigated to compute the rate of aftershocks. As mentioned earlier, the aftershock rate is time-dependent and decreases with the elapsed time after the mainshock.

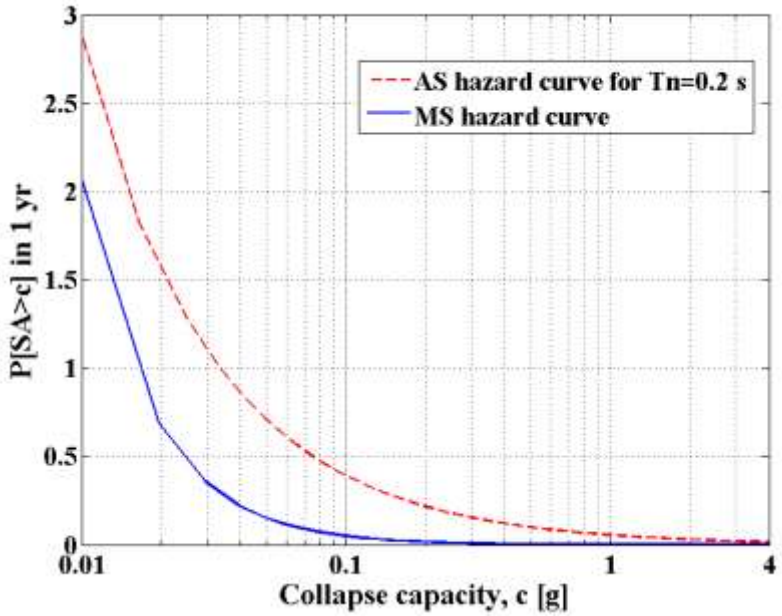

Figure 2.14. Mainshock and aftershock hazard curves for scenarios with M7.3 mainshock

2.6. Integration into Existing Performance-Based Earthquake Engineering (PBEE) Methodologies

Due to the increased collapse risk after the occurrence of the a mainshock, it is desirable to develop a methodology to quantify the damage states with more confidence by taking into account the aftershock uncertainty i.e. the probabilities assigned to different damage states might be revised substantially, narrowing the range of possible states. The aftershock seismic hazard and the resulting effect on building performance which was developed using the portfolio approach was examined and an aftershock adjustment were provided for the Direct Displacement Design (DDD) method, a performance-based seismic design approach. The aftershock adjustment factors could be applied to the design base shears used within the DDD method.

CHAPTER THREE: QUANTIFYING THE DESIGN CHANGES NEEDED DUE TO INTEGRATING THE AFTERSHOCK HAZARD

This chapter investigates a methodology that can quantify the changes that would be needed in the structural design of a building to account for aftershock hazard and illustrates it using a basic nonlinear model of a building. In other words, what changes to a structural design would be needed such that the building has the same collapse probability for the combined mainshock plus aftershock hazard as the collapse probability for the original building subjected to the MS only? The total collapse probability is computed using a combination of seismic fragility results convolved with the two types of hazard curves, namely a typical hazard curve and an aftershock hazard curve.

The methodology presented in Chapter Two of this dissertation was used in this chapter. The first section presents a methodology for quantifying the changes needed in the stiffness and strength hysteresis parameters. Section two of this chapter investigates the changes needed to account for the aftershock hazard using the Direct Displacement Design (DDD) approach. Three illustrative examples - a two-, four- and six-story woodframe building are presented in this chapter.

3.1. Quantifying the Changes Needed in Hysteresis Parameters of Stiffness and Strength due to the Aftershock Hazard

Quantifying the necessary changes to structural resistance and overall seismic behavior (hysteresis) for each story of a multi-story building to account for the aftershock risk was the objective of this chapter. This could be accomplished with a model of any complexity. However,

for development of the methodology a nonlinear shear building representation of the structures was felt to serve well. The basic concept relies on the fact that the total collapse probability is the summation of the collapse probability for the mainshock only occurrence plus the probability of collapse for both the Mainshock (MS) and Aftershock (AS) occurrence (i.e. $P(MS) + P(MS \cap AS)$ where P(MS) is the probability of collapse in mainshock and P(MS∩AS) is the probability of collapse under the occurrence of both mainshock and aftershock). Eq. 3.1 presents the collapse probability for mainshock plus aftershock mathematically as:

$$P(MS) + P(AS \cap MS) = P(MS) + P(AS) \times P(MS) = P(MS) + P(AS|\overline{MS_{MCE}}) \times P(MS) \quad (3.1)$$

Assuming that the $P(MS)$ and $P(AS)$ values are independent, the term $P(AS \cap MS)$ can be written as $P(AS) \times P(MS)$. Also, the terms $P(AS)$ and $P(AS|\overline{MS_{MCE}})$ can be used interchangeably here since the occurrence of an aftershock is conditioned on the occurrence of a previous MCE level mainshock. The bar means no collapse in the MCE level mainshock. In other words, $P(AS|\overline{MS_{MCE}})$ is calculated for only the buildings that have survived the MCE level mainshock. It should be noted that the mainshock in term $P(AS|\overline{MS_{MCE}})$ is different from the mainshock in term $P(MS)$.

The methodology presented herein lays out an approach to identify what change in structural design would be needed for each story of a multi-story building such that the MS+AS case gives the same total collapse probability as mainshock-only case. In order to account for the degraded model, the fragilities of the MS-damaged systems were developed by incremental dynamic analysis (IDA) using mainshock plus aftershock sequences. This process has been used many times to model a damaged structure (e.g. see Ryu et al., 2011). The methodology for quantifying the needed change in design due to the aftershock effects is summarized in the flowchart presented in Fig. 3.1 and the following text explains steps A through K using a two-

story woodframe building for illustration, when necessary. However, it should be noted that the methodology is general and can be applied to any type of structural system with a nonlinear model of any complexity.

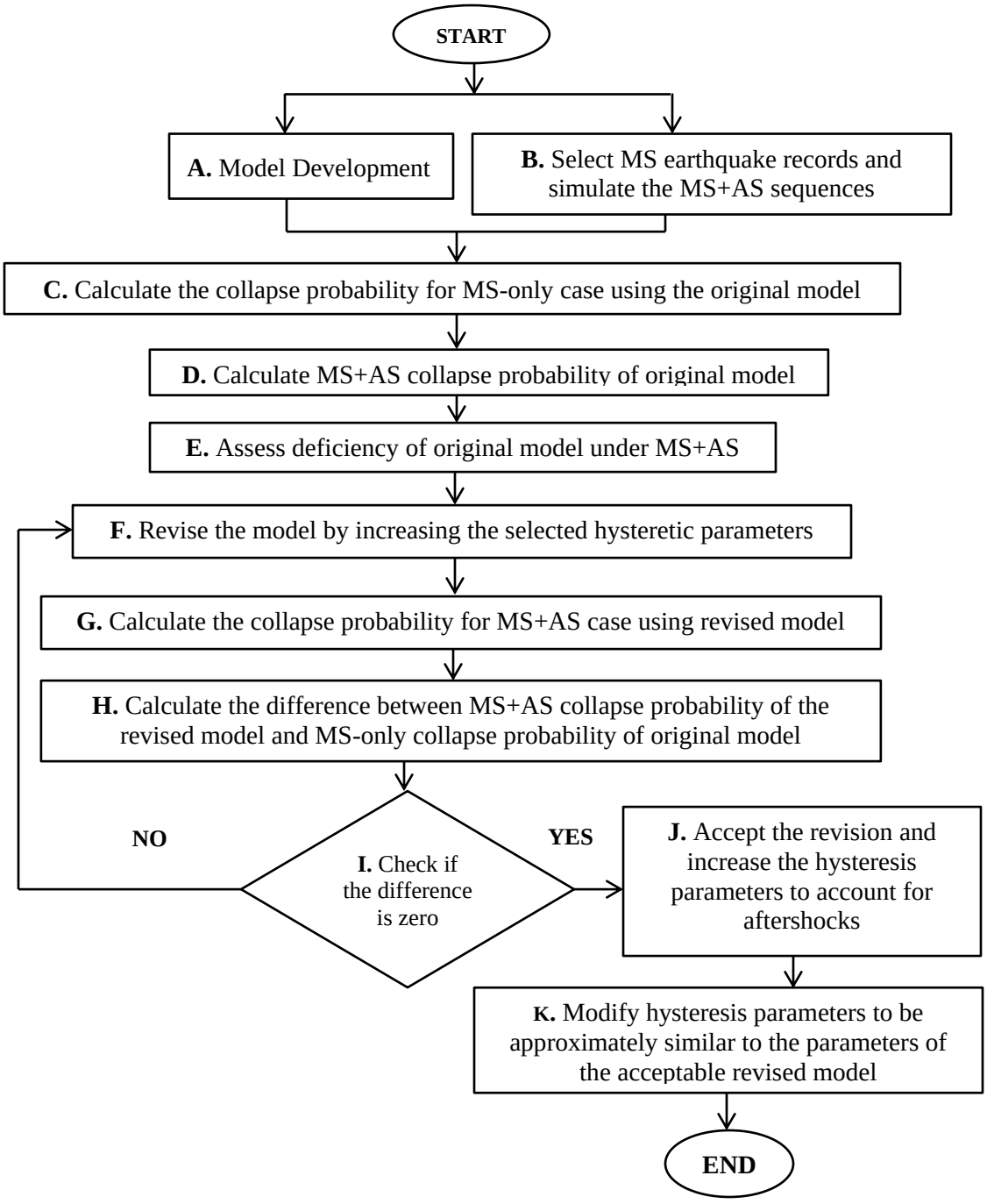

Figure 3.1. Flowchart outlining the methodology
(Note: MS stands for mainshock and AS stands for aftershock)

3.1.1. Analysis Methodology Using a Two-Story Illustrative Example

This section illustrates steps of the flowchart presented in Fig. 3.1.

Model Development (A)

The first step of the process is to develop a representative mathematical model of sufficient enough complexity such that the nonlinear hysteretic response of the building to earthquakes can be reproduced with confidence. This can be accomplished based on a detailed finite element formulation or a simplified hysteretic model if experimental data is available.

In order to calibrate a numerical model as shown in box A of Fig. 3.1, the building was simplified as a n-degree of freedom (DOF) system with lumped masses representing the seismic mass at each story. A CUREE-type hysteretic spring model was also used to represent each story of the n-DOF model. This nonlinear numerical model is capable of providing acceptable seismic response in a global sense. The 10-parameter CUREE model (Folz and Filliatrault, 2001) has been widely used in seismic wood research over the last decade (e.g. Pang et al., 2010; van de Lindt et al., 2010) and is generally accepted as a reasonable hysteretic model for examining woodframe building behavior under moderate to strong ground motions. The load-deformation behavior of wood shearwall components of the two-story building was modeled by fitting the 10-parameter CUREE model to the original NEEShub data in the N-S direction and the fits to this global hysteretic data are presented in Fig. 3.2. Table 3.1 provides the 10-parameters for the fitted CUREE model used in the analyses throughout this study. Stiffness and strength degradation in the CUREE model are accounted for by parameters α and β, respectively.

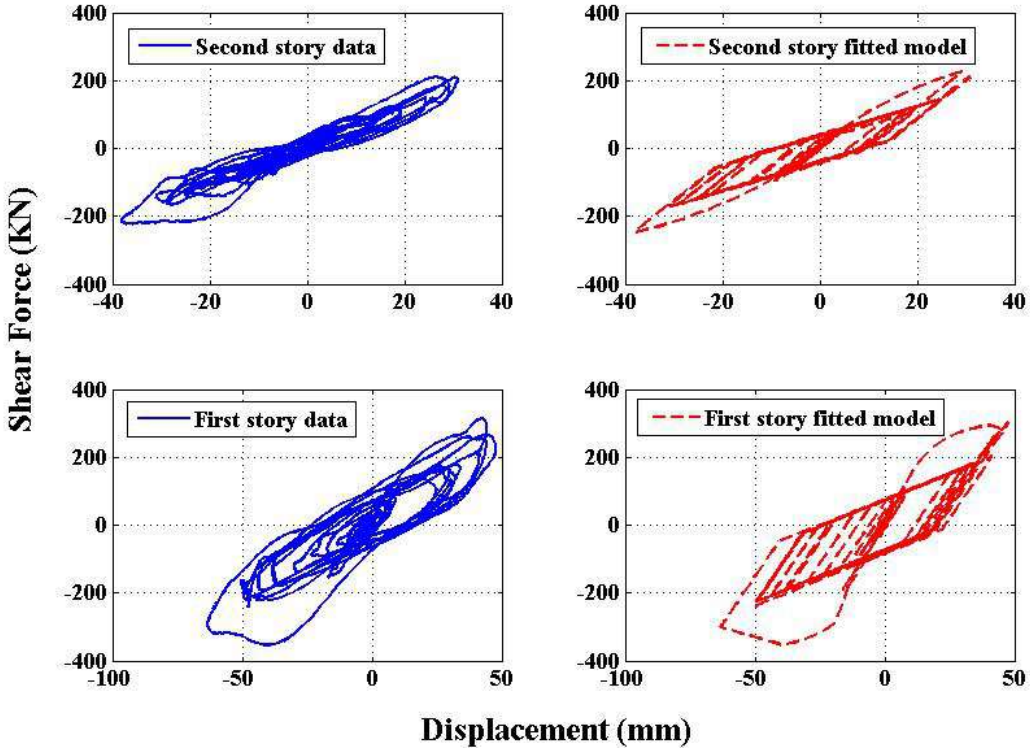

Figure 3.2 Response of the two-story test building at 100% Northridge-Rinaldi versus the CUREE model fitted to the hysteresis loops
(Note: The subplots in the left column show the test data hysteresis loops and, the subplots in the right column show the fitted model)

Table 3.1 10 parameters for the CUREE hysteretic model

Parameters (KN, mm)	First story	Second story
K_0	28.02	11.38
F_0	333.62	355.86
F_1	71.17	35.59
R_1	0.01	0.006
R_2	-0.08	-0.08
R_3	0.4	1
R_4	0.11	0.38
X_u	39.75	39.75
α	0.75	0.75
β	1.1	1.1

Select MS earthquake records and simulate MS+AS sequences (B)

Again referring back to the flowchart in Fig. 3.1, in step B the suite of ground motions is selected. The earthquake ground motion records used in this study were from the Applied Technology Council (ATC) Project 63 (see Table 2.3). The MS of specified moment magnitude is used in the Next Generation Attenuation (NGA) relationship at the natural period of the building. The only parameter that was changed between scaling the MS and AS using the attenuation relationship was the moment magnitude of the earthquake record. And, other input parameters are similar for both of the MS and AS cases.

Similar to the MS case, a spectral acceleration value is determined for an AS of smaller moment magnitude using the NGA attenuation relationship, by assuming the site-to-source distance remains the same. Using the procedure described above, a scenario for MS+AS with a MS of M8 and an AS of M7 was investigated.

Calculate the collapse probability for MS only case using the original model (C)

In step C of the flowchart presented in Fig. 3.1 the conditional probability of collapse (the fragility) determined using nonlinear time history analysis (NLTHA) is convolved with the site-specific seismic hazard curve to determine the unconditional probability of collapse when the structure is subjected to a MS at the prescribed magnitude. The MS hazard curve was generated based on the National Seismic Hazard Mapping Project (NSHMP) hazard application software (USGS, 2013). Fig. 3.3 presents the MS hazard curve for Los Angeles, CA (Latitude: 34.0537, Longitude: -118.2427).

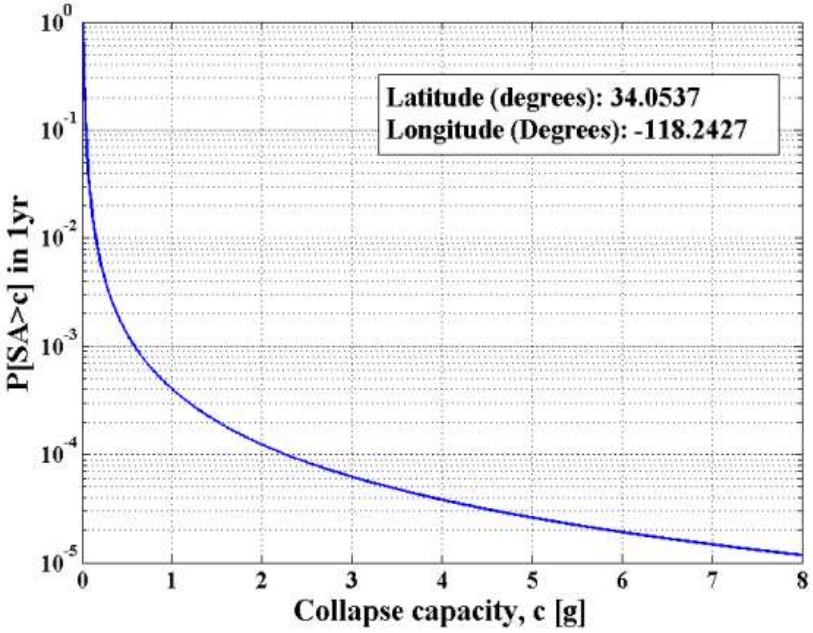

Figure 3.3 Mainshock hazard curve for Los Angeles, CA

The Incremental Dynamic Analysis (IDA) curves are provided using the scaled earthquake records. For the two-story building, the mainshocks are scaled to the spectral acceleration (S_a) of approximately 2.45g. This value is determined by Abrahamson and Silva (2008) NGA attenuation relationship for a M8 mainshock. A natural period of 0.2 seconds was used in determining the S_a value. The IDA curves for the 22 records have a near-flat slope at a drift of approximately 7% with a wide range of corresponding spectral accelerations for each record, as one might expect. It should be noted that some ground motion records do not excite particular building models and thus spectral accelerations corresponding to collapse were capped at a maximum of 4g, i.e. 4g spectral acceleration was assumed to collapse the building if the scaled record did not produce 7% drift numerically. Inter-story drift of 7% was used as the collapse drift from IDA curves for the woodframe example. The collapse spectral accelerations associated with 7% collapse drift were determined and MS fragility curve provided. Fig. 3.4 shows the MS collapse fragility curve for the model having the story hysteresis shown in Fig.

3.2. A lognormal distribution is fit to the cumulative distribution and the mean and standard deviation parameters are derived. The average collapse spectral acceleration was 3.014 g for the original model under MS earthquakes. Then, the probability density function (PDF) of an estimated lognormal distribution was also provided.

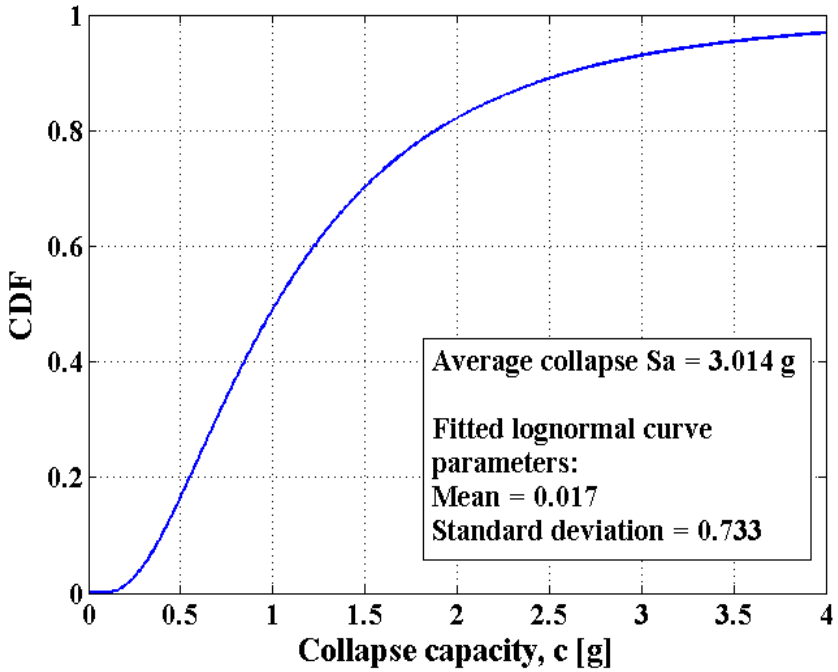

Figure 3.4 Mainshock fragility curve for the numerical model

The annual probability of collapse was calculated using the risk integral presented in Eq. 1.8. Calculation of the MS collapse probability for the numerical model presented earlier is shown in Fig 3.5. In the first subplot, a power curve is fit to the MS hazard curve shown earlier in Fig. 2.13. As presented in Fig. 3.5, this collapse probability (P(MS)) is approximately equal to 0.002307 which is quite small since it is an absolute collapse probability and not conditional. The probability is not conditioned on the occurrence of another earthquake since the hazard curve used in the convolution is unconditional in the MS-only case. However in the MS+AS case

the AS hazard curve is conditioned on the occurrence of the previous MS and thus results in the conditional collapse probability.

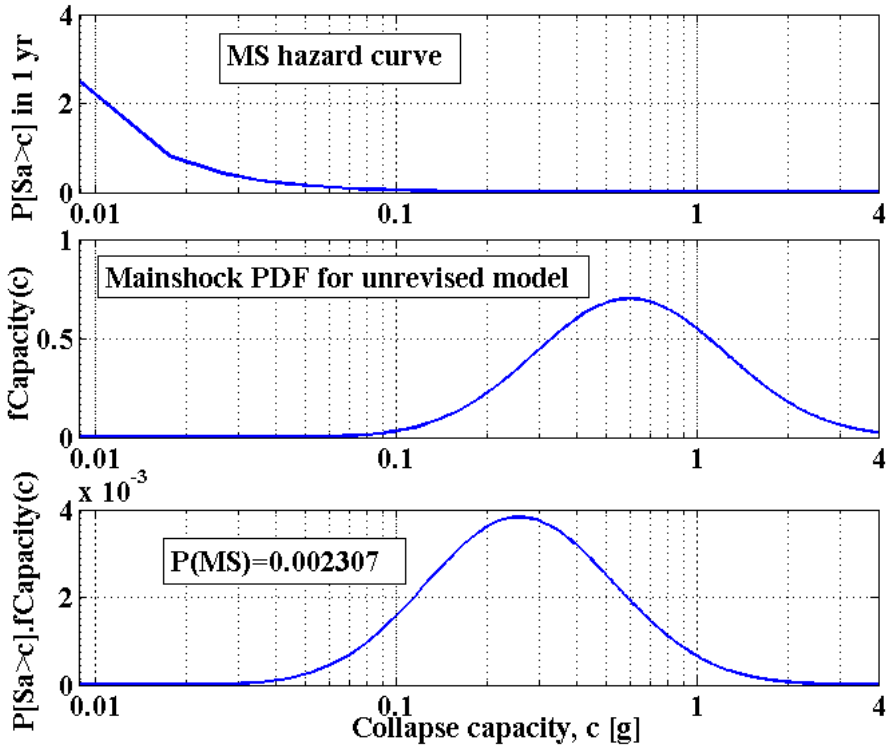

Figure 3.5 Calculation of the risk integral of the probability of collapse in 1 year for the two-story model for the mainshock

Calculate MS+AS collapse probability of original model (D)

The MS+AS collapse probability is also calculated using Eq. 1.8. Similar to section C of the flowchart in Fig. 3.1, the AS collapse probability can be computed. However, there are some differences in calculation of the AS hazard curve and the MS+AS fragility curves that are explained below. The AS hazard was developed using the procedure described by Yeo and Cornell (2005). This procedure was explained in more details in Chapter One of this dissertation. The mean number of aftershocks denoted by μ^* was calculated using Eq. 1.7. Parameters of the generic California model that were mentioned earlier in Eq. 1.4 were used in calculation of the mean number of aftershocks. The terms m_l and m_m in Eq. 1.7 are assumed to be M5.0 and M8.0

in this case. Also, time t following a MS of magnitude m_m was assumed to be t=0 days and T=1000 days using the approach developed by Yeo and Cornell (2005). Based on the above assumptions the scalar value of μ^* was approximately 100. This factor is then multiplied with the MS hazard curve which has the horizontal axis of PGA. However, the AS hazard curve in terms of S_a is needed for the purpose of convolving with the fragility curve. Therefore, the AS hazard curve with PGA horizontal axis is converted to the AS hazard curve with S_a horizontal axis by using a basic approximate procedure which is presented in Fig. 3.6. It has been shown that structural response can be sensitive to spectral shape (Haselton et al., 2011), but this was not explicitly accounted for in the present study.

It should be noted that the AS hazard curve developed using the procedure described herein is the AS hazard curve conditioned on the occurrence of the previous MS. Therefore, it can be convolved with the AS fragility curve. Fig. 3.7 shows the MS and AS hazard curves for Los Angeles, CA with a spectral acceleration horizontal axis. The natural period of 0.2 seconds was assumed for the two-story building for the purpose of scaling the earthquake records using the flowchart presented in Fig. 3.6.

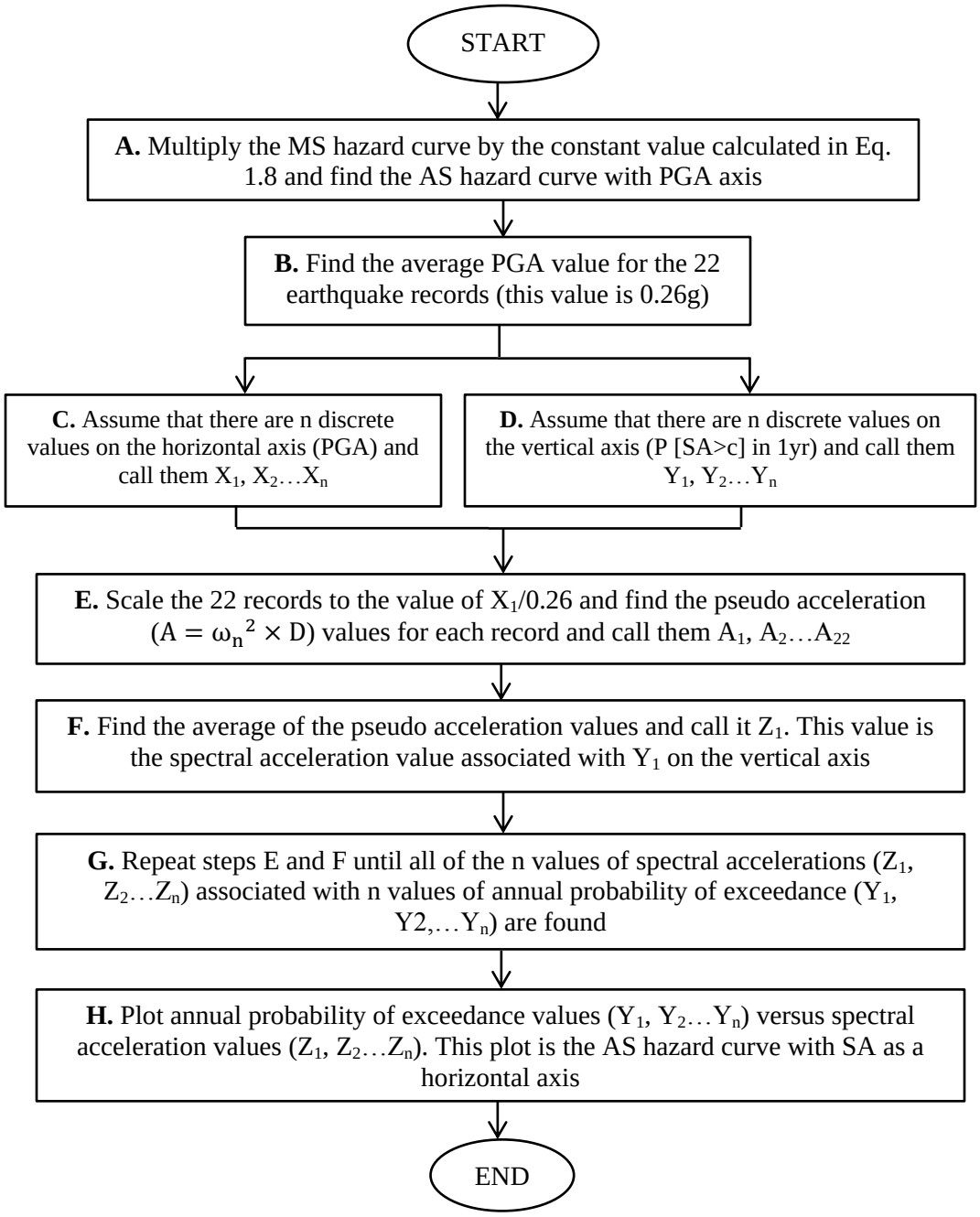

Figure 3.6. Flowchart for converting the horizontal axis from PGA to S_a for AS hazard curve

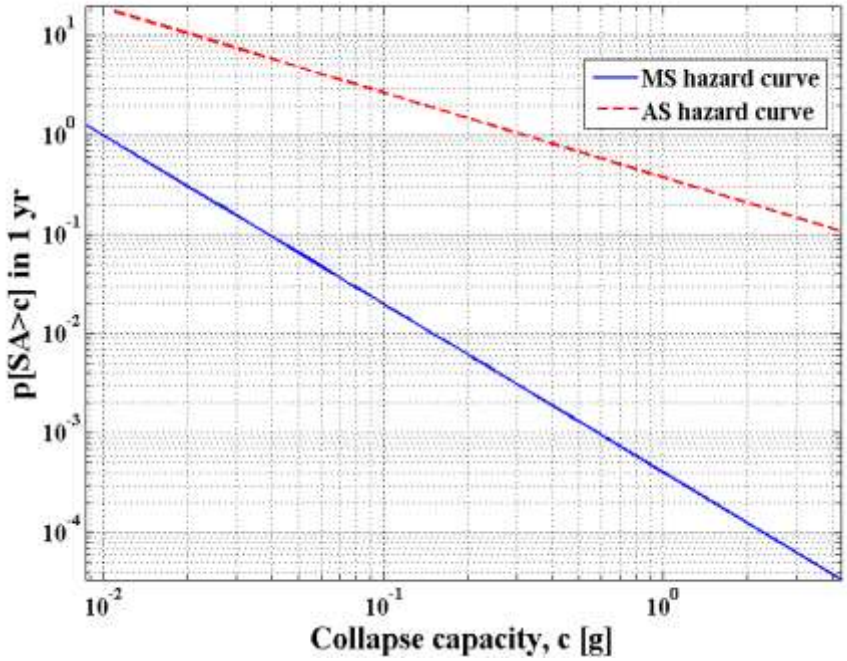

Figure 3.7 MS and AS hazard curves for MS(M8)+AS(M7) scenario

The aftershock IDAs are provided based on AS records scaled to the value computed from the attenuation relationship which is approximately 1.43g for M7 aftershock and natural period of 0.2 seconds for the two-story building. It should be noted that this is a smaller value compared to the value of 2.45g calculated for the MS. The only parameters that have changed in the attenuation relationship for the AS are the magnitude of the AS and the AS parameter, F_{AS}. The AS parameter is zero for the MS and unity for the AS (see Abrahamson and Silva, 2008). The collapse spectral accelerations for the AS fragility curves were provided by assuming 7% inter-story collapse drift similar to the MS case.

The degraded model with residual deformation (degraded stiffness and strength from the MS demand) was used to generate the IDA curves in the AS analysis. It was also assumed that the building comes to rest after the MS, a somewhat obvious but necessary assumption. Therefore, the initial acceleration of the damaged building is zero at the start of the AS analysis

process. A back-to-back IDA is performed on the MS-damaged building. Since the damaged model is used in the AS analysis, the IDA's start from non-zero values which represents the residual deformation in the degraded model under the MS. Fig. 3.8 shows the AS collapse probability for the original model. The AS collapse probability is larger than MS collapse probability presented in Fig. 3.5. Since, in MS+AS case the convolution is based on the fragility for the MS-damaged model and the conditional AS hazard curve.

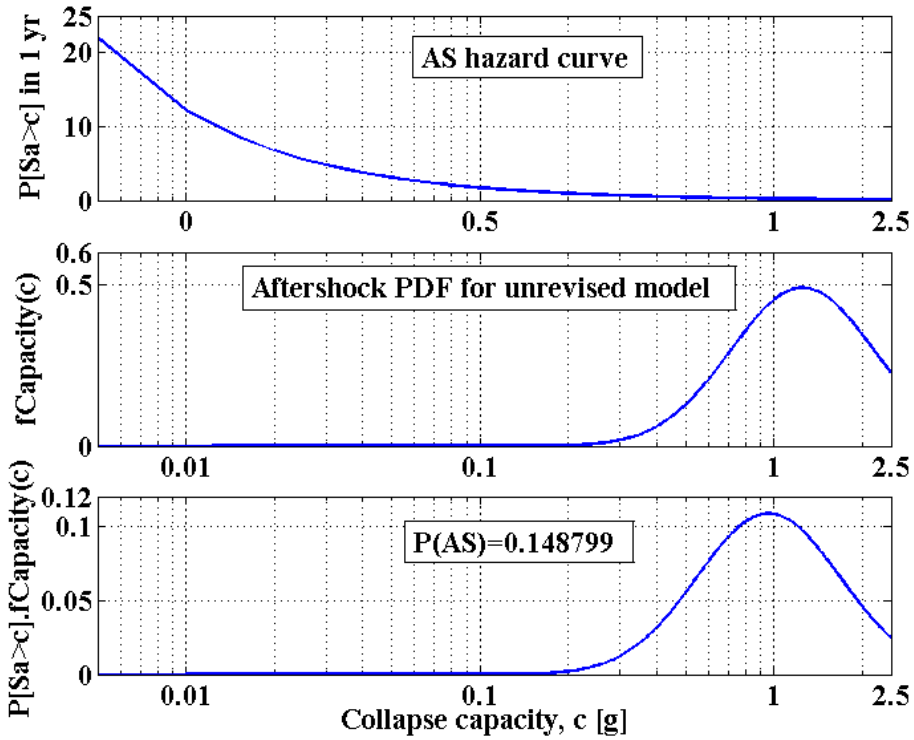

Figure 3.8 Calculation of the risk integral of the probability of collapse in 1 year for the two-story model for AS

Assess deficiency of original model under MS+AS (E)

In order to assess the deficiency of the original model under the MS+AS, the difference between the MS+AS collapse probability, calculated using Eq. 3.1 and the MS collapse probability was computed using the original model. The objective is to revise the building such that its' MS+AS collapse probability is equal to the MS-only collapse probability of the original

model. However, it is obvious that MS+AS collapse probability is higher than MS-only collapse probability for original model. Therefore, the design of original model has deficiency for MS+AS case.

Revise the model by increasing selected hysteretic parameters (F)

In order to obtain the same total collapse probability as in step C for the MS+AS case, the structure would have to be modified in some way since the probability of having a higher seismic demand will increase. In this section, two of the 10 hysteretic parameters in the model described earlier were selected. Specifically, the initial stiffness, K_0 and the resistance force, F_0 were modified in the revised model as follows. A vector of H_i^n with values equal to the ratio of the hysteretic parameters of a revised model to the hysteretic parameters for the original model is introduced. The H_i^n vector can be expressed as:

$$H_i^n = \left\{\frac{(K_0)_{\text{revised}}}{K_0}, \frac{(F_0)_{\text{revised}}}{F_0}, 1, 1, 1, 1, 1, 1, 1, 1\right\}$$

The superscript n indicates the iteration number (since there is clearly not a closed form solution to determine the collapse probability of even this simplified structural model) and the subscript i indicates the story number associated with the hysteretic model for each case. These ratios are set equal to 1 for all hysteretic parameters except for K_0 and F_0. The stiffness and strength parameters were selected for modification since, these hysteretic parameters are not dependent on the remaining 8 parameters in the CUREE model. The revised stiffness and strength parameters are shown by $(K_0)_{\text{revised}}$ and $(F_0)_{\text{revised}}$. Initial stiffness and initial strength are modified in each revision, but the entire vector is included herein. Since the addition of a new and/or supplemental lateral force resisting system could alter the shape of the hysteresis enough

such that additional hysteretic parameters need to be changed in the revised model. The revised K_0 and F_0 parameters for the revised models are provided in Table 3.2. A hypothetical method was used to derive the parameters for each revised model. It is assumed that the stiffness, K_0 and the strength, F_0 increase by 10% and 20% for the first and second revisions of model. It should be noted that the stiffness and strength are increased equally for each revision. For example, the 10% increase was for both the stiffness and strength hysteretic parameters in the first revision. This assumption requires a hysteresis model which has a linear relationship between changes in the stiffness , K_0 and the strength, F_0 parameters (see Fig. 2.9). However, the linear relationship between the stiffness and strength parameters is only an assumption and, it does not necessarily mean that there is a linear relationship between changes in the stiffness strength parameters of the CUREE hysteresis model presented in Fig. 2.9. This is an area that can be further investigated as additional analyses are performed. Based on the revised K_0 and F_0 parameters the H_i^n vectors for two iterations (n = 1, 2) can be calculated. In the presented example, the revision of the initial stiffness and strength parameters is done for the two stories of the model (i= 1, 2).

Table 3.2. Revised parameters of each story

	First Story Parameters		Second Story Parameters	
Model Type	K_0(KN/mm)	F_0(KN)	K_0(KN/mm)	F_0 (KN)
Original model	28.02	333.62	11.38	355.86
First revision	30.82	366.98	12.52	391.44
Second revision	33.62	400.34	13.66	427.03

Calculate the collapse probability for the MS+AS case using the revised model (G)

Similar to section D of the flowchart presented in Fig. 3.1, the MS+AS collapse probability is calculated for the revised model. Table 3.3 shows the calculated MS+AS collapse

probability values which are equal to the area under the curves resulted from the convolution of the fragility curves for the three revised models with the MS+AS hazard curves.

Table 3.3. Collapse probabilities and differences for different models

Model type	P(MS)	P(AS)	P(MS)+P(MS)×P(AS)	Difference (%)
Original model	0.002307	0.148799	0.002650	14.88
First revision	0.002045	0.144964	0.002341	1.49
Second revision	0.001820	0.143265	0.002081	-9.80

Calculate the difference between MS+AS collapse probability of the revised model and MS-only collapse probability of original model (H)

Recall that the structural modification which produces the same collapse probability for MS+AS as the original structural configuration under MS-only is being identified as the acceptable model herein based on the criteria introduced in section I of the flowchart in Fig. 3.1. The calculated difference is presented in Table 3.3.

Check if difference is zero (I)

In order to be able to compare different revised models, the MS collapse probabilities and MS+AS collapse probabilities were calculated for the original and revised models (see Table 3.3). The revision which resulted in the zero difference between the revised model's MS+AS collapse probability and the original model's MS-only collapse probability was considered acceptable.

In Table 3.3, it can be observed that the difference between the collapse probabilities for the original and revised model is the zero for a revised model with 10-20% increase in stiffness and strength parameters. It was assumed that interpolation can be used in order to find an estimate of the revised model which is associated with zero difference. Therefore, a revised

model with about 13.23% increase in stiffness and strength parameters is accepted as the modified model. The values of the stiffness, K_0 and strength, F_0 for the $_0$acceptable revision is presented in Fig. 3.9 with the intersection of the dashed lines in each subplot. Note that the intersection of the dashed lines is associated with the difference percent of zero. Fig. 3.9 presents the collapse probability difference versus the initial stiffness, K_0 and resistance force, F_0 parameters for each story of the building. Each marker point in the subplots is reperesentative of the revisions of the model.

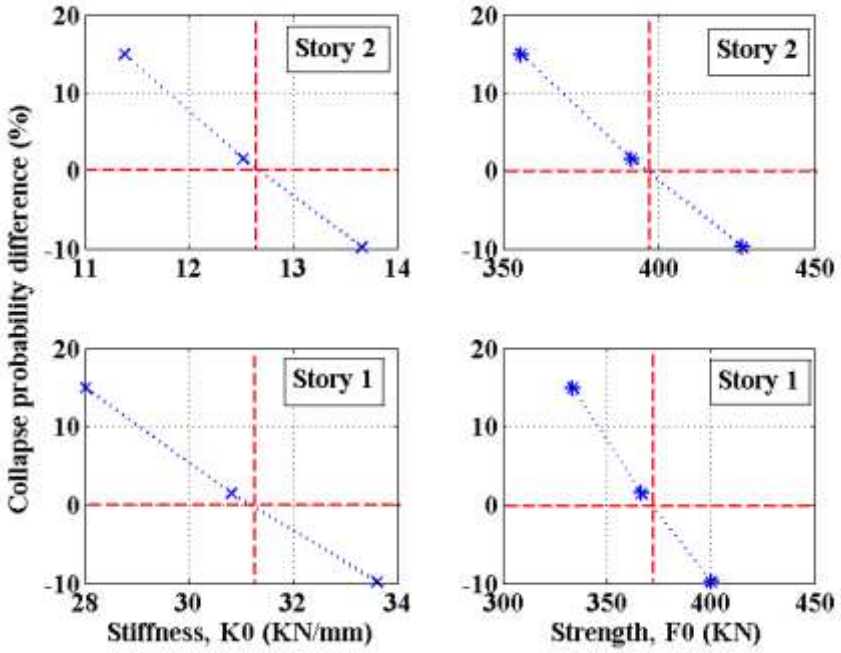

Figure 3.9 Revised hysteresis parameters versus collapse probability difference (Note: In each subplot, the markers from left to right refer to the original model, first and second revision of the model, respectively. The accepted revision of the model is specified with the intersection with zero collapse probability difference)

Accept the revision and increase the hysteresis parameters to account for aftershocks (J)

If the MS+AS collapse probability of the n^{th} revision of the model is equal to the MS-only collapse probability of the original model, then the n^{th} revised model is accepted and the

changes to the story hysteresis needed to account for the effect of aftershocks can be made based on the revised model. For example, the first revision of the model with H_i^n vectors of $H_1^1 = \{1.1, 1.1, 1, 1, 1, 1, 1, 1, 1, 1\}$ and, $H_2^1 = \{1.1, 1.1, 1, 1, 1, 1, 1, 1, 1, 1\}$ for the first and second story, respectively, is the acceptable model. In this example, the computed H_i^n vectors for the acceptable revision are $H_1^2 = H_2^2 = \{1.13, 1.13, 1, 1, 1, 1, 1, 1\}$.

Modify hysteresis parameters to be approximately similar to the parameters of the acceptable revised model (K)

It was observed that approximately a 13% increase in the initial stiffness and resistance force of the first and second stories is needed to account for the AS hazard effect in the scenario presented in this example. The increase in the parameters of the 10-parameter CUREE model such as the initial stiffness, K_0 and resistance force, F_0 can be accounted for by changing the nail patterns in the shear walls installed at each story of the structure. For example, the increase in the initial stiffness parameter of the CUREE model of the first story can be achieved by changing of the nail spacing from 152.4 mm to 76.2 mm (6 to 3 inches) in all of the shear walls. However, the larger increase in the initial stiffness parameter might require the change in the nail spacing from 152.4 mm to 50.8 mm (6 to 2 inches) in some shear walls or 101.6 mm to 76.2 (4 to 3 inches) in all of the shear walls of the associated story of the building.

There are numerous ways to modify a structural design to account for this increased stiffness and strength requirement. Fig. 3.10 presents the shear walls installed in the lower and upper levels of the two-story test structure designed to the 1988 Uniform Building Code (Filiatrault et al., 2010). These walls had nail spacing ranging from 50 mm to 150 mm along the sheathing panel perimeters. First, the shear walls in need of nail pattern modification are selected

for each story but recall there are a large number of possible changes to a design that could provide the new stiffness and strength required, so the changes presented herein represent only one possible design modification scenario. Shear walls E16, I1, E13, I27, E11, E6, E8, E12, E9, E10, E37 and E36 from the first story and shear walls E34X, E34Y, E32 and E26 from second story were selected for modification. Then, the design modification is performed such that the global hysteresis model for each story is as close as possible to the fitted CUREE model with increased parameters for the revised model. In this case, some of the selected single-sheathed standard shear walls for the first story are replaced with 101.6 mm/304.8 mm (4”/12”) double-sheathed and single-sheathed shear walls. Also, the shear wall E12 was replaced with a 76.2 mm/304.8 mm (3”/12”) single-sheathed shear wall for the first story. This modification results in an increase in the parameters of the CUREE model fitted to the backbone curves of the modified model. Table 3.4 shows the increase in the initial stiffness and resistance force for the two stories of the model. It was sought to achieve an approximate increase of 13% in the parameters however, this change resulted in approximately 11% for the first and second story and was felt to be acceptable. Fig. 3.11 shows the comparison between the backbone curves of the original and modified model for the two stories of the model. The backbone curves are derived by pushover analysis of the two-story woodframe building by using a predefined monotonic displacement protocol. The two-story building model is loaded by this protocol and the backbones associated with Y-direction (transverse direction) of the two-story model are derived.

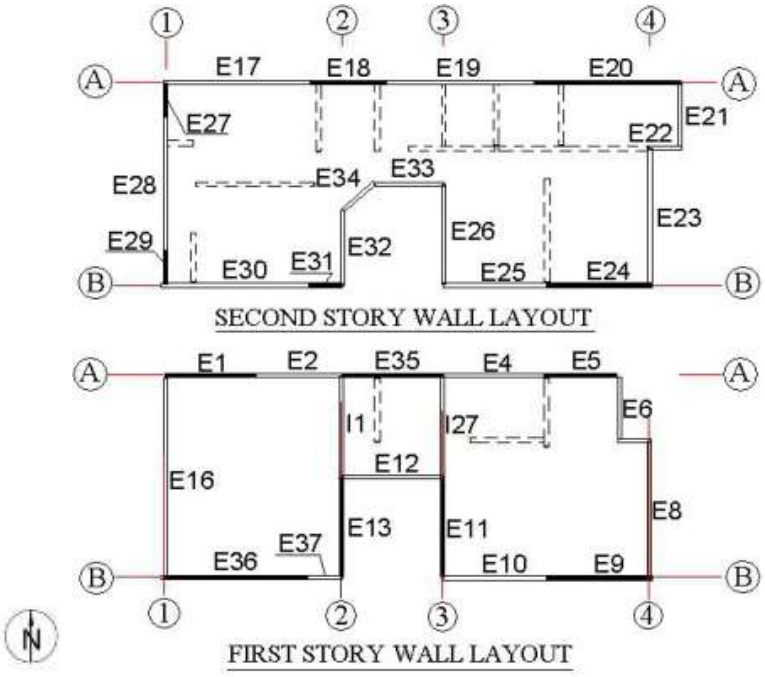

Figure 3.10 Wall elements considered in the numerical model (Excerpted from van de Lindt et al., 2010)

Table 3.4 Increase in hysteresis parameters of the modified model

% of increase	K_0	F_0
Story1	11.22	11.20
Story2	11.24	11.22

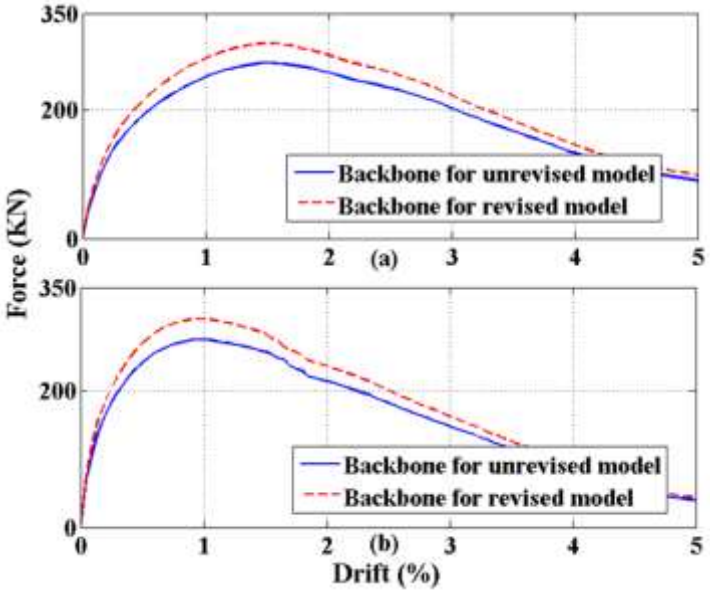

Figure 3.11 Comparison of the backbone curves of the original and modified model, (a) first story (b) second story

3.1.2. Four-Story Example

The numerical four-story building model introduced in section 2.1 was used in this example. The backbone curves for each story are derived by pushover analysis of separate stories of the four-story woodframe building. A predefined monotonic displacement protocol was used for the pushover analysis using the SAPWood software. Fig. 3.12 presents the backbone curves for the four separate stories of the building. The 10 parameter model was fit to the backbone curves using SAPWood software. The parameters of the CUREE model for the four-story building are presented in Table 3.5.

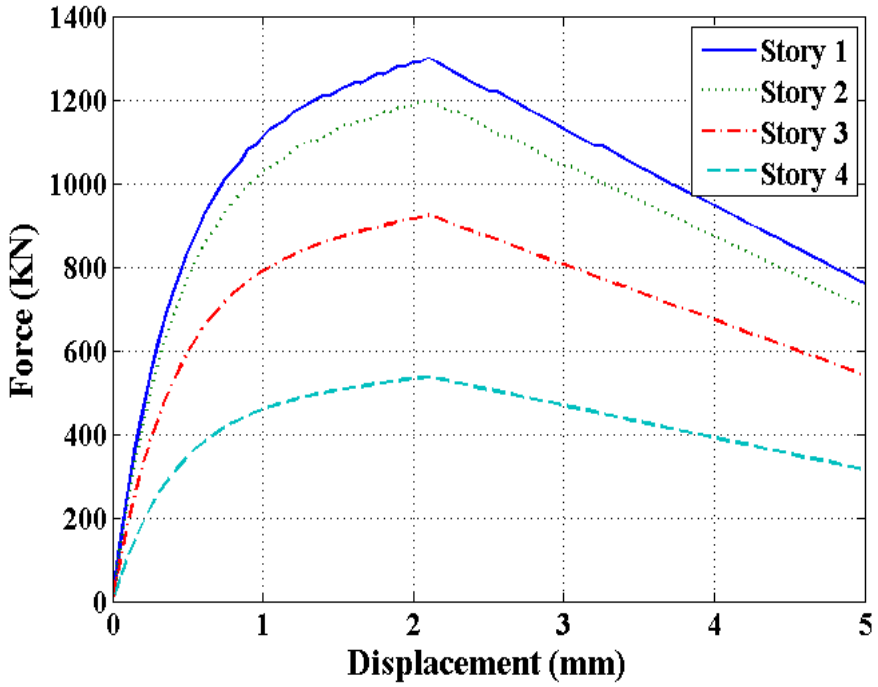

Figure 3.12 Backbones from pushover analysis

Table 3.5. 10 parameters for the CUREE hysteretic model

Parameters (KN, mm)	First story	Second story	Third story	Fourth story
K_0	115.62	104.34	82.66	47.28
F_0	1104.94	1041.77	786	457.72
F_1	194.57	179.57	138.43	80.42
R_1	0.028	0.026	0.028	0.028
R_2	-0.063	-0.064	-0.062	-0.064
R_3	1	1	1	1
R_4	0.02	0.02	0.02	0.02
X_u	52.07	52.07	52.07	52.07
α	0.75	0.75	0.75	0.75
β	1.1	1.1	1.1	1.1

A similar analysis procedure used in the two-story example was used in the four-story building. The computed collapse probabilities are presented in Table 3.6. The collapse probabilities of the mainshock, aftershock and the total collapse probabilities are presented in Table 3.6. The last column of the table shows the difference percent between the total collapse probability and the mainshock collapse probability of the original model. The difference percent computed for the original model and the first revision is presented in Table 3.6. Fig. 3.13 presents the MS fragility for the four-story building. The average collapse spectral acceleration was found to be approximately 2.17g for the four-story model.

Table 3.6. Collapse probabilities and differences for different models

Model type	P(MS)	P(AS)	P(MS)+P(MS) ×P(AS)	Difference (%)
Original model	**0.000453**	0.107113	**0.000502**	10.71
First revision	0.000384	0.103730	**0.000423**	-6.58

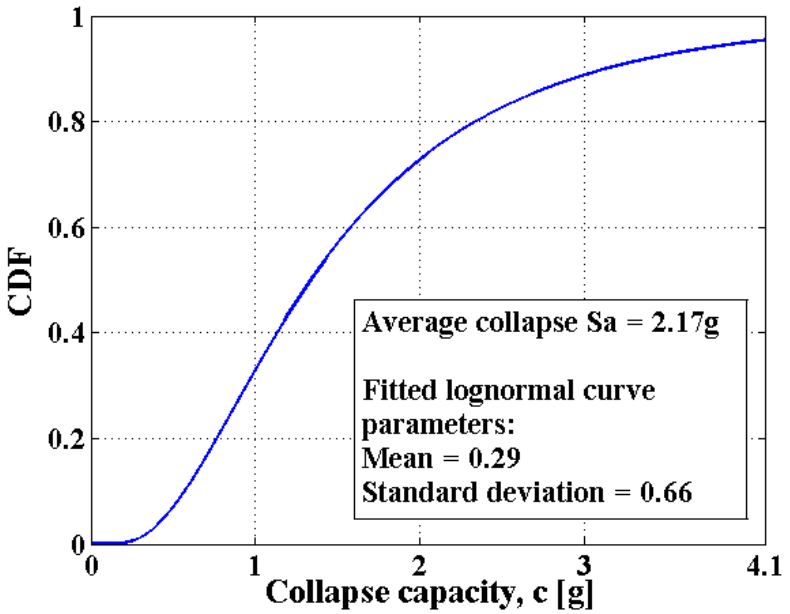

Figure 3.13 MS fragility curve for the numerical model

Similar to the two-story example presented earlier, the increase in the stiffness and strength parameters at the first revision is 10%. As observed in Table 3.6, the acceptable revision of the four-story has an increase in parameters of approximately between 0% and 10%. Since, the zero difference percent occurs between the difference percent computed for the original model and the first revised model. This increase is determined to be approximately 6.2% for the four-story building model.

3.1.3. Six-Story Example

This example uses the test results of the six-story capstone building introduced in section 2.1. This full-scale mid-rise building was tested in order to validate the performance-based seismic design procedure developed as part of the overall NEESWood project. The E-Defense shake table in Miki City, Japan was used for Testing of a building the size of the Capstone test specimen. This shake table is the largest tri-axial shake table in the world with a payload

capacity of 2.5 million pounds and the ability to reproduce the largest historical records from many of the world's largest earthquakes. The facility was built following the 1995 Kobe earthquake and opened in 2004. The NEESWood Capstone test was the first U.S. led test conducted at E-Defense and represents the largest building ever tested at full scale on a shake table.

The architecture of the Capstone test structures was based on a realistic multi-family apartment building or condominium that might be typical of an urban infill building in Northern or Southern California. The building was seven stories total: six-stories of light-frame wood containing twenty-three living units and a bottom story Steel Special Moment Frame (SMF) at level 1. The building was tested in two phases. Phase 1 was testing the seven-story mixed-use building. In phase 2, the SMF was locked down to become an extension of the shake table and the six-story light-frame wood building was tested. In this example, the test results from phase 2 were used. Thus, it was assumed that the building is behaving as a six-story building with the first story being locked down. One set of tri-axial historical ground motions were used for all seismic tests: an ordinary ground motion recorded during the Northridge earthquake at the Canoga Park recording station was used. The ground motion was scaled to represent a frequent earthquake having a probability of exceedance of 50% in 50 years, a Design Basis Earthquake (DBE) having a probability of exceedance of 10% in 50 years (10%/50 years), and a Maximum Credible Earthquake (MCE) having a probability of exceedance of 2% in 50 years (2%/ 50 years), or a return period of 2475 years. The response of the six-story test building under MCE level earthquake was used in the example presented in this section. The performance of the building was very well at MCE level and, it sustained only gypsum wall board damage without any structural damage. This level of performance satisfied the performance expectations outlined

during the design process. Therefore, the NEESWood PBSD philosophy has been validated to the extent a single test can. The hysteresis data from the response of the test building at MCE level Northridge-Canoga Park earthquake is presented in Fig. 3.14. The CUREE model was fitted to these test data at each story of the building. The fitted CUREE model is also presented in Fig. 3.14. Table 3.7 presents 10 parameters of the fitted CUREE model to the hysteresis loop of each story.

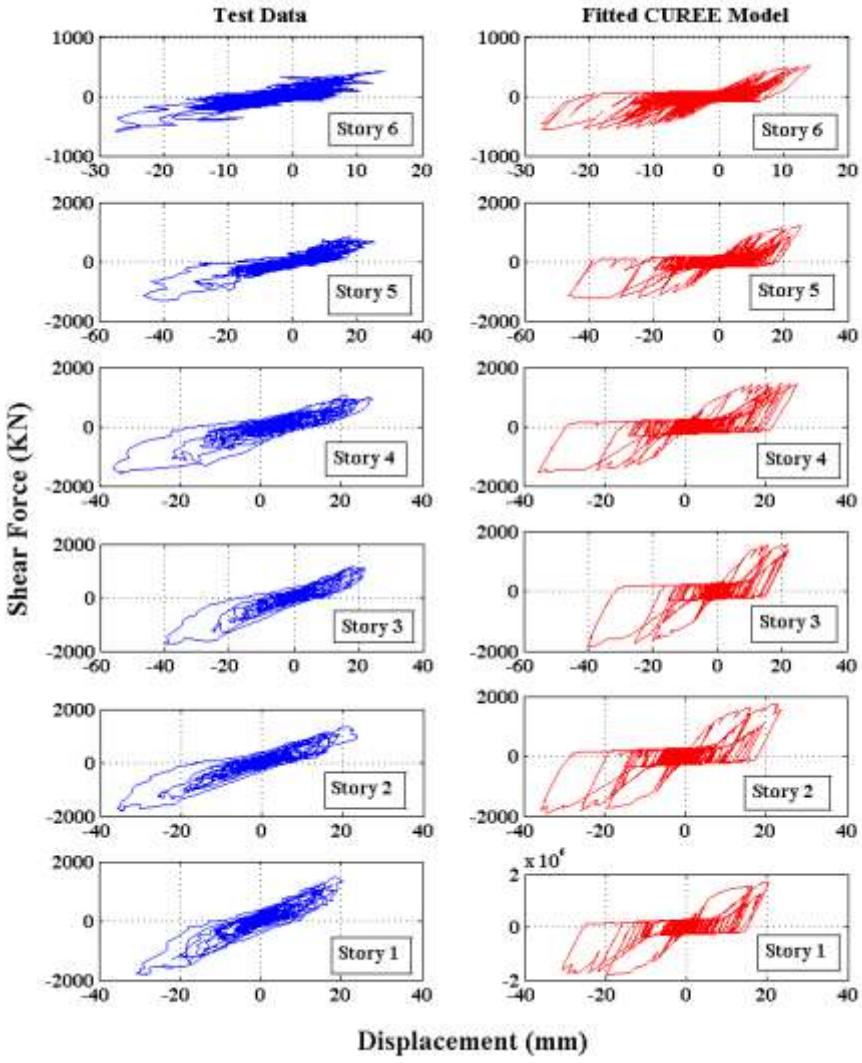

Figure 3.14 Response of the test building at MCE level Northridge-Canoga Park earthquake versus the CUREE model fitted to the hysteresis loops

Table 3.7. 10 parameters for the CUREE hysteretic model

Parameters (KN, mm)	First story	Second story	Third story	Fourth story	Fifth story	Sixth story
K_0	308.22	264.44	217.16	229.42	161.47	109.1
F_0	1641.39	1619.15	1547.98	1436.78	1169.88	533.79
F_1	273.57	270.01	258.04	239.23	194.83	89.1
R_1	0.01	0.01	0.01	0.01	0.01	0.01
R_2	-0.08	-0.08	-0.08	-0.08	-0.08	-0.08
R_3	1	1	1	1	1	1
R_4	0.02	0.02	0.02	0.02	0.02	0.02
X_u	29.54	34.01	39.55	34.7	40.21	27.2
α	0.75	0.75	0.75	0.75	0.75	0.75
β	1.1	1.1	1.1	1.1	1.1	1.1

A similar procedure presented earlier for the two-story example was followed in this section. The revisions also were the same as the two-story example. The MS fragility curve is presented in Fig. 3.15. The average collapse spectral acceleration was found to be approximately 1.77g for the six-story model. The similar procedure presented in section 2.5 was used to compute the collapse probabilities in this example. Mainshock and aftershock collapse probabilities for the unrevised six-story model are presented in Fig. 3.16 and Fig. 3.17.

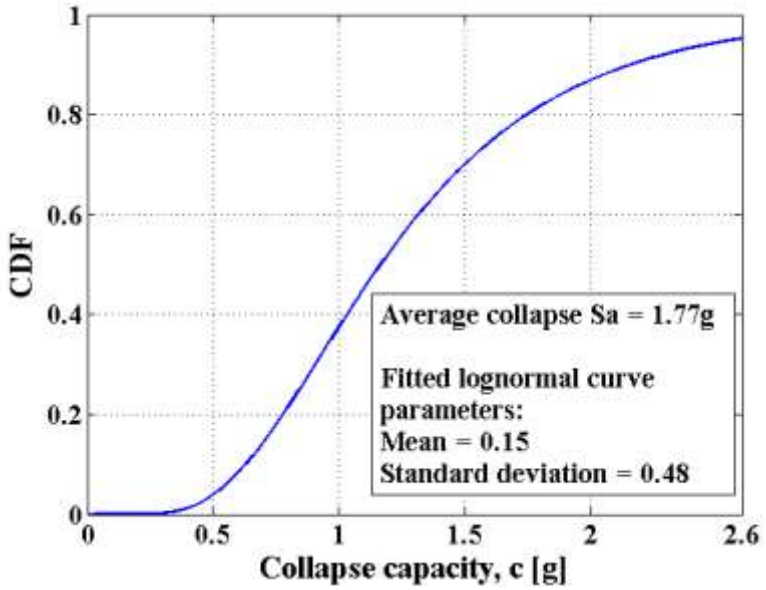

Figure 3.15 MS fragility curve for the numerical model

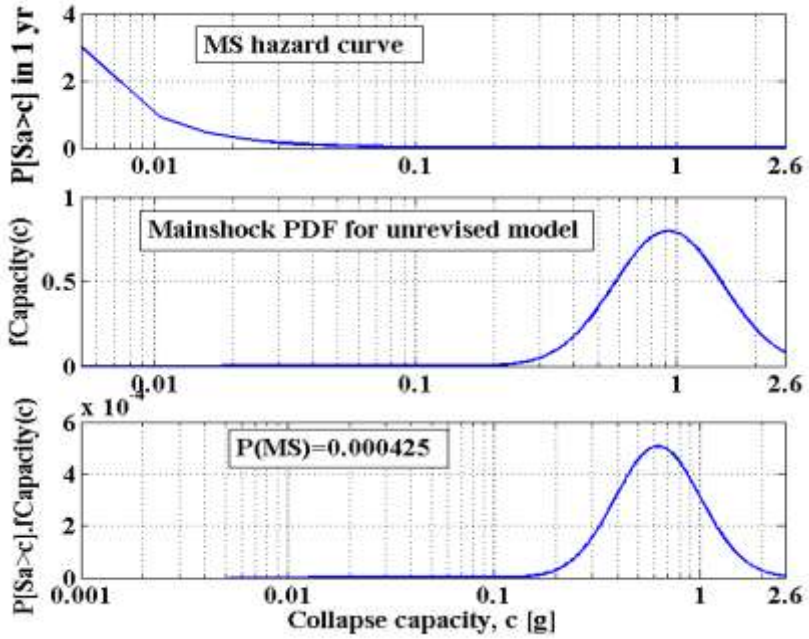

Figure 3.16 Calculation of the risk integral of the probability of collapse in 1 year for the six-story model for MS

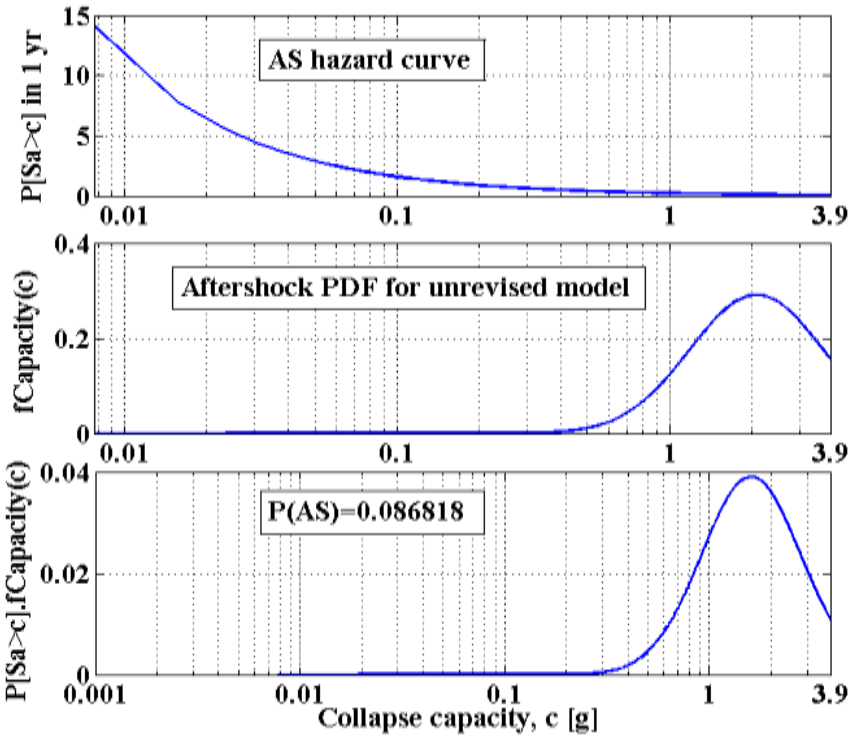

Figure 3.17 Calculation of the risk integral of the probability of collapse in 1 year for the six-story model for AS

The collapse probabilities were calculated and presented in Table 3.8 for the six-story model. As observed in Table 3.8, the collapse probabilities calculated for the revised model are generally smaller than the values for the original model.

Table 3.8. Collapse probabilities and differences for different models

Model type	P(MS)	P(AS)	P(MS)+P(MS) ×P(AS)	Difference (%)
Original model	0.000425	0.086818	0.000462	8.68
First revision	0.000325	0.08088	0.000351	-17.38

The collapse probabilities presented in Table 3.8 show that the acceptable revision has a parameter increase between 0% and 10%. The interpolated value for percent of increase in

hysteresis parameters of K_0 and F_0 is found to be about 3.5% for the six-story Capstone test building.

3.1.4. Summary

In this chapter, a methodology was presented to quantify the changes in structural design that would be needed to account for AS hazard. To achieve this objective, the calculated MS collapse probability for a building model was set equal to the total collapse probability (MS+AS) of the model with modified structural design requirements. Structural design modifications such as changes in the nail patterns of the shear walls in each story can then be made for the MS+AS case in order to get the same total collapse probability as the MS-only case.

Based on the methodology presented in this chapter, it was observed that approximately 13%, 6% and 3.5% increase in the initial stiffness and restoring force is needed to account for AS effect for the two-, four- and six-story buildings presented in the examples. These increases are specific to a scenario with MS(M8)+AS(M7). Although these percentages are specific to this scenario, it can be observed that the stiffness and strength requirement is not insignificant and, if accounted for in design, would result in an increase in building cost. Further, it should also be noted that only one building type was examined and that multiple building types such as steel and concrete buildings should be examined to generalize the conclusions.

3.2. Quantifying the Design Changes Needed to Account for Aftershock Hazard in Direct Displacement Design (DDD) Method

The objective of this section is to develop a methodology that allows one to quantify the change that would be needed in the design drift of a building to account for aftershock (AS)

hazard when applying Direct Displacement Design (DDD). The target is for the modified building to have the same collapse probability for the combined mainshock and aftershock hazard as the original building has for only the mainshock. The different probabilities of collapse are computed using a combination of seismic fragility results convolved with two different types of hazard curves, namely a typical hazard curve and an aftershock hazard curve. An illustrative example is presented for a four-story woodframe building and the design drift adjustment factors needed for the procedure were calculated.

Direct Displacement-Based Design (DDD) is one of the Performance-Based Engineering (PBE) methods. In this method, inter-story drift defines the performance level of a structure and displacement is considered as an engineering demand parameter that correlates well with both structural and non-structural damage. More details about DDD approach can be found in section 1.3 of this dissertation.

3.2.1. Analysis Methodology

Table 3.9 presents the steps of the analysis methodology that were used in this section.

Table 3.9. Steps of the Analysis Methodology

Step 1: Design building (A) using DDD method and calibrate the n-DOF model
Step 2: Use a suite of earthquake records to compute the building (A) mainshock fragility
Step 3: Convolve the mainshock fragility with the annual hazard curve for the mainshock to obtain the probability of collapse under mainshock, P(MS)
Step 4: Use the simulated MS+AS earthquake sequences to compute the building (A) aftershock fragility
Step 5: Develop the aftershock seismic hazard curve
Step 6: Convolve the building fragility with the aftershock seismic hazard curve to obtain the probability of collapse under aftershock to obtain the aftershock collapse probability, P(AS) for the building that survived the MCE level mainshock
Step 7: Compute the MS+AS collapse probability, P(MS)+P(AS∩MS)
Step 8: Find the difference between MS+AS collapse probability, P(MS) + P(AS∩MS) and mainshock collapse probability, P(MS)
Step 9: Design a new building, (B) for a lower design displacement limit using DDD and calibrate the n-DOF model
Step 10: Repeat steps 2 to 8 for building (B)
Step 11: Find the difference between MS+AS collapse probability of building (B) and mainshock collapse probability of building (A)
Step 12: Repeat step 10 to 13 until the difference calculated in step 12 is equal or less than zero
Step 13: Interpolate between the differences (calculated in steps 9 and 12) and the design base shears of buildings A and B (calculated in steps 1 and 10) in order to find the design base shear needed to account for the aftershock hazard
Step 14: Find the adjusted design drift limit in DDD method which results in the design base shear computed in step 14

In step 1, a building is designed using the simplified DDD approach presented by Pang et al. (2010) for a specific design drift, a probability of non-exceedance (P_{NE}) and a performance level (see section 1.3). The design consists of computing the required story shears and then selecting the seismic force resisting elements by summing the hysteretic backbones to achieve

these story shears at the target drift. Next, a representative mathematical model of sufficient enough complexity is developed such that the nonlinear time history response of the building to earthquakes can be determined. The building was simplified as a shear building model in this section, but a more complex model could be used if desired. Once the backbone curves are determined for each story, a hysteretic model is fit to each backbone curve (see section 2.2). In the next step (2), a suite of earthquake ground motions (see Table 2.3) is used to represent the record-to-record variation representing the total earthquake variability for the MS. Then, the mainshock fragility is obtained by following a procedure similar to that presented earlier in section 2.4. In step 3 the MS-only fragility curve is convolved with the location-specific MS hazard curve to obtain the probability of collapse of the building under mainshock (P(MS)). See section 2.5 for more details.

The MS+AS sequences simulated using the procedure presented in section 2.4 are used to generate the aftershock fragilities in step 4 of Table 3.9. In order to compute the aftershock collapse probability, P(AS), the AS fragility curve is convolved with the aftershock hazard curve in step 7. See section 2.5 and 3.1.1(D) for details about the aftershock hazard curve derivation and convolution of the fragility curve with the hazard curve. In step 8, the MS+AS collapse probability is calculated using Eq. 3.1. The difference between the MS+AS collapse probability, computed in the previous step and the MS collapse probability (see step 3) was calculated in step 9. The objective is to modify the design of the building (A) such that the difference between the collapse probabilities calculated in step 9 is zero. Therefore, a new building (B) was designed for a design drift smaller than the original building (A) in step 10 and a n-DOF model was calibrated to building (B). Steps 2 to 8 of Table 3.9 were repeated for building (B) in order to compute the MS+AS collapse probability. Once the MS+AS collapse probability is calculated for building

(B), the difference between this probability and the MS collapse probability of building A is computed in step 12. If the difference calculated in step 12 is equal or less than zero then, building (B) with the smaller design drift is acceptable. The design base shear needed can be computed by interpolation between the collapse probability differences (calculated in steps 9 and 12) and the design base shears of buildings A and B which were calculated in steps 1 and 10 (see step 14 in Table 3.9).

After determining the design base shear needed which accounts for the aftershock hazard in step 14, the adjusted design drift can be found by iterating different design drifts smaller than the design drift of building A in DDD method (see step 15). This iteration in the DDD method continues until obtaining a design base shear approximately equal to the needed design base shear value calculated in step 14. However, if the difference in collapse probabilities calculated in step 12 was not equal or less than zero, steps 10 to 13 would be repeated and another building (e.g. building C) with design drift smaller than the design drift of building B would be used to compute the MS+AS collapse probability.

3.2.2. Illustrative Example

A 4-story woodframe building is designed by using the simplified DDD method using design drifts of 4%, 3%, 2% and 1%. It is assumed that the building is located in Los Angeles, CA. See section 2.1 for more details about the 4-story woodframe building. A probability of non-exceedance (P_{NE}) of 50% is used in the DDD approach. Seismic design category is assumed to be D for Los Angeles and spectral values are determined following the ASCE 7-10 standard. Mapped values for short spectral acceleration (S_s) and one-second spectral acceleration (S_1) are 2.448g and 0.858g based on ASCE 7-10. These values are obtained from USGS website (see

http://earthquake.usgs.gov/designmaps/us/application.php). Soil category for Los Angeles is assumed to be D therefore, site coefficients are found to be F_a=1 and F_v=1.5 based on ASCE/SEI 7-05, Table 11.4-1 and Table 11.4-2. The Maximum Credible Earthquake (MCE) is calculated based on ASCE/SEI 7-05 section 11.4 to be equal to 2.448g for the short spectral acceleration ($S_{MS} = S_s \times F_a = 2.448 \times 1 = 2.448$) and, 1.288g for one second spectral acceleration ($S_{M1} = S_1 \times F_v = 0.858 \times 1.5 = 1.288$). More details can be found in Appendix A.

Using the above spectral accelerations, base shear demands are calculated by simplified DDD for four different design drifts. Calculated base shear values are presented in Table 3.10. The change needed in design due to aftershock hazard was calculated for three different cases where the design drift of the original building is 4%, 3% and 2%.

Table 3.10. Design base shears calculated using DDD method

Story	Design Drift (%)	Vs(KN)	Design Drift (%)	Vs(KN)	Design Drift (%)	Vs(KN)	Design Drift (%)	Vs(KN)
4	4	512	3	747	2	1219	1	1824
3		894		1308		2135		3194
2		1152		1681		2749		4106
1		1277		1868		3051		4559

The design points versus backbone curves for the four stories of the buildings designed for 4%, 3%, 2% and 1% design drifts can be found in Appendix C of this dissertation. In order for the building designed by simplified DDD approach to be satisfactory, the design points should be below the backbone curves for each story of the woodframe building. This criterion is satisfied and each story's design point falls below the associated backbone curve.

By following the steps presented in Table 3.9, the procedure was completed and the results were provided in Tables 3.11 to 16 for the scenario with MCE level mainshock. The results presented in tables were for a single MS+AS scenario with M8 mainshock and M7 aftershock. The spectral acceleration values calculated using the Abrahamson and Silva NGA (2008) relationship at the natural period of the building (Tn=0.5s) are 1.424g and 0.773g for the mainshock and aftershock, respectively. These values were used in scaling procedure used in simulation of MS+AS records (see section 2.4).

Each building is calibrated with a 4-DOF numerical model with a lumped mass and a CUREE model for each story based on the illustration in section 2.2. The 10 parameters for the fitted CUREE model used in the analyses of the four numerical models throughout this study are presented in Appendix D. These parameters were obtained by fitting the CUREE model to the backbone curves of each story of the buildings designed using DDD approach. Fig. 3.18 shows a backbone curve for the first story of the building designed for a 4% design drift and non-exceedance probability (P_{NE}) of 50%. See Appendix A for design details of the building.

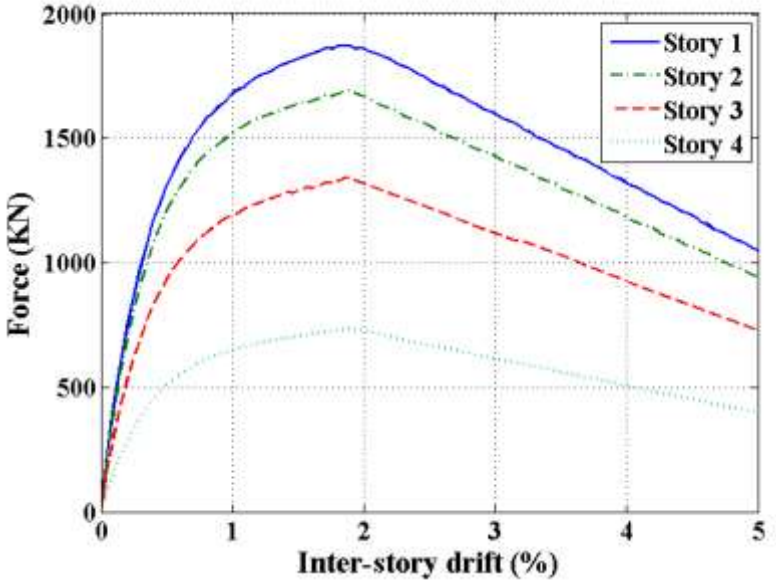

Figure 3.18 Backbone curves for the four-story building designed for 4% design drift and P_{NE}=50%

Fig. 3.19 presents the Cumulative Distribution Function (CDF) form of a fragility curve for a four-story building designed for 4% design drift and P_{NE} of 50% in the illustrative example. The fragility curve shows probability of exceedance ($P[S_a>c]$) versus collapse capacity (c) parameter which in this study is selected as spectral acceleration (S_a[g]) was developed for the mainshock. A lognormal curve is fitted to data points generated from the analysis and the parameters for the lognormal fit are presented in Fig. 3.19. The average collapse spectral acceleration is 2.62g for the four-story building.

The MS and AS hazard curves can be generated based on the procedure presented in section 2.5. Note that the natural period of 0.5 seconds was used for generating the AS hazard curve for the four-story building. Therefore, the AS hazard curve presented in Fig. 3.20 is slightly different from the AS hazard curve in Fig. 3.7 since the previous one was generated for the two-story building with natural period of 0.2 seconds.

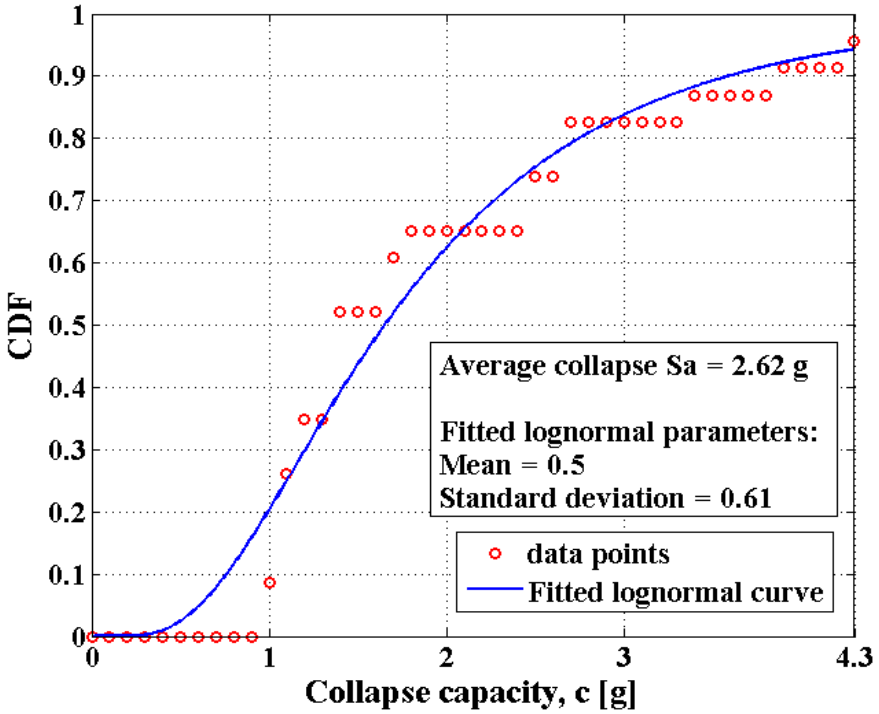

Figure 3.19 Mainshock fragility curve for the building designed for 4% design drift

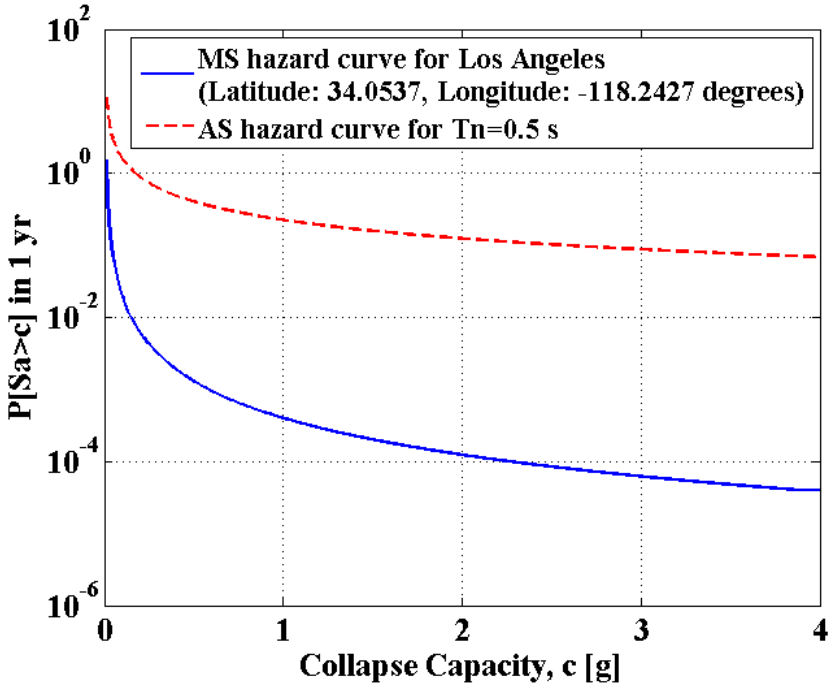

Figure 3.20 Mainshock hazard curve for Los Angeles, CA vs. the aftershock hazard curve for the 4-story building

Once the PDF form of the fragility curve and the seismic hazard curve are known, the fragility can be convolved with the site-specific seismic hazard curve to determine the probability of collapse when the structure is subjected to a MS. This represents a typical scenario in which the probability of collapse might allow one to determine if a design meets a particular collapse probability. See section 2.5 for more details about the convolution of the fragility curve and hazard curve. Fig. 3.21 presents an example of a collapse probability for the MS (P(MS)) computed based on Eq. 1.8.

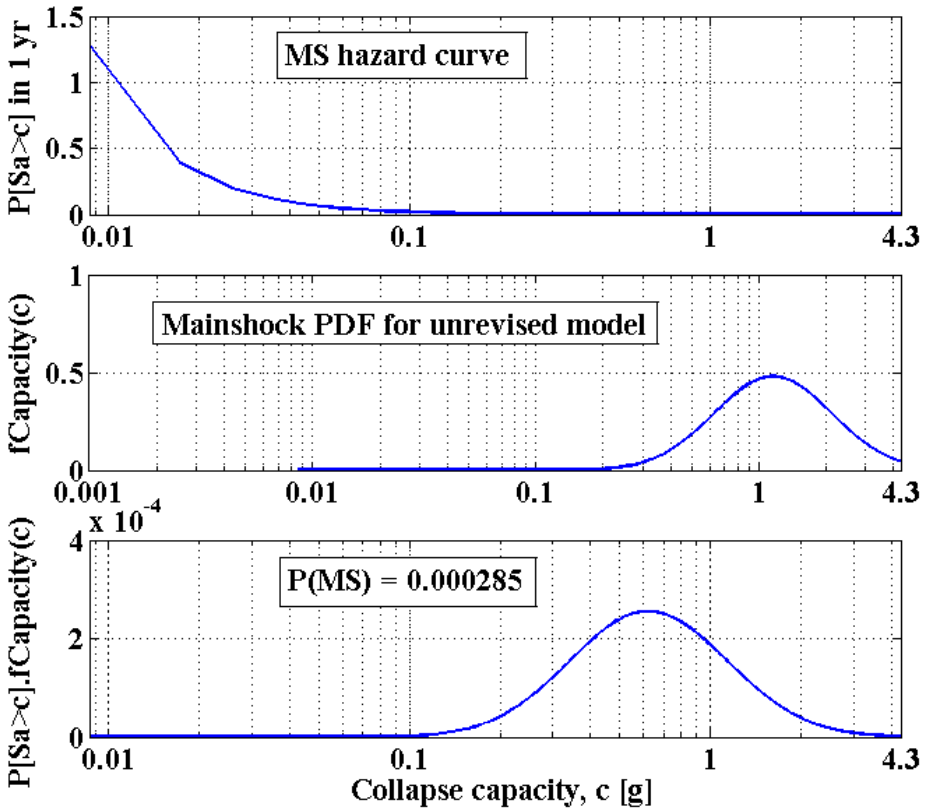

Figure 3.21 Calculation of the MS collapse probability of the 4-story model

Fig. 3.22 presents the CDF form of the AS fragility curve for the building designed for 4% design drift. It was also assumed that a MCE level MS scaled to 2.4g for Los Angeles, CA is applied on the building before the occurrence of the aftershocks. The value of collapse spectral

acceleration and the parameters of the lognormal curve were also presented in Fig. 3.22. The average collapse S_a is 0.88g for the aftershock analysis.

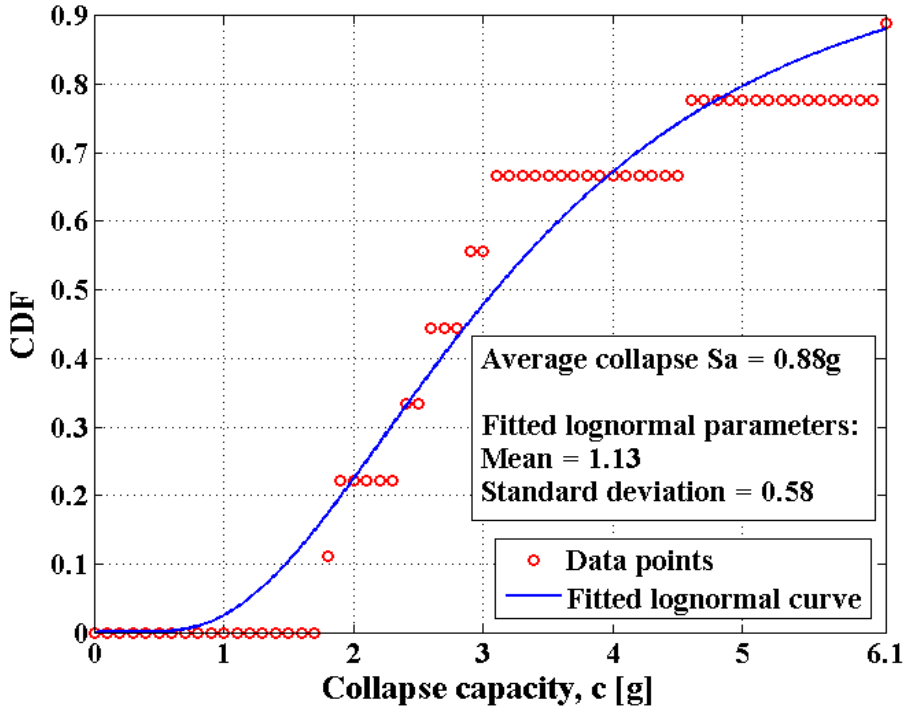

Figure 3.22 Aftershock fragility curve for the building designed for 4% design drift

Also, it should be noted that the AS fragility curve produced by step 4 of the procedure presented in Table 3.9 was conditioned on the occurrence of the previous MS. Therefore, it must be convolved with the conditional AS hazard curve presented in Fig. 3.20. Therefore, in step 7 of the procedure the AS fragility curve is convolved with the AS hazard curve and the collapse probability for AS case (P(AS)) is calculated. Fig. 3.23 shows the AS collapse probability for the numerical model. In the end, the total collapse probability for the MS+AS was computed using Eq. 3.1. Table 3.11 presents the mainshock, aftershock and total collapse probabilities calculated for different four-story buildings with 4%, 3%, 2% and 1% design drift. The difference of the total collapse probability with the MS-only collapse probability is presented in the last column of

Table 3.11. This difference percent is computed using the total collapse probability and the mainshock collapse probability of the original model which are shown in bold in Table 3.11.

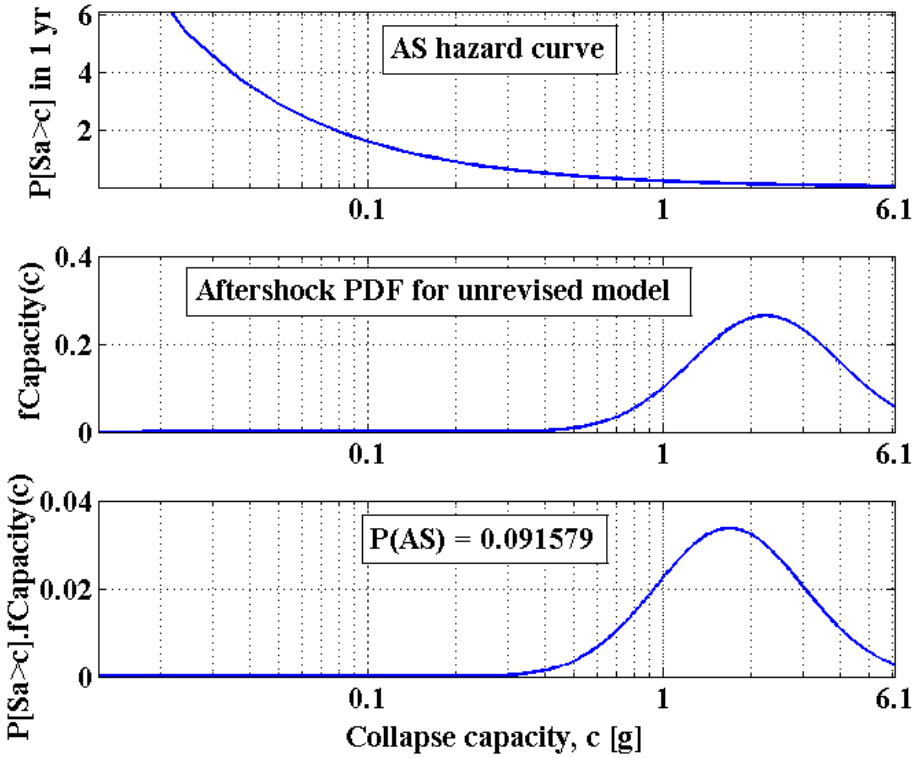

Figure 3.23 Calculation of the AS collapse probability of the 4% DDD 4-story model with MCE level MS

Table 3.11 Collapse probabilities and differences for buildings with different design drifts

Model type	Design drift	P(MS)	P(AS)	P(MS)+P(MS)×P(AS)	Difference (%)
Original	4%	**0.000285**	0.091579	0.000311	9.16
Modified	3%	0.00024051	0.086547	0.000261	-8.37
Original	3%	**0.000241**	0.086547	0.000261	-8.37
Modified	2%	0.00018258	0.085638	0.000198	-17.59
Original	2%	**0.000183**	0.085638	0.000198	-17.59
Modified	1%	7.2854E-05	0.049071	7.64E-05	-58.14

Step 2 and 8 of the procedure should be repeated for the stronger model designed for 3% drift in step 5. The difference of the total collapse probability of the 3% DDD building with the

MS-only collapse probability of the 4% DDD building (original building) is approximately -8.37% which means that these two collapse probabilities are equal somewhere between the 3%DDD and 4% DDD buildings. It is assumed that interpolation between the values of the difference between the total collapse probability of the revised model and MS collapse probability of the original model is accurate. The exact base shear adjustment factor (X_v) associated with the 0% difference between the total collapse probability of the revised model and the MS collapse probability of the original model was determined by interpolation using the difference percent of the two cases. The interpolated base shear that results in 0% difference between collapse probabilities is 1586KN in this case (see Table 3.12). This value results in the base shear adjustment factor (X_v) equal to 1586/1277=1.24. The value of 1277 is the design base shear of the first story for the 4%DDD 4-story building (see Table 3.10). Table 3.12 shows the interpolated design base shear and base shear adjustment factors for the four-story building with different design drifts. As observed in Table 3.12, the base shear adjustment factor, X_v is 1.21 and 1.06 for original models designed for 3% and 2% drift, respectively. However, if the two values of total probability of collapse differ, then the building is not acceptable and must be re-designed to be stronger than before. In this case, steps 10 to 13 are repeated until the two values of collapse probability are equal.

Table 3.12. Interpolated design base shear of the first story and base shear adjustment factors for buildings with different design drifts

Model type	Design drift	Design base shear needed for the first story(KN)	Base shear adjustment factor(Xv)
Original	4%	1586	1.24
Modified	3%		
Original	3%	2258	1.21
Modified	2%		
Original	2%	3246	1.06
Modified	1%		

The design base shear needed for the first story is presented in Table 3.12. These values were used to find the associated adjusted design drift of the acceptable model by iterations using DDD method. The design base shear is calculated using DDD approach for different design drifts less than that of the original model e.g. 3.1%, 3.2% …3.9% for the original model with 4% design drift. The iterations continue until obtaining an approximately equal design base shear to the one calculated above by interpolation. The design drifts that resulted in an equal design base shear to the interpolated value is defined as the adjusted design drift, denoted as X_d. For instance, the adjusted design drift that result in the interpolated base shear of 1586KN (see Table 3.12) is approximately equal to 3.22% (see Table 3.13). A design drift adjustment factors (X_d) was defined as the ratio of the adjusted drift limit and the original drift limit (e.g. X_d = 3.22/4= 0.81). Finally, the values of adjusted design drift computed by iterations in DDD method and associated design drift adjustment factors are presented in Table 3.13.

Table 3.13. Adjusted design drift and design drift adjustment factors for buildings with different design drifts

Model type	Design drift	Adjusted design drift (%)	Design drift adjustment factor (X_d)
Original	4%	3.22	0.81
Modified	3%		
Original	3%	2.48	0.83
Modified	2%		
Original	2%	1.88	0.94
Modified	1%		

As observed in Table 3.13, the adjusted design drift is 3.22%, 2.48% and 1.88% for the original model with 4%, 3% and 2% design drifts, respectively. The design drift adjustment factors are smaller for the stronger building which is designed for a smaller design drift. For example, X_d is 0.94 for the original model designed for 2% drift, however, the design drift adjustment factor is 0.81 for the building with 4% design drift. This means that the stronger

building which is designed for a smaller design drift needs less change in design due to the effect of aftershock hazard.

CHAPTER FOUR: SENSITIVITY ANALYSIS OF NEEDED CHANGE IN DESIGN DUE TO THE AFTERSHOCK EFFECTS

This chapter presents a comprehensive sensitivity analysis of the change needed in design due to the aftershock effects. More specifically, the change needed in design base shear is investigated. Recall from section 3.2 that a design adjustment factor was introduced for quantifying the design changes needed. In this chapter sensitivity of the base shear adjustment factor, Xv, was examined with respect to several parameters using the Direct Displacement Design (DDD) approach (Pang et al., 2010). These parameters include the number of stories for the building, the location of the building, and the design drift for the building used within the DDD approach. Also, the sensitivity of the base shear adjustment factor, X_v, was investigated using different mainshock plus aftershock (MS+AS) scenarios. The effect of mainshock level including the Maximum Considered Earthquake (MCE) and Design Basis Earthquake (DBE) level X_v is also studied in this chapter. The duration of interest, T, and the elapsed time from the initial mainshock, t can change the computed aftershock hazard and thus the base shear adjustment factor, X_v. Therefore, the effects of these factors were also studied. The collapse probabilities were computed for different damage states (DS) for the MS-only and MS+AS case. The objective was to show the aftershock effect on the collapse probabilities associated with different damage states.

4.1. Effect of Number of Stories on Base Shear Adjustment Factor, X_v

In order to quantify the needed change in design base shear, a base shear adjustment factor denoted as X_v was defined in section 3.2. The base shear adjustment factor was calculated

for the two-, four- and six-story buildings using a similar procedure presented in section 3.2. These buildings were designed for a 4% design drift using DDD at a 50% probability of non-exceedance (P_{NE}) for that design drift. Design base shears and the backbone curves for each story of the buildings are presented in Appendix B and C, respectively. The fitted CUREE hysteretic parameters used in the building model are also presented in Appendix D.

Fig. 4.1 presents the mainshock collapse fragility curves for each building using the methodology presented earlier in Chapter Two. Earthquakes having a magnitude of M8 and M7 were used as the mainshock plus aftershock (MS+AS) scenario, respectively, for the two-, four- and six-story buildings. The location of the buildings is assumed to be Los Angeles, CA and, the associated hazard curves were used in the calculation of the base shear adjustment factors.

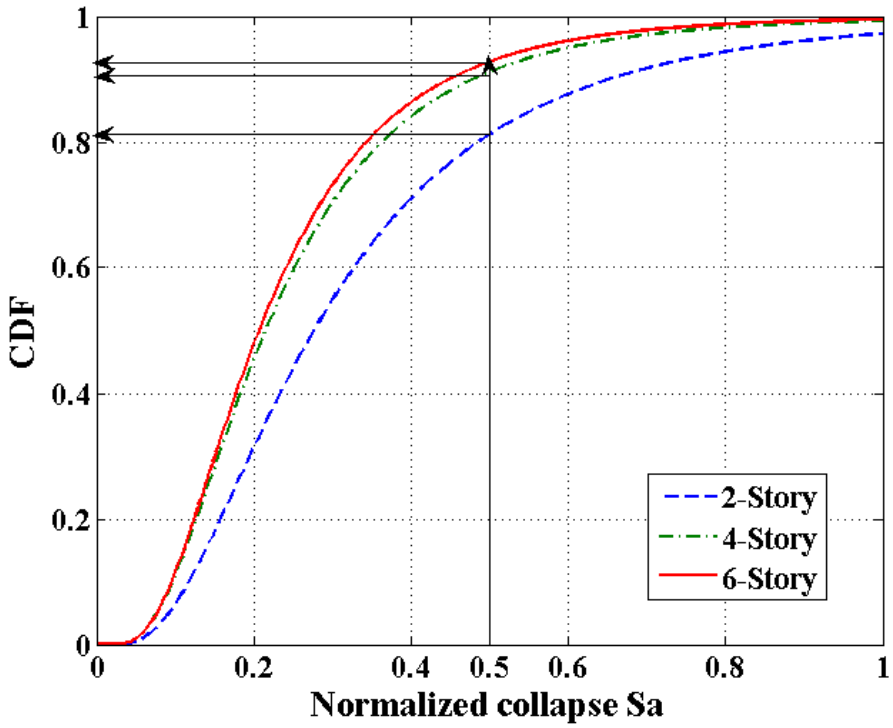

Figure 4.1. Mainshock collapse fragility curves for different buildings computed using Non-Linear Time History Analysis (NLTHA)

As presented in Fig. 4.1, the collapse fragility curve has a higher value for the six-story and the four-story buildings compared to the two-story building. For example, at a normalized spectral acceleration (S_a) of 0.5, the collapse fragility curve is approximately equal to 0.81, 0.9 and 0.92 for the two-, four- and six-story buildings, respectively. Following the procedure presented in section 3.2, the total collapse probabilities and the percent difference when aftershock is included versus excluded were computed for each building. Table 4.1 presents the total collapse probabilities and differences for the two-, four- and six-story buildings. Similar to section 3.2, each building is modified and designed for a smaller design drift. For example, the 4-story building originally designed for 4% design drift has a smaller design drift of 3% making the modified building stronger than the original one. Design drifts of the original and modified buildings are presented in Table 4.1.

The modified buildings were used in the MS and MS+AS analysis and their collapse probabilities are presented in Table 4.1. The percent difference when aftershock is included versus excluded are all presented for the modified buildings as well as the original buildings.

Table 4.1. Collapse probabilities and differences for different buildings

Building type	Model type	Design drift	P(MS)	P(AS)	P(MS)+P(MS)×P(AS)	Difference (%)
2-story	Original	4%	**0.000626**	0.102388	0.00069	10.24
	Modified	0.5%	0.000407	0.080761	0.00044	-29.76
4-story	Original	4%	**0.000285**	0.091579	0.000311	**9.16**
	Modified	3%	0.000241	0.086547	0.000261	**-8.37**
6-Story	Original	4%	**0.000294**	0.094869	0.000322	9.49

For example, consider the calculated design base shear needed and the base shear adjustment factor for the four-story building with the original design drift of 4%. These values are shown in bold in Table 4.2. The value of design base shear needed for the first story which is

1586 KN was calculated by interpolation between the design base shears for the first story of the original and modified four-story building which are 1277 KN and 1868 KN, respectively (see Table 3.10). The percent difference of 9.16 and -8.37 for the original and modified four-story building were used for the purpose of interpolation, too. These percent difference values are shown in bold in Table 4.1. Finally, the base shear adjustment factor for the four-story building with 4% design drift is calculated by taking the ratio of the design base shear needed for the first story to the design base shear for the first story of the original building with 4% design drift (1586/1277 = 1.24) (see Table 4.2). Fig. 4.2 shows sensitivity of the calculated base shear adjustment factor with respect to the number of stories of the building. As observed in Fig. 4.2, the six-story building needs a higher base shear adjustment factor. However, the two-story building needs the least modification in the design base shear. This is consistent with the fragility curves presented earlier in Fig. 4.1.

Table 4.2. Interpolated design base shear of the first story and base shear adjustment factors for buildings with different design drifts

Building type	Model type	Design drift	Design base shear needed for the first story(KN)	Base shear adjustment factor(X_v)
2-story	Original	4%	445	1.05
	Modified	0.5%		
4-story	Original	4%	**1586**	**1.24**
	Modified	3%		
6-Story	Original	4%	927	1.35
	Modified	3%		

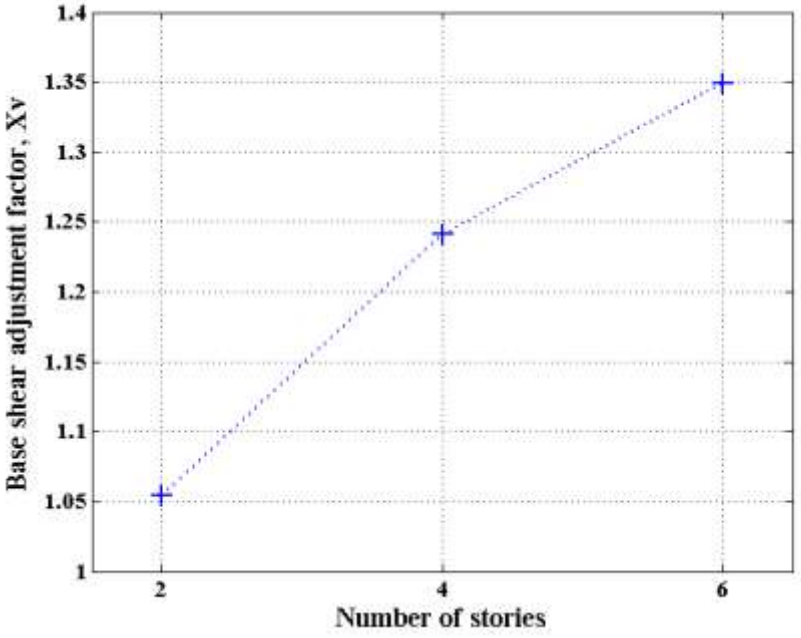

Figure 4.2 Calculated base shear adjustment factors for different buildings

4.2. Effect of Building Location on Base Shear Adjustment Factor, X_v

In this section, three new two-, four- and six-story buildings were designed using the spectral acceleration values associated with the low seismic zone in Sacramento, CA. Additional details are presented in Appendix A. The buildings were designed for a design drift of 4% with a 50% probability of non-exceedance. Fig. 4.3 presents the MS hazard curves for Los Angeles, CA (Latitude: 34.0537°, Longitude: -118.2427°) and Sacramento, CA (Latitude: 38.5816°, Longitude: -121.49.44°) with a spectral acceleration horizontal axis. A MS+AS scenario of for a mainshock of M8 and an aftershock of M7 was used in the analysis of this section.

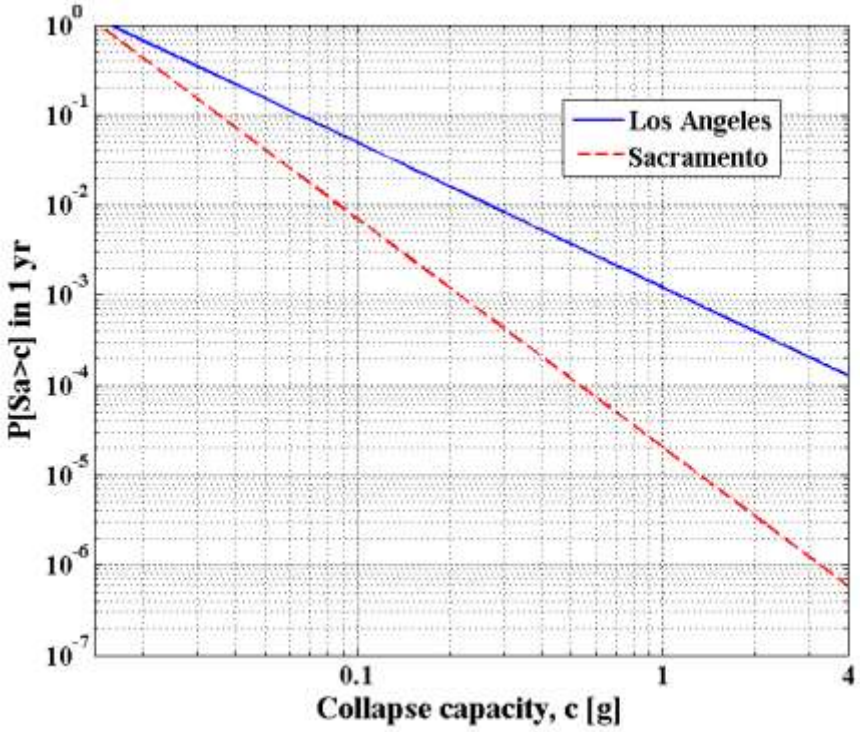

Figure 4.3 Mainshock hazard curves for Los Angeles and Sacramento

The computed mainshock fragility curves for the two-, four- and six-story buildings are presented in Fig. 4.4. As can be seen from Fig. 4.4, the buildings designed for Sacramento, CA have higher collapse fragility than the buildings designed for Los Angeles, CA. This means that the collapse spectral acceleration is lower for the buildings designed for Sacramento, CA. In other words, the weaker buildings designed for the low hazard seismic zone of Sacramento, CA reaches the collapse criteria sooner than the stronger buildings designed for Los Angeles, CA.

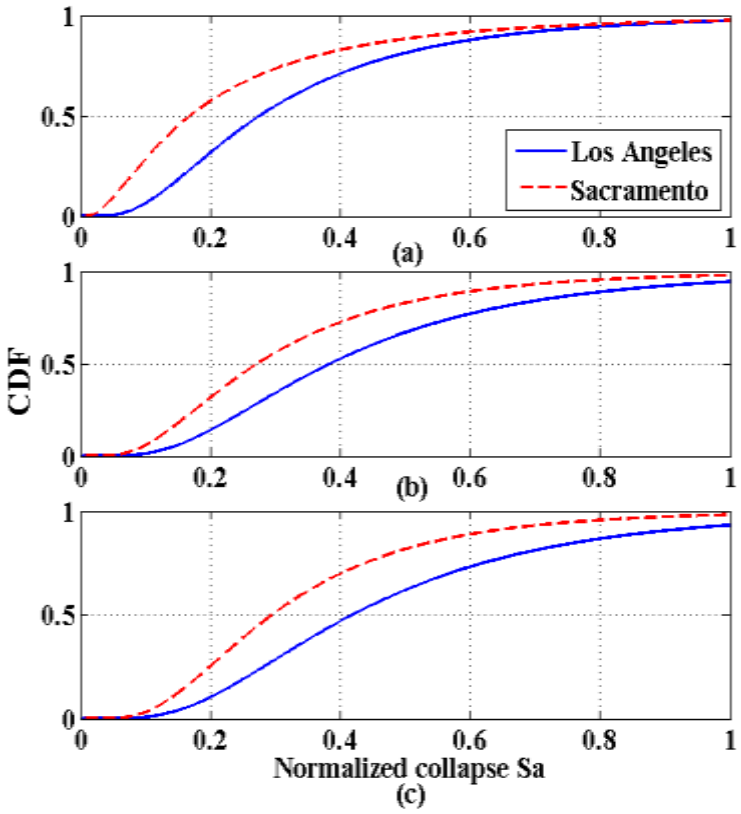

Figure 4.4 Mainshock collapse fragilities computed by NLTHA for 4%DDD buildings located in Los Angeles and Sacramento, (a) 2-story building, (b) 4-story building, (c) 6-story building

The design base shear needed for the first story was calculated for the buildings located in Sacramento, CA using the procedure presented in section 2.5. These values and the associated base shear adjustment factors are presented in Table 4.3. The base shear adjustment factors, X_v increase with increasing the number of stories of the building. This is similar to the increasing trend of X_v presented earlier in Table 4.2 for Los Angeles, CA. However, the adjustment factors are much smaller for Sacramento, CA compared to those of Los Angeles, CA.

Table 4.3. Interpolated design base shear of the first story and base shear adjustment factors for buildings with different design drifts

Building type	Model type	Design drift	Design base shear needed for the first story(KN)	Base shear adjustment factor(X_v)
2-story	Original	4%	185	1.004
	Modified	0.50%		
4-story	Original	4%	563	1.009
	Modified	3%		
6-Story	Original	4%	306	1.022
	Modified	3%		

Fig. 4.5 presents the base shear adjustment factors computed for both Los Angeles, CA and Sacramento, CA. As observed in Fig 4.5, the base shear adjustment factors for the low seismic hazard zone of Sacramento is much lower than the associated values for Los Angeles, CA which is considered a high seismic zone. This is in line with what one would expect. Therefore, the change needed in design due to the aftershock hazard is negligible in case of Sacramento, CA. This is resulted from the lower hazard curves for Sacramento, CA compared to that of Los Angeles, CA (see Fig. 4.3).

In the case of the low hazard seismic zone such as Sacramento, CA, the low hazard curve convolves with the collapse fragilities resulting in small site-specific collapse probabilities. As observed in Fig. 4.4, the collapse fragilities for Sacramento CA are higher than those for Los Angeles, CA. However, the effect of lower hazard curves dominates the effect of higher collapse fragilities in this case. Therefore, the calculated total collapse probabilities are approximately similar to the mainshock collapse probabilities of the original model resulting in small change needed in design due to the aftershock hazard.

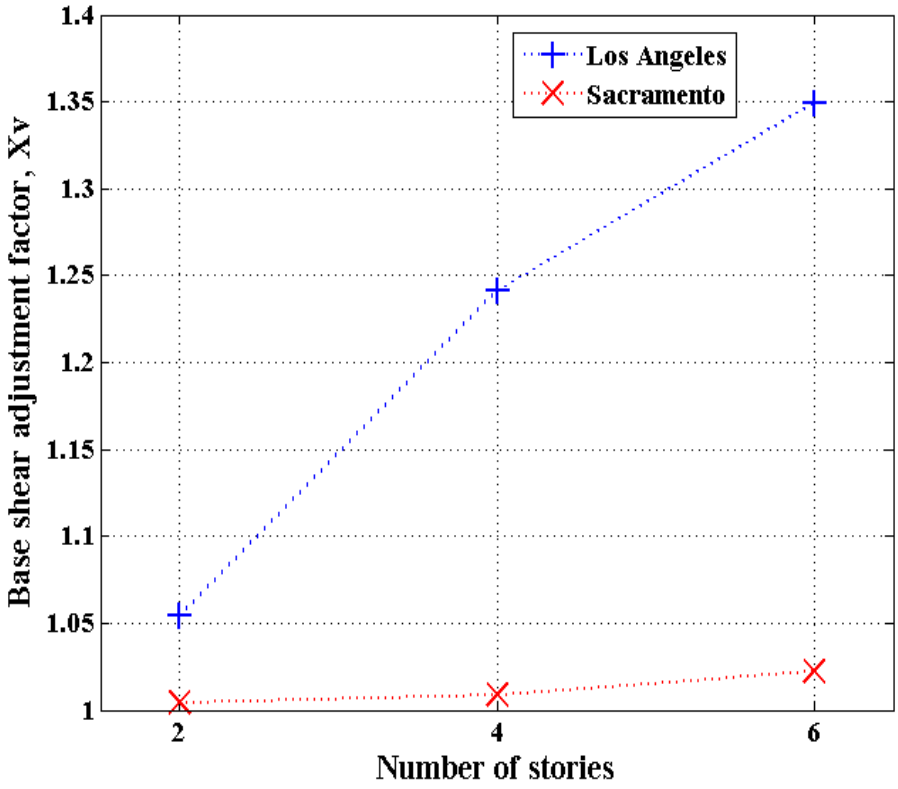

Figure 4.5 Base shear adjustment factors for different buildings located in Los Angeles and Sacramento

4.3. Effect of Design Drift of the Building on Base Shear Adjustment Factor, X_v

In this section the base shear adjustment factor is calculated for the four-story and six-story buildings designed for design drifts of 4%, 3% and 2% as an illustration. The location of the buildings is Los Angeles, CA and the MS+AS scenario of MS of M8 and AS of M7 was used for the analysis. See Appendix A and B for details of the DDD design of the buildings.

Fig. 4.6 presents the design base shear for the first story of the four-story and six-story buildings. As observed in Fig 4.6., the design base shears have an increasing trend as the design drift decreases. In other words, the buildings designed for smaller design drifts are stronger than the buildings designed for higher drifts. The design base shears calculated using DDD approach

show approximately linear decreasing trend with increasing design drifts for the four-story building. However, this decreasing trend is not linear for the six-story building. The design base shears resulted from DDD approach were used in interpolation which resulted in the design base shear adjustment factor, X_v (see more details in section 3.2).

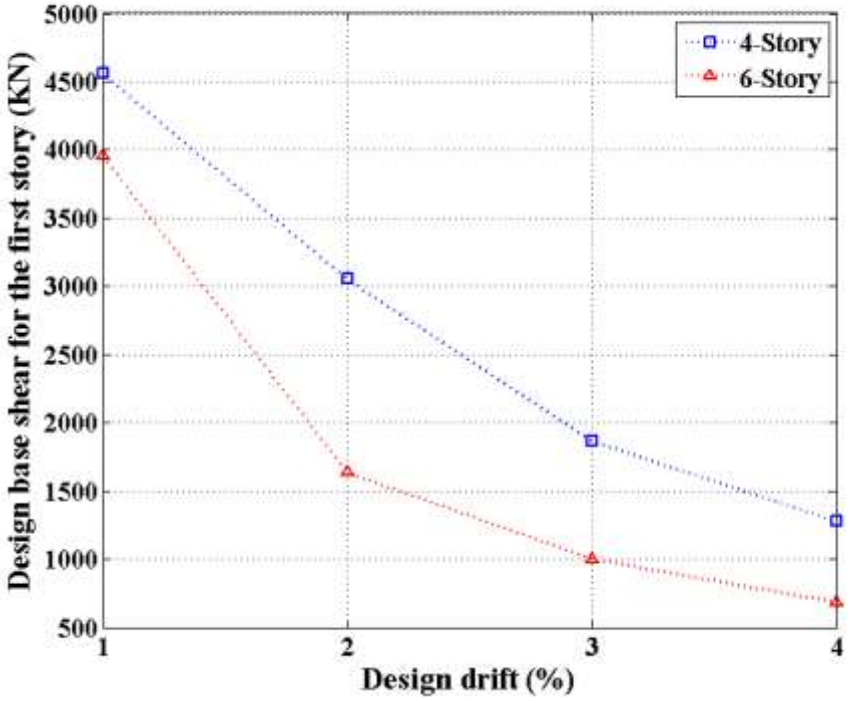

Figure 4.6 Design base shears of the first story of the buildings

The mainshock collapse fragilities were developed for the four-story and six-story buildings designed for different drifts. The collapse fragilities for the buildings with higher design drifts have higher values. For example, at normalized collapse S_a of 0.5, the value of the mainshock collapse fragility is approximately 0.52, 0.79, 0.82 and 0.85 for the four-story building designed for 4%, 3%, 2% and 1% design drift. These fragility curves are presented in Fig. 4.7 and 4.8. The higher collapse fragility indicates sooner collapse of the building which is associated with the weaker building with 4% design drift. As the building becomes stronger, the

collapse fragilities are lower. In this case, the building with 1% design drift is the strongest building and has the lowest collapse fragility.

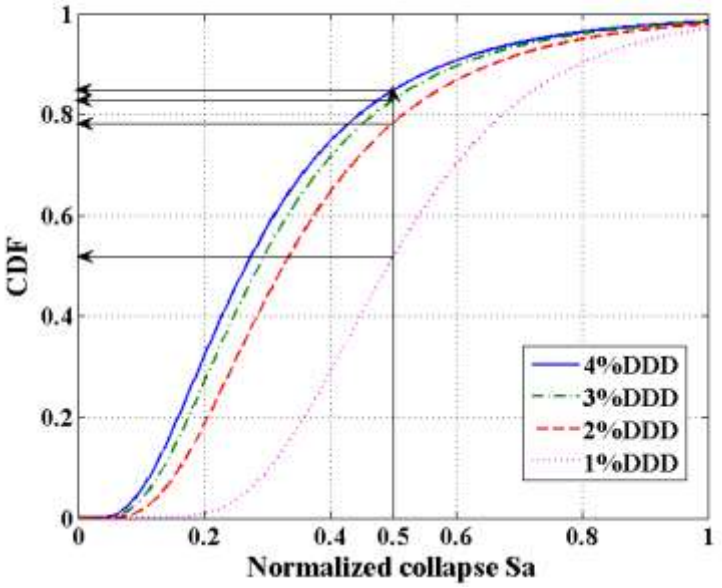

Figure 4.7 Mainshock fragility curves computed by NLTHA for the 4-story building

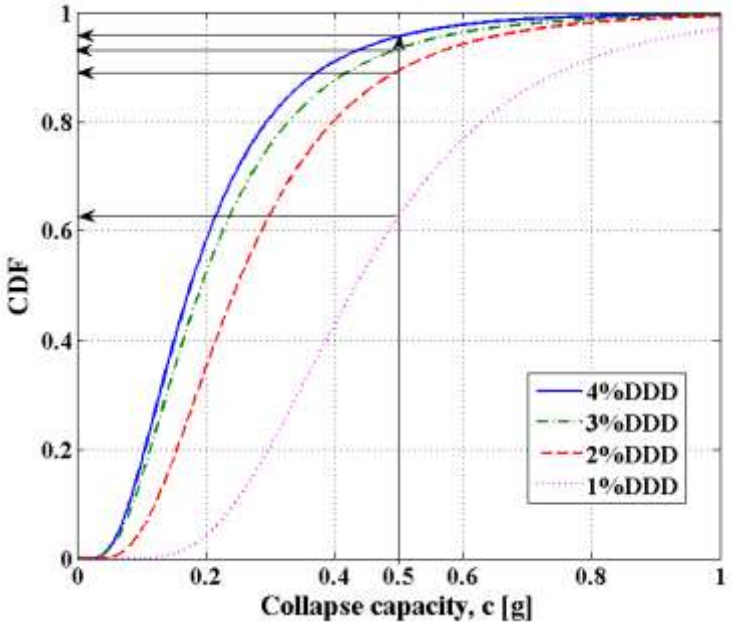

Figure 4.8 Mainshock fragility curves computed by NLTHA for the 6-story building

The base shear adjustment factor for each building was computed following the procedure presented in section 3.2. The values of the base shear adjustment factors are presented in Table 4.4 and Fig. 4.9.

Table 4.4. Design base shear needed and the base shear adjustment factors

Building type	Model type	Design drift	Design base shear needed for the first story(KN)	Base shear adjustment factor(X_v)
4-Story	Original	4%	1586	1.24
	Modified	3%		
	Original	3%	2258	1.21
	Modified	2%		
	Original	2%	3246	1.06
	Modified	1%		
6-Story	Original	4%	927	1.35
	Modified	3%		
	Original	3%	1129	1.13
	Modified	2%		
	Original	2%	1880	1.15
	Modified	1%		

As it is presented in Fig. 4.9, the base shear adjustment factor has a general decreasing trend for the buildings designed for lower design drifts. As observed in Table 4.4, the values of X_v are 1.24, 1.21 and 1.06 for the four-story building with design drift of 4%, 3% and 2%. The stronger building with 2% design drift has smaller X_v (1.06) compared to that of the weaker building with 4% design drift (X_v=1.24). In other words, the weaker building needs more change in design due to the aftershock hazard which is in line with what one would expect.

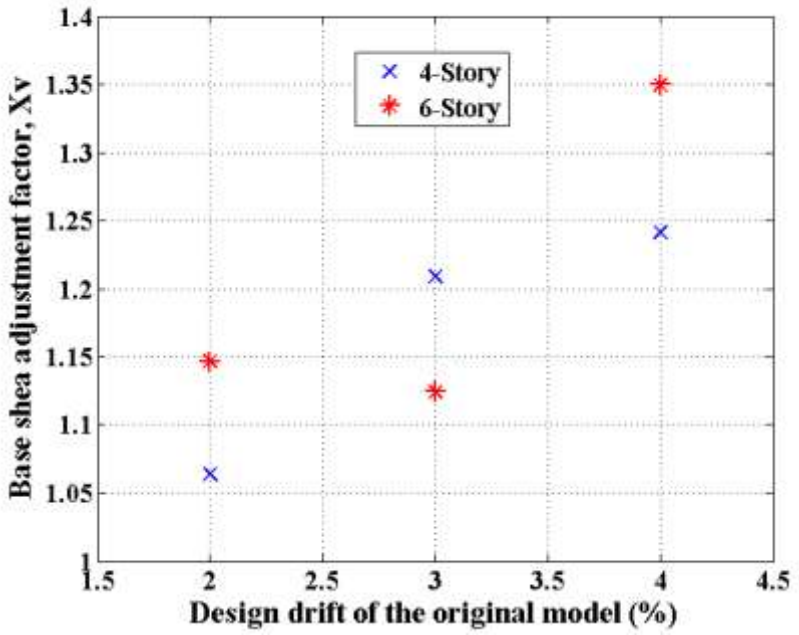

Figure 4.9 Base shear adjustment factors for different design drifts

4.4. Base Shear Adjustment Factors for Different Mainshock + Aftershock Scenarios

The objective of this section is to show the effect of mainshock and aftershock magnitude on the design base shear adjustment factors. To achieve this objective, the MS+AS scenarios were simulated using the scaling factors generated by the Abrahamson and Silva Next Generation Attenuation (NGA) relationship (Abrahamson and Silva, 2008). These simulated MS+AS scenarios were used for the analysis in order to compute the base shear adjustment factors for each scenario.

Tables 4.5 to 4.11 presents the computed base shear adjustment factors for MS+AS scenarios with mainshocks of M8.5-M5.5 and aftershocks of M8-M5. Table 4.5 presents the base shear adjustment factors computed for the two-story building designed for 4% design drift in Los Angeles, CA. For example, the base shear adjustment factor of 1.05 which was computed for a scenario with a mainshock of magnitude M8 and aftershock of magnitude M7 is shown in bold in

Table 4.5. It should be noted that the design base shears of the original and modified models used in the interpolation to generate the base shear adjustment factors in Table 4.5 were 4% and 0.5%, respectively.

As observed in Table 4.5, the needed change in design base shear is less than 5% for most MS+AS scenarios. The MS+AS scenarios which have design base sear adjustment factors, (X_v) more than 1.05 are MS(M8.5)+AS(M8), MS(8.5)+AS(M7.5), MS(M8.5)+AS(M7), MS(M8.5)+AS(M6.5), MS(M8)+AS(M7.5) and MS(M8)+AS(M7). Therefore, the low-rise two-story building needs a considerable change in design due to the effect of aftershocks only for MS+AS scenarios with large magnitudes.

Table 4.5. Base shear adjustment factors of the 4%DDD, 2-story building located in Los Angeles, CA for different MS+AS scenarios

		Aftershock magnitude						
		M8	M7.5	M7	M6.5	M6	M5.5	M5
Mainshock magnitude	M8.5	1.14	1.13	1.12	1.08	1.04	1.04	1.03
	M8	N/A	1.06	**1.05**	1.03	1.02	1.01	1.01
	M7.5	N/A	N/A	1.02	1.01	1.01	1.00	1.00
	M7	N/A	N/A	N/A	1.00	1.00	1.00	1.00
	M6.5	N/A	N/A	N/A	N/A	1.00	1.00	1.00
	M6	N/A	N/A	N/A	N/A	N/A	1.00	1.00
	M5.5	N/A	N/A	N/A	N/A	N/A	N/A	1.00

Note: N/A stands for not applicable

Base shear adjustment factors are presented in Tables 4.6, 4.7 and 4.8 for the four-story building designed for 4%, 3% and 2% design drift respectively. The location of the buildings is assumed to be in Los Angeles, CA. The base shear adjustment factors associated with the MS(M8)+AS(M7) scenario are 1.24, 1.21 and 1.06 for the four-story building designed for 4%, 3% and 2% design drift, respectively. These values are shown in bold in Tables 4.6, 4.7 and 4.8.

Table 4.6. Base shear adjustment factors of the 4%DDD, 4-story building located in Los Angeles, CA for different MS+AS scenarios

		Aftershock magnitude						
		M8	M7.5	M7	M6.5	M6	M5.5	M5
Mainshock magnitude	M8.5	1.76	1.69	1.58	1.32	1.17	1.12	1.09
	M8	N/A	1.27	**1.24**	1.13	1.07	1.05	1.03
	M7.5	N/A	N/A	1.08	1.04	1.02	1.01	1.01
	M7	N/A	N/A	N/A	1.02	1.01	1.01	1.01
	M6.5	N/A	N/A	N/A	N/A	1.00	1.00	1.00
	M6	N/A	N/A	N/A	N/A	N/A	1.00	1.00
	M5.5	N/A	N/A	N/A	N/A	N/A	N/A	1.00

In Tables 4.6 and 4.9, it should be noted that the cells colored in grey indicate cases where the 0% difference was not achieved for the modified building. For example, if the design drift of the original and modified building were 4% and 3%, respectively, the percent difference is still positive for the modified 3% designed building. Therefore, the building would need to be modified again using a smaller design drift e.g. 2%. Thus, the resulting base shear adjustment factors specified with grey cells are much larger than the other cells in the table.

By comparison of Table 4.5 and 4.6, it can be seen that the base shear adjustment factors for the mid-rise four-story building are generally larger than those for the low-rise two-story building. Also, the number of MS+AS scenarios with design base shear adjustment factors larger than 1.05 are more in the case of four-story building.

Table 4.7. Base shear adjustment factors of the 3%DDD, 4-story building located in Los Angeles, CA for different MS+AS scenarios

		Aftershock magnitude						
		M8	M7.5	M7	M6.5	M6	M5.5	M5
Mainshock magnitude	M8.5	1.59	1.54	1.49	1.28	1.15	1.11	1.07
	M8	N/A	1.24	**1.21**	1.11	1.06	1.04	1.03
	M7.5	N/A	N/A	1.08	1.04	1.02	1.02	1.01
	M7	N/A	N/A	N/A	1.01	1.01	1.00	1.00
	M6.5	N/A	N/A	N/A	N/A	1.00	1.00	1.00
	M6	N/A	N/A	N/A	N/A	N/A	1.00	1.00
	M5.5	N/A	N/A	N/A	N/A	N/A	N/A	1.00

Table 4.8. Base shear adjustment factors for the 2%DDD, 4-story building located in Los Angeles, CA for different MS+AS scenarios

		Aftershock magnitude						
		M8	M7.5	M7	M6.5	M6	M5.5	M5
Mainshock magnitude	M8.5	1.19	1.17	1.16	1.09	1.05	1.04	1.02
	M8	N/A	1.07	**1.06**	1.04	1.02	1.01	1.01
	M7.5	N/A	N/A	1.02	1.01	1.01	1.00	1.00
	M7	N/A	N/A	N/A	1.00	1.00	1.00	1.00
	M6.5	N/A	N/A	N/A	N/A	1.00	1.00	1.00
	M6	N/A	N/A	N/A	N/A	N/A	1.00	1.00
	M5.5	N/A	N/A	N/A	N/A	N/A	N/A	1.00

The decreasing trend in the design base shear adjustment factors (X_v) with decreasing the design drift is observed by comparing the values presented in Table 4.6, 4.7 and 4.8 (see section 4.3 for more details). As expected the number of MS+AS scenarios with X_v values larger than 1.05 are more for the weaker building with 4% design drift compared to that of the stronger building with 2% design drift. This can be observed by comparing the design base shear values presented in Tables 4.6 and Table 4.8. Similarly, the base shear adjustment factors were calculated for the six-story building designed for 4%, 3% and 2% design drift.

Table 4.9. Base shear adjustment factors for the 4%DDD, 6-story building located in Los Angeles, CA for different MS+AS scenarios

		Aftershock magnitude						
		M8	M7.5	M7	M6.5	M6	M5.5	M5
Mainshock magnitude	M8.5	1.83	1.82	1.76	1.56	1.38	1.26	1.20
	M8	**N/A**	**1.41**	**1.35**	**1.20**	**1.10**	**1.07**	**1.05**
	M7.5	N/A	N/A	1.14	1.08	1.04	1.03	1.02
	M7	N/A	N/A	N/A	1.03	1.01	1.01	1.01
	M6.5	N/A	N/A	N/A	N/A	1.00	1.00	1.00
	M6	N/A	N/A	N/A	N/A	N/A	1.00	1.00
	M5.5	N/A	N/A	N/A	N/A	N/A	N/A	1.00

By comparing the design base shears presented in Table 4.9 versus Table 4.6, it can be seen that the needed change in design is generally more in the case of six-story building compared to that of that of the four-story building. It should be noted that the base shear adjustment factors in Tables 4.6 through 4.11 were calculated for a 1000 days (T=1000 days) period beginning at the time of mainshock (t=0 days).

Table 4.10. Base shear adjustment factors for the 3%DDD, 6-story building located in Los Angeles, CA for different MS+AS scenarios

		Aftershock magnitude						
		M8	M7.5	M7	M6.5	M6	M5.5	M5
Mainshock magnitude	M8.5	1.35	1.34	1.30	1.18	1.09	1.06	1.05
	M8	N/A	1.14	1.12	1.07	1.03	1.02	1.02
	M7.5	N/A	N/A	1.05	1.03	1.01	1.01	1.01
	M7	N/A	N/A	N/A	1.01	1.00	1.00	1.00
	M6.5	N/A	N/A	N/A	N/A	1.00	1.00	1.00
	M6	N/A	N/A	N/A	N/A	N/A	1.00	1.00
	M5.5	N/A	N/A	N/A	N/A	N/A	N/A	1.00

Table 4.11. Base shear adjustment factors for the 2%DDD, 6-story building located in Los Angeles, CA for different MS+AS scenarios

		Aftershock magnitude						
		M8	M7.5	M7	M6.5	M6	M5.5	M5
Mainshock magnitude	M8.5	1.44	1.41	1.36	1.21	1.11	1.08	1.06
	M8	N/A	1.17	1.15	1.08	1.04	1.03	1.02
	M7.5	N/A	N/A	1.05	1.03	1.01	1.01	1.01
	M7	N/A	N/A	N/A	1.01	1.00	1.00	1.00
	M6.5	N/A	N/A	N/A	N/A	1.00	1.00	1.00
	M6	N/A	N/A	N/A	N/A	N/A	1.00	1.00
	M5.5	N/A	N/A	N/A	N/A	N/A	N/A	1.00

Reasenberg (1994) presents a table containing the probabilities for the occurrence of one or more aftershock equal to or greater than a given magnitude ($M \geq 5$, $M \geq 5.5$, $M \geq 6$, $M \geq 6.5$, $M \geq 7$ and $M \geq 7.5$). The table presented by Reasenberg (1994) gives probabilities for aftershocks of the Loma Prieta earthquake. Bayesian model parameters were used for generating these probabilities. The probabilities are presented in Table 4.12 for a 1000 day period 0 beginning at the time of mainshock. The probability values presented in Table 4.12 can be used as weights in order to compute a single base shear adjustment factor for each row of Tables 4.6 to 4.11 with a specific mainshock magnitude. Consider the base shear adjustment factors in the second row of Table 4.9 which is associated with mainshock magnitude of M8. This row of table is associated with different MS+AS scenarios with aftershocks with magnitude of M7.5, M7, M6.5, M6, M5.5 and M5. A weighted base shear adjustment factor can be calculated using the probabilities presented in Table 4.12 which takes into account the probability of occurrence of aftershocks with different magnitudes. The weighted base shear adjustment factor for mainshock of M8 is calculated to be approximately 1.09 for the 6-story building with 4% design drift (see Table 4.9).

Table 4.12. Probability of occurrence of aftershocks with different magnitudes (Reasenberg, 1994)

Aftershock magnitude	Probability
M>7.5	0.019
M>7	0.048
M>6.5	0.115
M>6	0.264
M>5.5	0.536
M>5	0.854

Fig. 4.10 and 4.11 were plotted in order to show the effect of aftershock and mainshock magnitude on the base shear adjustment factor. The calculated base shear adjustment factors in Table 4.6 for the four-story building designed for 4% design drift were used in Fig. 4.10 and 4.11. Fig. 4.10 presents the base shear adjustment factors versus mainshock magnitude. The aftershock magnitude is fixed for each dataset. Therefore, the effect of aftershock magnitude can be investigated.

The base shear adjustment factor has an increasing trend with increasing the mainshock magnitude assuming that the aftershock magnitude has a fixed value. This increasing trend becomes steeper with increase in the aftershock magnitude which is fixed for each dataset. In other words, the effect of mainshock magnitude on the design base shear adjustment factor, X_v is more for the datasets with higher aftershock magnitude. This means that the X_v becomes more sensitive to the mainshock magnitude when the aftershock magnitude increases.

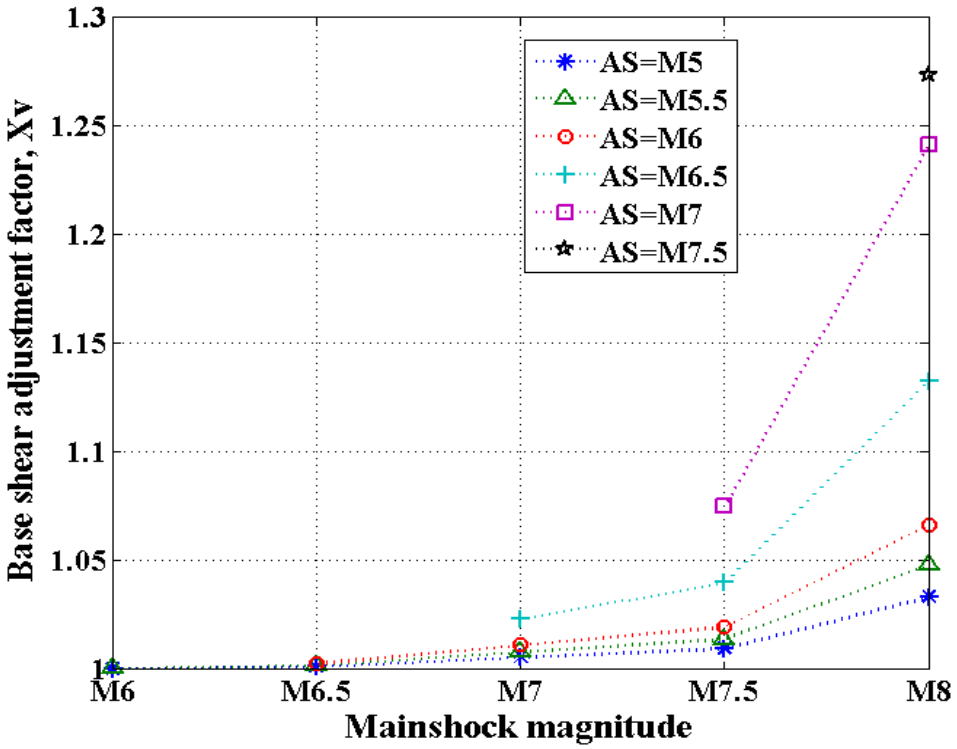

Figure 4.10 Base shear adjustment factor versus mainshock magnitde for the 4-story building with 4% design drift (Note that the aftershock magnitude is fixed for each dataset)

Fig. 4.11 presents the base shear adjustment factor versus aftershock magnitude. The magnitude of the mainshock is fixed for each dataset and the effect of mainshock magnitude was investigated. The base shear adjustment factors increase with increasing the mainshock magnitude assuming that the magnitude of aftershock has a constant value.

The general trends observed in Fig 4.11 are similar to that of Fig. 4.10. As expected, for each dataset with fixed MS magnitude, the base shear adjustment factor, X_v increases with increase in the aftershock magnitude. The increasing trend for X_v becomes steeper for datasets with larger magnitudes. For example, the increasing trend for dataset with MS of M8 is much steeper than the increasing trend of the dataset with MS magnitude of M6. In other words, the X_v

values become more sensitive to the changes in the aftershock magnitude as the mainshock magnitude increases.

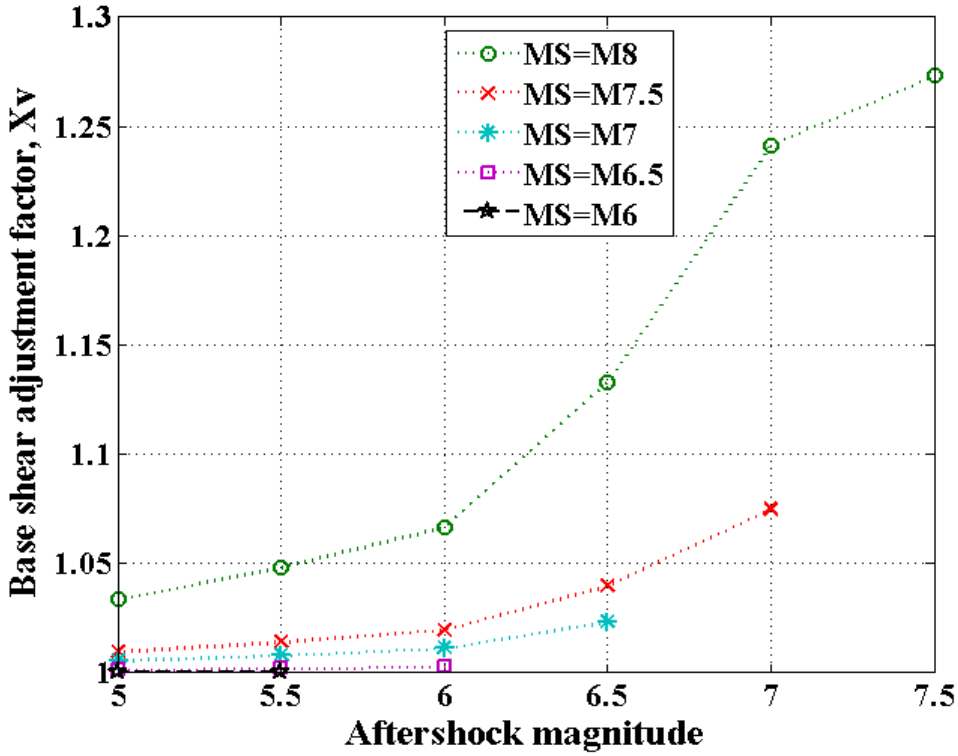

Figure 4.11 Base shear adjustment factor versus aftershock magnitde for the 4-story building with 4% design drift
(Note: The mainshock magnitude is fixed for each dataset)

By comparing Fig. 4.10 and Fig. 4.11, it can be seen that the datasets for the fixed aftershocks presented in Fig. 4.10 are much closer to each other compared to the datasets with fixed mainshocks presented in Fig. 4.10. This means that the base shear adjustment factor, X_v is more sensitive to the changes in mainshock magnitude compared to the changes in the aftershock magnitude. This conclusion was expected since the mean aftershock hazard rate value is more sensitive to the mainshock magnitude (see Eq. 1.8). Recall that the aftershock rate was used in generating the aftershock hazard curve which was used in the convolution with the collapse fragility curves (see section 2.5).

Fig. 4.12 shows variation of base shear adjustment factors with respect to the aftershock magnitude for the two-, four- and six-story buildings. It was assumed that the mainshock magnitude is fixed at M8 for the MS+AS scenarios. As can be seen in Fig. 4.12, the base shear adjustment factor has an increasing trend with the increasing aftershock magnitude for the two-, four- and six-story building. However, the increasing trend for the low-rise two-story building is much smoother than the increasing trend for the mid-rise four- and six-story buildings. In other words, sensitivity of the base shear adjustment factor, X_v with respect to the aftershock magnitude is more for the mid-rise four- and six-story buildings compared to the low-rise two-story building. As observed in Fig. 4.12, for the four- and six-story buildings, there is a steep increase in the base shear adjustment factor computed for the MS(M8)+AS(M6.5) and MS(M8)+AS(M7) scenarios. This increase in X_v becomes smoother between MS(M8)+AS(M7) and MS(M8)+AS(M7.5). In other words, in case of mid-rise buildings a considerable change in design is needed due to the aftershock hazards for the aftershock magnitudes of M7 and higher.

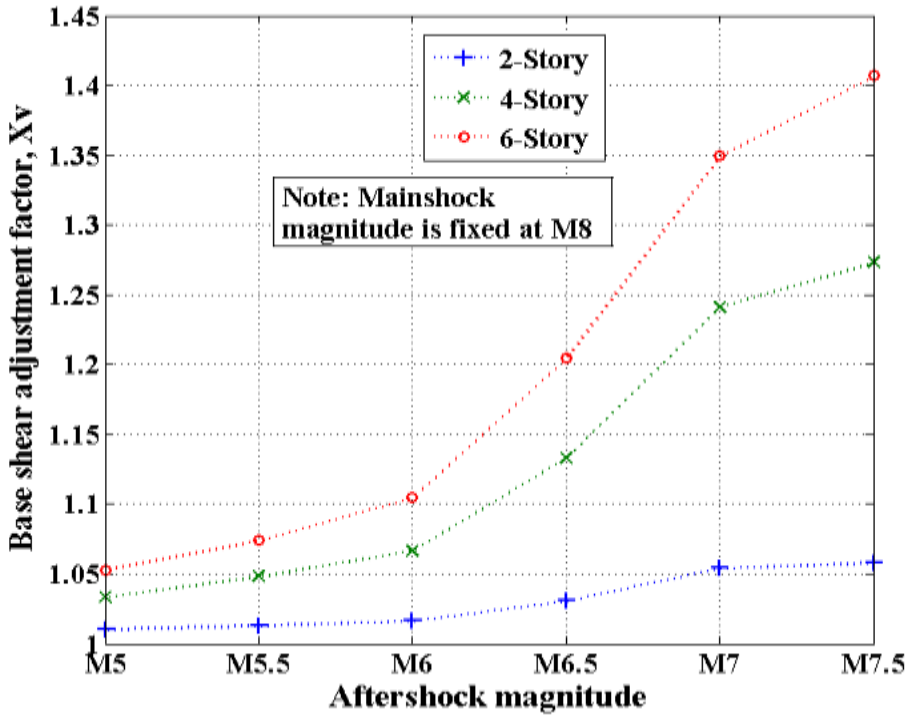

Figure 4.12 Base shear adjustment factor versus aftershock magnitude for the 2-, 4-, and 6-story buildings

4.5. Effect of Intensity of the Mainshock + Aftershock Scenario on Base Shear Adjustment Factor, X_v

In this section the effect of the intensity the MS+AS scenario was studied. The intensity of the MS+AS scenarios used in the analysis is assumed to be MCE in the first case and DBE in the second case. The two-, four- and six-story buildings with 4% design drift located in Los Angeles, CA were used for the analysis in this section.

The MCE level spectral acceleration for Los Angeles, CA is approximately 2.4 g (www.USGS.gov). Also, the DBE level spectral acceleration for Los Angeles, CA is 1.6 g which is equal to 2/3 of the MCE level spectral acceleration of 2.4 g. The mainshock collapse fragilities for the two-, four- and six-story buildings with 4% design drift and P_{NE}=50% are presented in

Fig. 4.13. The solid line shows the fragility curve for the MCE level mainshock and, the dashed line which is lower than the solid line, shows the collapse fragility curve for the DBE level mainshock. This means that the collapse occurs sooner (or at lower spectral accelerations) for the MS+AS scenario with MCE level.

By comparing Fig. 4.13(b) and Fig. 4.13(c) for the mid-rise four- and six-story buildings with Fig. 4.13(a) for the low-rise two-story building, it can be seen that the difference between the collapse probabilities generated for MCE and DBE level is more in case of mid-rise buildings. For example, at normalized S_a of 0.4 in Fig. 4.13(b) and 4.13(c), the difference between the MCE and DBE level fragility curves is about 0.25. This value is higher than the similar difference value in Fig. 4.13(a) which is about 0.15. Therefore, the mid-rise four- and six-story buildings are more sensitive to the change in the MS+AS level compared to the low-rise two-story building.

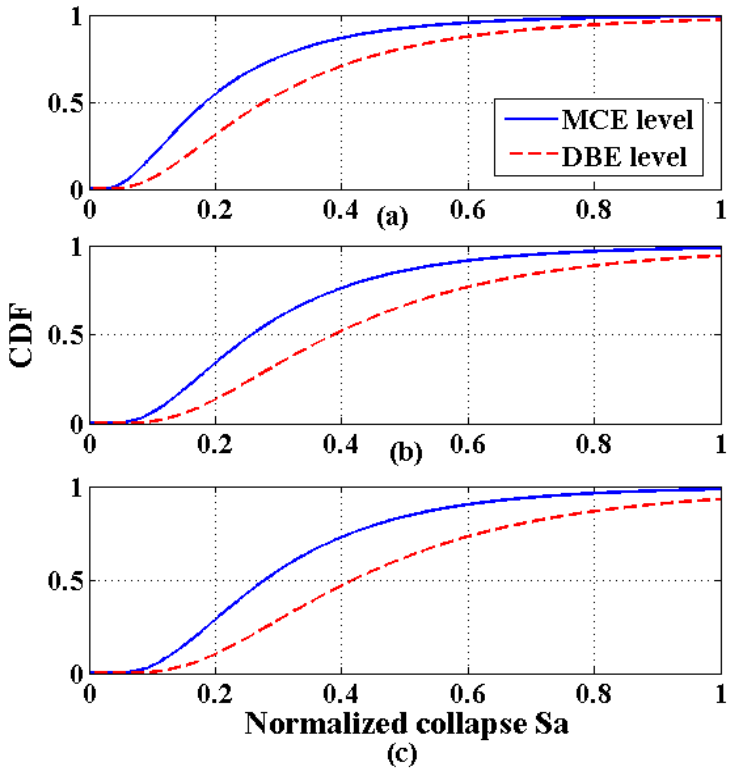

Figure 4.13 Mainshock collapse fragilities computed using NLTHA for MCE and DBE level mainshock for different buildings, (a) 2-story, (b) 4-story, (c) 6-story

Table 4.12 presents the collapse probabilities computed for the DBE level MS+AS scenario. The magnitude of the mainshock and aftershock was assumed to be M8 and M7, respectively. The collapse probabilities for MCE level MS+AS scenario were presented earlier in Table 4.1.

Table 4.13. Collapse probabilities and differences for different buildings

Building type	Model type	Design drift	P(MS)	P(AS)	P(MS)+P(MS)×P(AS)	Difference (%)
2-story	Original	4%	**0.000323**	0.070181	0.000346	7.02
	Modified	0.50%	0.000212	0.056928	0.000224	-30.74
4-story	Original	4%	**0.000142**	0.075517	0.000153	7.55
	Modified	3%	0.000121	0.074254	0.00013	-8.35
6-Story	Original	4%	**0.000148**	0.066103	0.000158	6.61
	Modified	3%	0.000133	0.062774	0.000142	-3.99

The design base shear needed for the first story of each building was determined and the associated base shear adjustment factor was presented in Table 4.13 for MS(M8)+AS(M7) scenario with DBE level mainshock and aftershock. The base shear adjustment factors for MCE level MS+AS scenario were presented earlier in Table 4.2.

Table 4.14. Design base shear needed and the base shear adjustment factors

Building type	Model type	Design drift	Design base shear needed for the first story(KN)	Base shear adjustment factor(X_v)
2-story	Original	4%	439	1.04
	Modified	0.50%		
4-story	Original	4%	822	1.22
	Modified	3%		
6-Story	Original	4%	868	1.29
	Modified	3%		

The base shear adjustment factors computed for the MS+AS scenario with MCE and DBE level MS(M8)+AS(M7) scenario were plotted in Fig. 4.14. As observed in this figure, the base shear adjustment factor is lower in the case of DBE level MS+AS scenario. The lower adjustment factors for the DBE level which is 2/3 of MCE level is reasonable. Also, the difference between the base shear adjustment factor computed for MCE level and DBE level MS+AS scenario are higher in case of the four-story and six-story building compared to the two-story building. This is in line with the earlier discussion mentioned about Fig. 4.13.

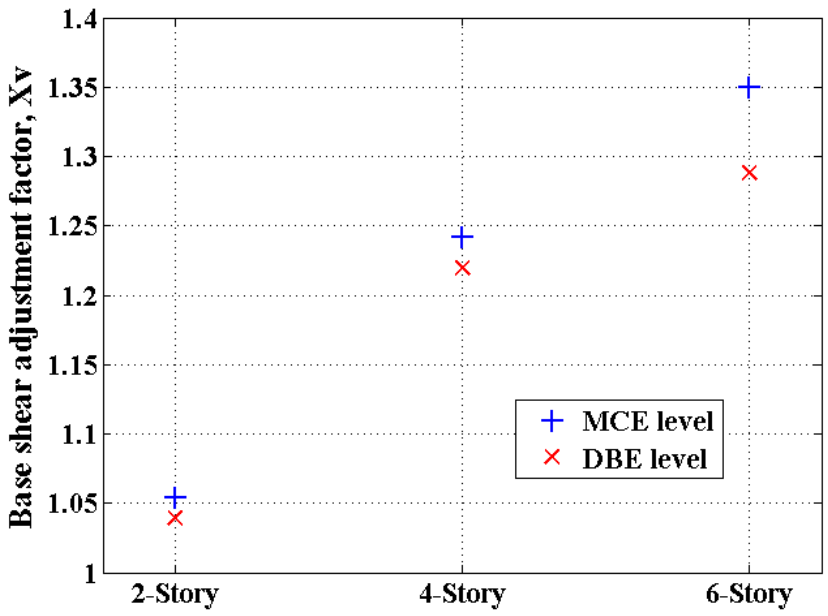

Figure 4.14 Base shear adjustment factors for MCE and DBE level

4.6. Base Shear Adjustment Factors for Different Time Intervals, (t, t+T)

Effects of duration (T) and the elapsed time from the initial rupture (t) on aftershock hazard are investigated by Yeo and Cornell (2005). It was concluded that by increasing the elapsed number of days from the initial mainshock, the aftershock occurrence frequency decreased and the durations considered become more significant in determining the difference in aftershock hazard. Also, the aftershock hazard is almost insensitive to the duration of interest, [t, t+T] beyond six months.

Yeo and Cornell (2005) state that more than one year is needed for the aftershock hazard to decrease to the original total pre-mainshock hazard level. And, aftershock hazard contribution to the total (mainshock and aftershock) hazard becomes negligible (<10%) after more than approximately 30 years. It is clear that aftershock hazard is significantly dependent on the mainshock magnitude, m_m. The increase in the aftershock hazard with increasing m_m values is

mainly due to the increase in the mean rate of aftershocks (dependent only on m_m) and to a significantly lesser extent, a factor due to the increase implied in the upper bound aftershock magnitude (where this factor is dependent on m_m and PGA level). The aftershock hazard is also sensitive to the structural period (T_0) (Yeo and Cornell, 2005).

As was mentioned in Chapter One, the aftershock rate is dependent on the time interval that is being considered, which is the duration, T, and the time elapsed after the mainshock, t (see Eq 1.8). Fig. 4.15 presents sensitivity of the aftershock rate (denoted by μ^* in Eq. 1.8) with respect to the mainshock magnitude, elapsed time after the mainshock (t) and the duration after time t (T). Considering Fig. 4.15(a), it can be observed that the mean number of aftershocks is highly dependent on the mainshock magnitude and has a steep increasing trend with increasing magnitude of the mainshock. For example, the mean aftershock rate is approximately 34 for a M7.5 mainshock while, this value increases to 100 for a M8 mainshock. It should be noted that the time values of t and T were fixed at t=0 days and T=1000 days in order to compute the values of aftershock rate using Eq. 1.8. Fig. 4.15(b) shows the variation of the mean aftershock rate with change in the time after the mainshock. The values of mean aftershock rates are calculated for time t equal to 0, 7, 14 and 30 days. A decreasing trend with increasing time t is observed in the calculated mean aftershock rates (see Fig. 4.15(b)). The effect of the duration after time t (denoted by T) was investigated in Fig. 4.15(c). The duration of interest that were used in calculation of mean aftershock rated in Fig. 4.15(c) were one month (T=30 days), two months (T=60 days), three months (T=180 days), one year (T=365 days) and T=1000 days. The mean rate aftershocks show an increasing trend with increasing the duration after time t, T. However, sensitivity of the aftershock rate decreases as the duration of T increases.

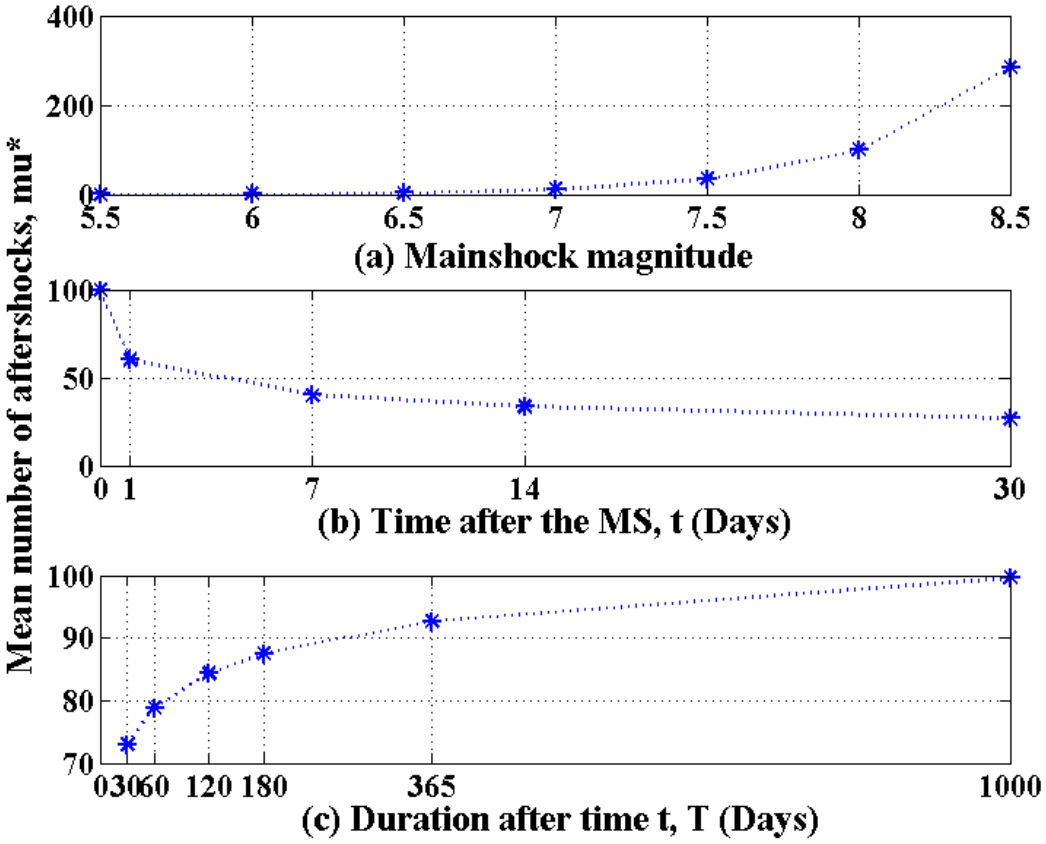

Figure 4.15 Mean number of aftershocks versus (a) mainshock magnitude, (b) time after the mainshock, t and (c) duration after time t

In order to show effects of the time after the mainshock, t and duration after time t (denoted by T) on the base shear adjustment factors, Fig. 4.16 was plotted. The base shear adjustment factors were computed for a four-story building with 4% design drift located in Los Angeles, CA. Fig. 4.16(a) presents the calculated base shear adjustment factors for different times of t= 0, 1, 7, 14 and 30 days. As expected, the base shear adjustment factor decreases with increasing the time after the mainshock. It should be noted that duration of T was fixed at 1000 days in calculation of aftershock rates which were used to generate base shear adjustment factors in Fig. 4.16(a). The effect of duration after time t (T) was investigated in Fig. 4.16(b) where the time after the maishock is fixed at t=0 days. The mean aftershock rates used in calculation of base shear adjustment factors were computed for T= 30, 60, 120, 180, 365 and 1000 days in Fig.

4.16(b). It is observed that the base shear adjustment factor has an increasing trend with increasing the duration, T. By comparing Fig. 4.16(a) and 4.16(b) with Fig. 4.15(b) and 4.15(c) one can observe that variation of the base shear adjustment factor with time t and T is approximately similar to the variation of mean aftershock rate with time t and T.

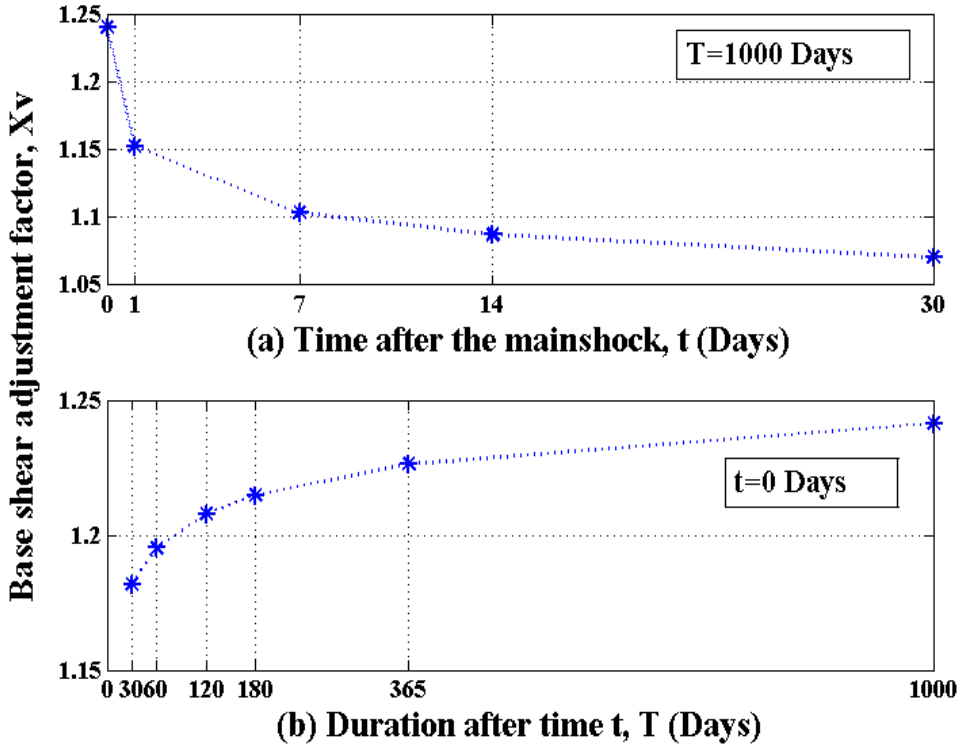

Figure 4.16 Base shear adjustment factors versus (a) Time after the mainshock and (b) Duration after time t, T

4.7. Aftershock Effect on Collapse Probability of Different Damage States

The objective of this section is to show the aftershock effect on the collapse probabilities associated with different damage states (see Table 2.4). The four-story building with 4% design drift located in Los Angeles,CA was used for the analysis in this section. The MS+AS scenario of M8 mainshock and M7 aftershock was used in the analysis and the collapse probabilities were calculated following a similar procedure to that presented in section 3.2.

Fig. 4.17(a) presents the mainshock collapse fragility curves for the four-story building with 4% design drift. As was mentioned earlier in Table 2.4, damage states DS1, DS2, DS3 and DS4 are associated with the drift of 1%, 2%, 4% and 7%. As observed in Fig. 4.17(a), the fragility associated with DS1 has the highest fragility while the DS4 has the lowest fragility curve. It should be noted that the fragilities presented in Fig. 4.17(a) were generated for the undegraded (or intact) building. However, the aftershock fragilities presented in Fig. 4.17(b) were calculated for the mainshock-damaged (or degraded) model. Since the degraded model was used in Fig. 4.17(b), the fragility curve for DS1 was equal to zero indicating that all of the 22 earthquake records cause the building model to reach 1% drift during the MCE level mainshock. Also, it is observed in Fig. 4.17(b) that DS2, DS3 and DS4 have lower fragility curves compared to the similar fragility curves in Fig. 4.17(b) where the undegraded model was used.

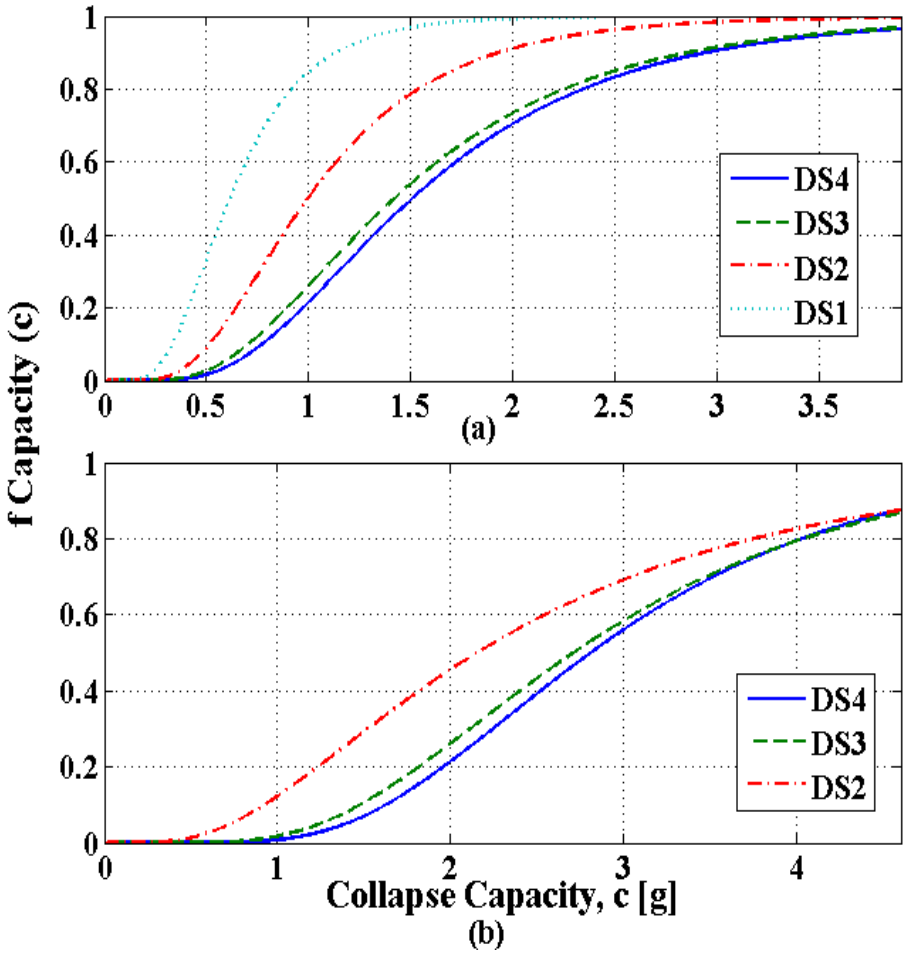

Figure 4.17 Fragility curves computed by NLTHA for the 4-story building with 4% design drift and P_{NE}=50% (a) mainshock collapse fragility curves for the undegraded (intact) system (b) aftershock collapse fragility curves for degraded system (Note: The aftershock fragilities were plotted only for the buildings survived from the MCE level mainshock)

Table 4.14 shows the average collapse spectral acceleration values for the intact and degraded models. The values in the first row of Table 4.14 for the intact model were computed by taking the average of the collapse spectral accelerations from the mainshock analysis of the undegraded model. However, the second row of the table presents the average spectral acceleration values generated from the MS+AS analysis of the degraded model under an MCE level mainshock. Therefore, the second row of Table 4.14 has smaller values compared to the first row of the table which is associated with the undegraded (or intact) model. Note that the

average collapse spectral acceleration for the degraded model and DS1 is equal to zero indicating that all of the 22 earthquake records cause the collapse of the 4-story model in the MCE level mainshock.

Table 4.15. Average collapse spectral accelerations

From\To	DS1	DS2	DS3	DS4
Intact	0.93	1.52	2.21	2.34
Degraded	**0.00**	0.18	0.65	0.67

Table 4.15 presents the calculated collapse probabilities for different damage states. The first row of the table shows the collapse probabilities for the intact model in the mainshock analysis and, the second row of the table shows the collapse probabilities for the mainshock-damaged degraded model in the aftershock analysis.

A similar procedure to section 3.2 was followed for convolution of the fragility curves with the hazard curves and computing the collapse probabilities in 1 year. Eq. 1.9 was used to calculate the 50 year collapse probabilities presented in Table 4.15. As observed in Table 4.15, the collapse probabilities in the second row of the table which is associated with the degraded model are higher than the collapse probabilities in the first row of the table for the intact model. The solid line and the dashed line in Fig. 4.18 present the 50 year collapse probabilities for the intact and degraded model, respectively.

Table 4.16. Collapse probabilities in 50 years

From\To	DS1	DS2	DS3	DS4
Intact	0.001229	0.000568	0.000334	0.000291
Degraded	0.001229	0.000634	0.000366	0.000318

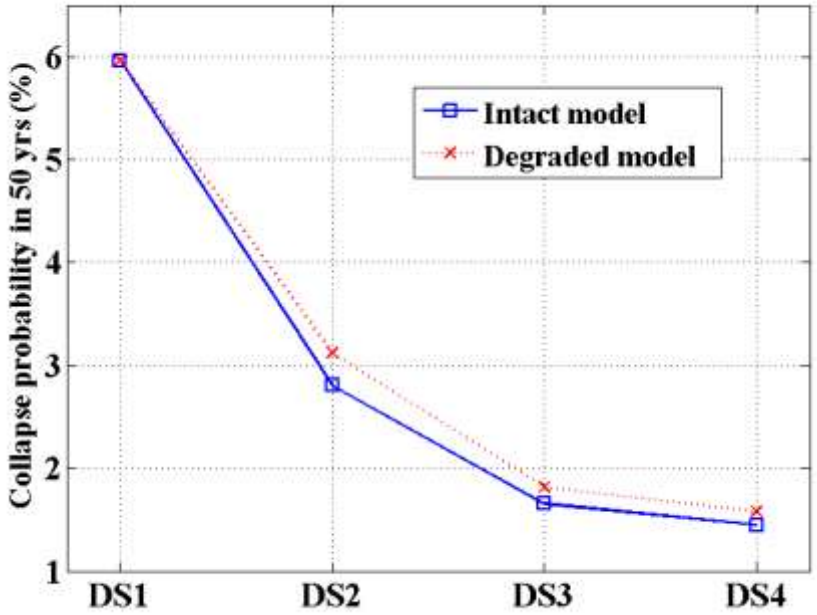

Figure 4.18 Collapse probabilities in 50 yrs for different damage states

The reliability indices associated with the 50 year collapse probabilities presented in Table 4.15 were shown in Table 4.16. The reliability indices associated with the degraded model are approximately 0.95%, 0.75% and 0.7% less than the similar values for the intact model for DS2, DS3 and DS4, respectively. The collapse probabilities and reliability indices for the intact model and degraded model were equal in case of DS1 since, there was no survived model from the MCE level mainshock.

Table 4.17. Reliability indices for 50 yrs collapse probabilities

From\To	DS1	DS2	DS3	DS4
Intact	3.03	3.25	3.40	3.44
Degraded	3.03	3.22	3.38	3.42

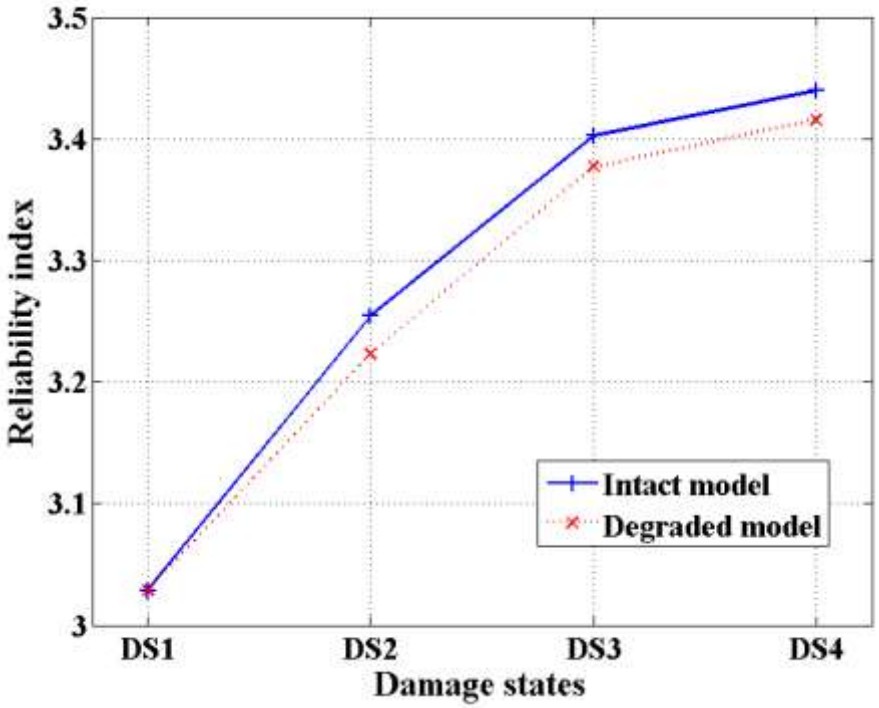

Figure 4.19 Reliability indices for different damage states (Note: Reliability indices were calculated for 50 yrs collapse probabilities presented in Fig. 4.17)

As observed in Fig. 4.19, the degraded model has smaller reliability indices compared to the intact model. This means that the mainshock-damaged degraded model is more susceptible to collapse than the undamaged model which is reasonable.

CHAPTER FIVE: EFFECT OF AFTERSHOCK INTENSITY ON SEISMIC COLLAPSE PROBABILITIES

This chapter examines the sensitivity of a mainshock (MS)-damaged building's collapse probability to aftershock earthquake intensity. Fig. 5.1 shows the shift in the collapse fragility curve which is due to the aftershock effect. As observed in Fig 5.1, the collapse S_a associated with a single value on the collapse fragility curve is smaller in the MS+AS case. This means that the collapse occurs sooner in the case of MS+AS due to the shift to the left resulting from the aftershocks.

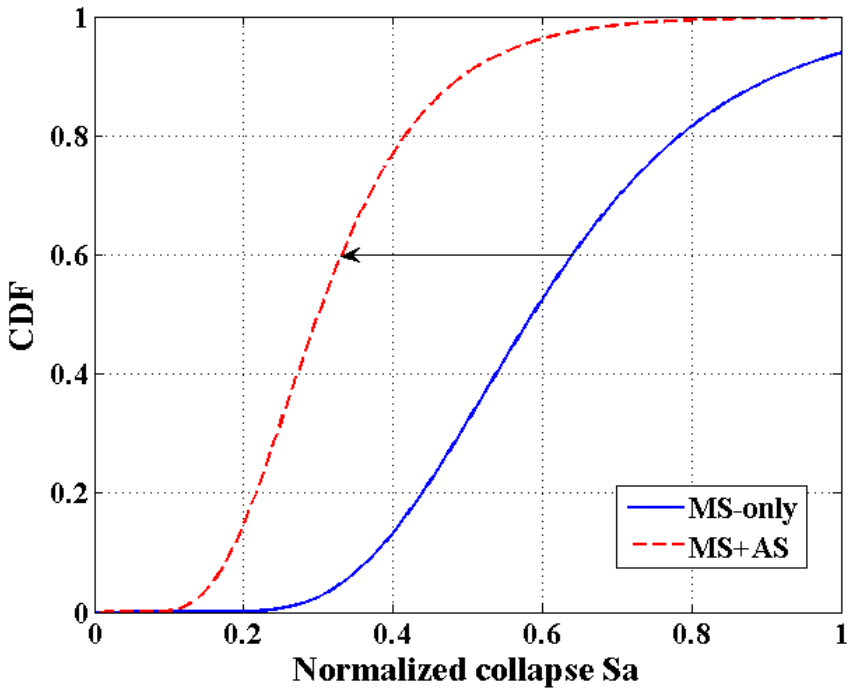

Figure 5.1 Collapse fragility curves for MS-only case (solid line) and MS+AS case (dashed line)

Specifically, the effect of earthquake magnitude and spatial distribution of aftershocks on collapse fragilities was investigated. Aftershock (AS) fragilities for different site-to-source

distances are generated via incremental dynamic analysis (IDA) using a sequence of MS+AS ground motions. The effect of MS damage is to alter the fragilities which can be quantified for the building investigated.

5.1. Methodology

Earthquake intensity is dependent on several parameters including two key parameters: earthquake magnitude and site-to-source distance. Therefore, a logical procedure to investigate the effect of earthquake intensity is to investigate the effect of modifying the earthquake magnitude or the site-to-source within an attenuation equation on the probability of building collapse.

In this chapter, two cases are investigated; case no. 1, with the magnitude parameter as a variable and a fixed site-to-source-parameter and case no. 2, with the site-to-source distance and a fixed magnitude. Scenarios for MS+AS analysis for a hypothetical (or generic) site in California were used to quantify this sensitivity. For scenarios in case no. 1, the AS site-to-source distance is fixed at 10 kilometers and the AS magnitudes are varied over the range of M7.2 down to M6.3. For the scenarios in case no. 2, the AS magnitude was fixed at M6.7 and the AS site-to-source distances varied over the range of 5 up to 25 kilometers. Recall that in both cases it is only the AS that is varied, and the MS magnitude and the MS site-to-source-distance are fixed at M7.3 and 10 kilometers, respectively. Figure 5.2 presents a flowchart summarizing the steps followed in this chapter to develop fragilities for MS-damaged buildings in aftershocks.

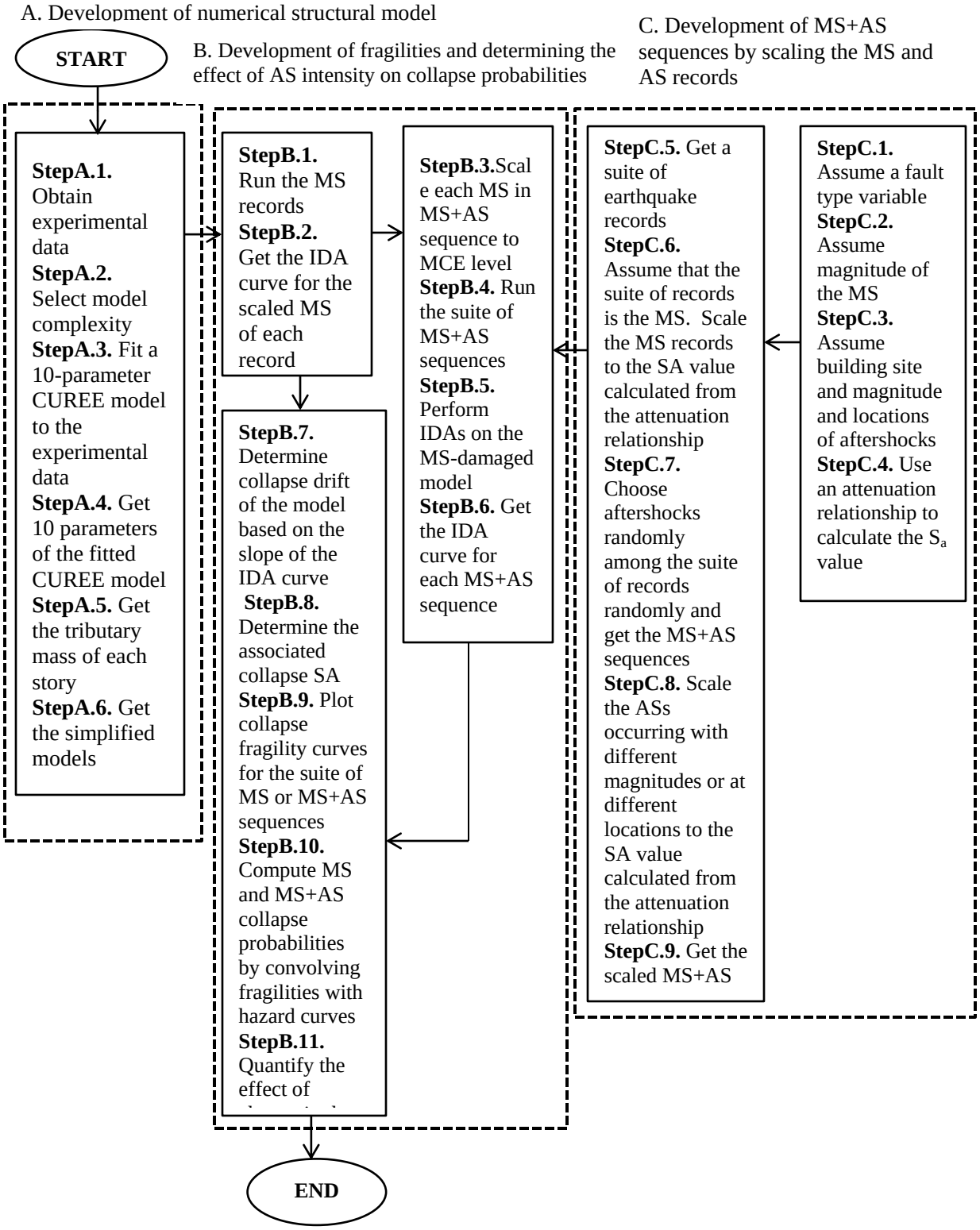

Figure 5.2. Flowchart of the steps followed in the procedure

Section A of the flowchart contains the steps required for development of the numerical structural model. The first step is to obtain the experimental data for the hysteresis loops for each story of a building from resources such as NEEShub (www.nees.org). However, it is noted here that a purely analytical model could be used, if desired by the analyst. In the present case, the 10-parameter CUREE (Consortium of Universities for Research in Earthquake Engineering) model was fit to this data. The complexity of the model must also be determined, which can range from a single degree of freedom (DOF) to a complex nonlinear finite element model. Section C of Fig. 5.2 outlines the steps for development of the scaled MS+AS scenarios through the use of an attenuation relationship. Section B of Fig. 5.2, which is the main branch of the flowchart, uses the information from sections A and C such as the degraded hysteresis information and MS+AS sequences in order to compute the total collapse fragilities under the effect of MS and AS. Then, the effect of AS intensity can be investigated based on the variation of collapse fragilities and the collapse probabilities obtained in this section.

5.2. Development of Numerical Structural Model

The two-story structure introduced in the building portfolio (see section 2.1) was used as an illustrative (or working) example in this chapter. Initially, existing experimental data is obtained in order to accurately model the seismic behavior of the structure. However, as mentioned it is equally possible to utilize a comprehensive analytical model without the use of experimental data. The CUREE model calibrated for the two-story building in Chapter Three was used as a simplified 2-DOF model in the illustrative example. See Table 3.1 for 10 parameters of the CUREE model at each story of the building. Sequence of MS+AS were used in

the analysis. In other words, the degraded model with residual deformation (degraded stiffness and strength from the MS demand) was used to generate the aftershock IDA curves.

5.3. Mainshock + Aftershock Sequence Simulation

The suite of 22 far field (ordinary) ground motions (FEMA, 2009) presented in Table 2.3 were used in the analysis in this chapter. It is assumed that site-to-source distance can be altered, but it should be kept in mind that as the distance decreases below 10 kilometers the velocity of the records has been shown to change and produce pulse-like velocity profiles, but that near fault effect is beyond the scope of the current effort.

In this study, the NGA relationship developed by Abrahamson and Silva (2008) was used for scaling. In all cases, the fault type is set constant as a normal-oblique fault. Fig. 5.2 shows the fault geometry and the parameters used in the NGA relationship. The site-to-source distance parameter used in this dissertation is the parameter R_x defined as the horizontal distance from top of rupture measured perpendicular to fault strike (see Fig. 5.3). The mainshocks and aftershocks of specified moment magnitude and site-to-source-distance are used in the attenuation relationship at the natural period of the building (T_n=0.2 seconds) with 5% elastic damping to determine the response spectrum for record scaling.

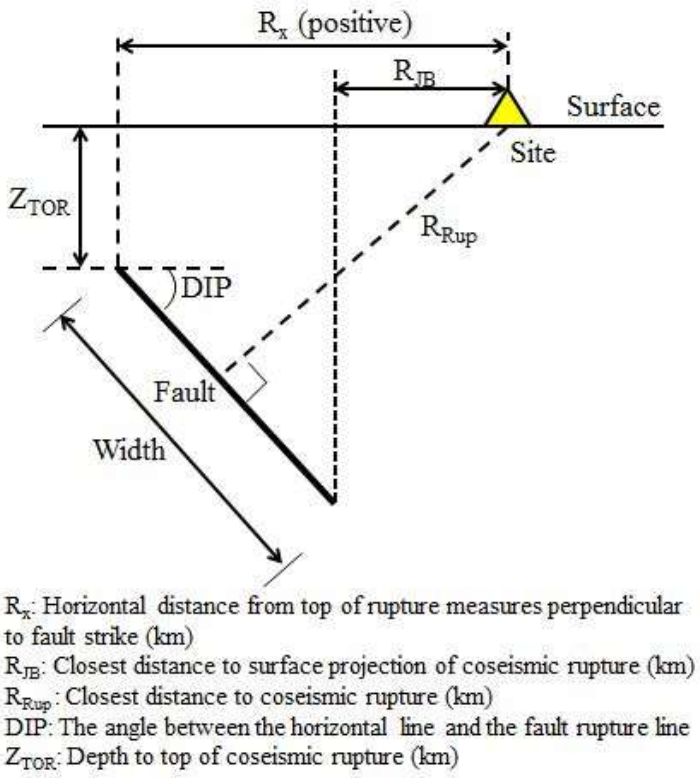

Figure 5.3. Definition of fault geometry and distance measures for reverse or normal faulting, hanging-wall site

The reason that the mainshocks and aftershocks are scaled to the spectral acceleration calculated from attenuation relationships is to be able to show the lower intensity level of aftershocks compared to the mainshocks. Since, the aftershocks usually have smaller magnitude than the mainshock. For instance, the spectral acceleration value for a M7.3 mainshock and a M6.8 aftershock were calculated to be 2.17g and a smaller value of 1.09g, respectively. Then, in order to get the IDA curves for the AS, the different levels of S_a will be multiplied by the value of 2.17g and, the MS fragilities are generated using the IDA curves. Similarly, in the AS case the S_a levels will be multiplied by the smaller value of 1.09g and the IDA curves are generated.

The AS intensity values for the scenarios in the two cases introduced in section 5.1 are presented in Table 5.1.

Table 5.1. Aftershock intensity levels for case no. 1

Case No. 1	variable: Magnitude	Aftershock Intensity, Sa (g)
Scenario No. 1	MS(M7.3)	2.17
Scenario No. 2	MS+AS(M7.2)	1.50
Scenario No. 3	MS+AS(M7)	1.43
Scenario No. 4	MS+AS(M6.8)	1.09
Scenario No. 5	MS+AS(M6.7)	0.94
Scenario No. 6	MS+AS(M6.4)	0.59
Scenario No. 7	MS+AS(M6.3)	0.51

Table 5.2. Aftershock intensity levels for case no. 2

Case No. 2	variable: Site-to-source distance	Aftershock Intensity, Sa (g)
Scenario No. 1	MS(M7.3)	2.17
Scenario No. 2	MS+AS(R5)	0.83
Scenario No. 3	MS+AS(R10)	0.51
Scenario No. 4	MS+AS(R15)	0.36
Scenario No. 5	MS+AS(R20)	0.28
Scenario No. 6	MS+AS(R25)	0.22

In order to determine the MS+AS sequences, the aftershocks are generated on a random basis from the suite of 22 earthquakes. The MS is scaled to a (Maximum Considered Earthquake) MCE level associated with the location of the structure. For example, an MCE with a spectral acceleration of 2.4g for Los Angeles, CA was used in the example presented in this chapter. These MCE level mainshocks degrade the model for the AS analysis.

5.4. Development of Fragilities and Determining the Effect of Aftershock Intensity on Collapse Probabilities

The initial process involves using the procedure to generate MS fragilities described in section 2.4 of this dissertation. Once the IDA curves are developed, the collapse spectral accelerations associated with the collapse drift (7%) were used to generate the MS fragility curve. Similar to the MS-only analysis, the collapse spectral accelerations are then determined for all 22 MS+AS earthquake records using the process explained in section 2.4 of this dissertation. Figures 8.3 and 8.4 show the cumulative probability of exceedance versus normalized collapse S_a curves for different scenarios for case no. 1 and case no. 2 (see section 4.1). The development of AS fragility curves is based on using only the earthquake records that do not cause the collapse of the building model. Aftershock intensities presented in Tables 5.1 and 5.2 were used for scaling the earthquake records in each scenario of cases no. 1 and 2, respectively.

The MS+AS fragility curves were conditioned on the occurrence of the previous MCE level MS. However the MS-only fragility curve presented in Figures 5.4(a) and 5.5(a) were not conditioned on the occurrence of a previous earthquake. Therefore, it should be noted that the fragility curve presented in Figures 5.4(a) and 5.5(a) for MS-only cannot be compared to the MS+AS fragility curves in Figures 5.4(b) and 5.5(b).

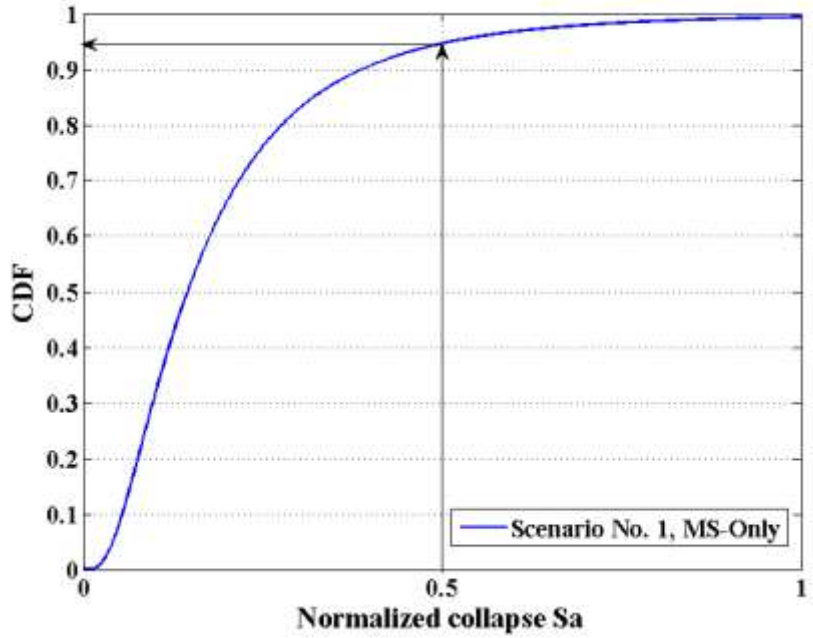

(a)

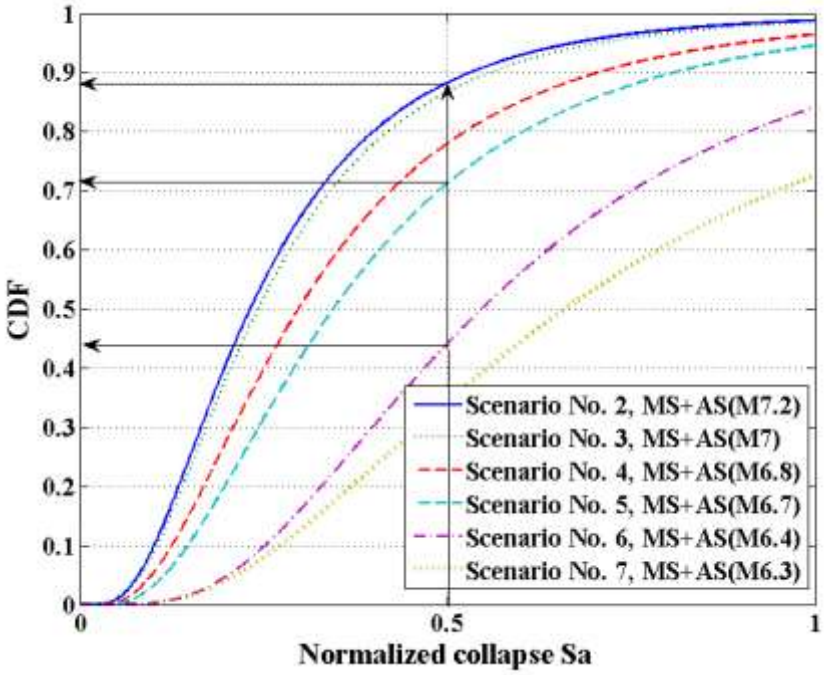

(b)

Figure 5.4 Fragility curves for different scenarios in case no. 1, (a) MS-Only scenario, (b) MS+AS scenarios

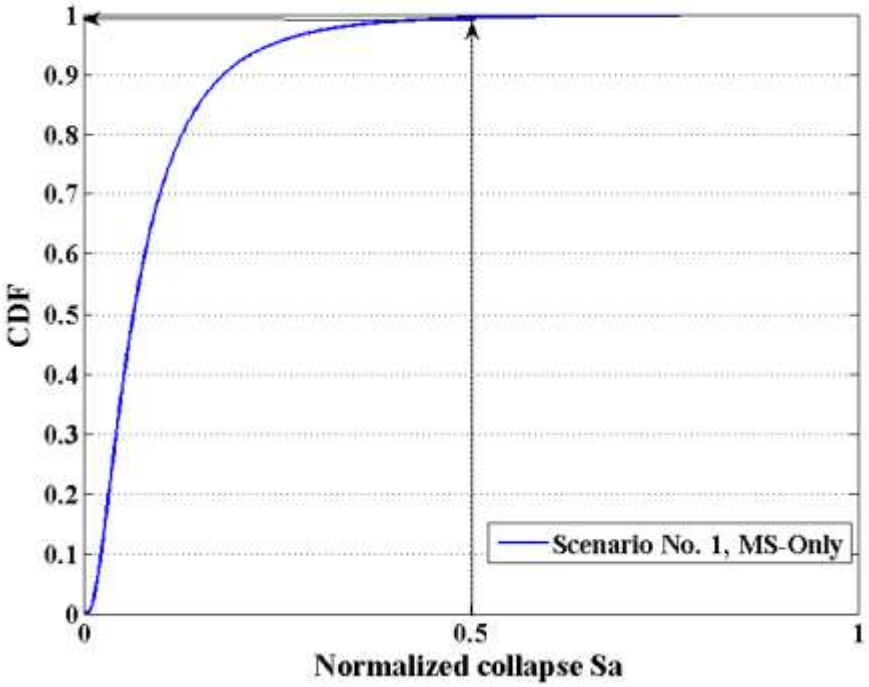

(a)

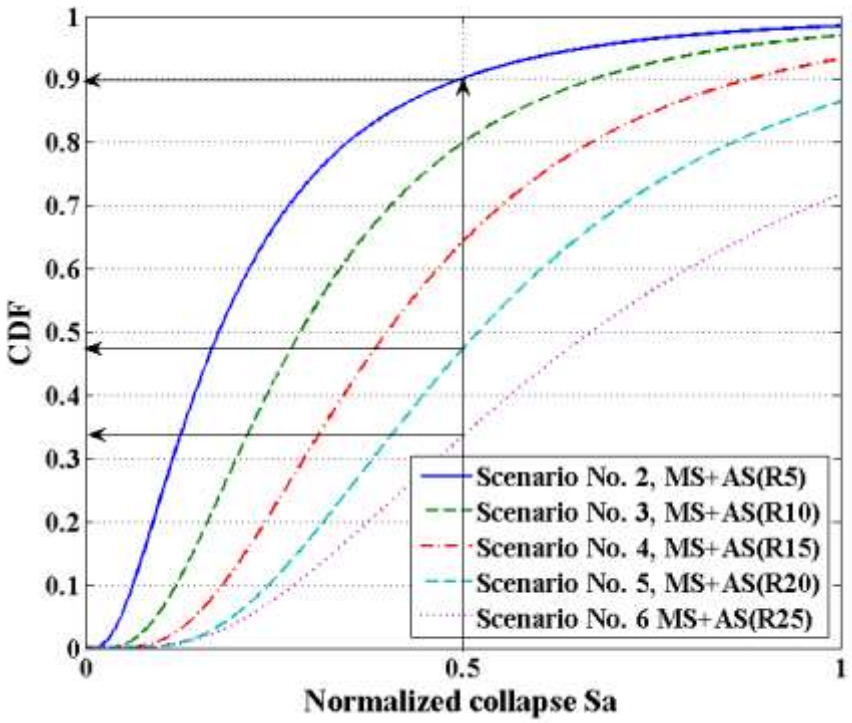

(b)

Figure 5.5 Fragility curves for different scenarios in case no. 2, (a) MS-Only scenario, (b) MS+AS scenarios

The mean and standard deviation for the different MS+AS scenarios are provided in Tables 4.3 and 4.4 as a means of comparison between the fragility curves. Note that the lognormal curve parameters are associated with the MS+AS collapse probability conditioned on the occurrence of the MS.

Table 5.3. Fragility curve parameters for magnitude distribution of aftershocks

Case No. 1	variable: Magnitude	Mean	Std. dev.
Scenario No. 1	MS(M7.3)	0.02	0.77
Scenario No. 2	MS+AS(M7.2)	0.48	0.65
Scenario No. 3	MS+AS(M7)	0.53	0.65
Scenario No. 4	MS+AS(M6.8)	0.73	0.65
Scenario No. 5	MS+AS(M6.7)	0.88	0.67
Scenario No. 6	MS+AS(M6.4)	1.34	0.60
Scenario No. 7	MS+AS(M6.3)	1.53	0.69

Table 5.4. Fragility curve parameters for spatial distribution of aftershocks

Case No. 2	variable: Site-to-source distance	Mean	Std. dev.
Scenario No. 1	MS(M7.3)	0.01	0.81
Scenario No. 2	MS+AS(R5)	1.02	0.81
Scenario No. 3	MS+AS(R10)	1.50	0.67
Scenario No. 4	MS+AS(R15)	1.84	0.61
Scenario No. 5	MS+AS(R20)	2.10	0.59
Scenario No. 6	MS+AS(R25)	2.35	0.69

Fig. 5.6 presents the AS intensity versus mean and standard deviation of fitted lognormal parameters, respectively. It is observed that the mean has an overall linear increasing trend with decreasing AS intensity for both cases of AS magnitude and spatial distribution. However, the standard deviation does not have any specific trend with increasing AS intensity for the cases of magnitude and spatial sensitivity analysis. As it was observed in Fig. 5.4(b) and 5.5(b), the fragility curve associated with the highest AS intensity is above the other fragility curves

meaning that the probability of exceedance is higher for higher AS intensities as it was expected. By comparison of the AS intensity values presented in Tables 5.1 and 5.2 with the values of mean and standard deviation in Tables 5.3 and 5.4, it is observed that the least mean is associated with the highest AS intensity value.

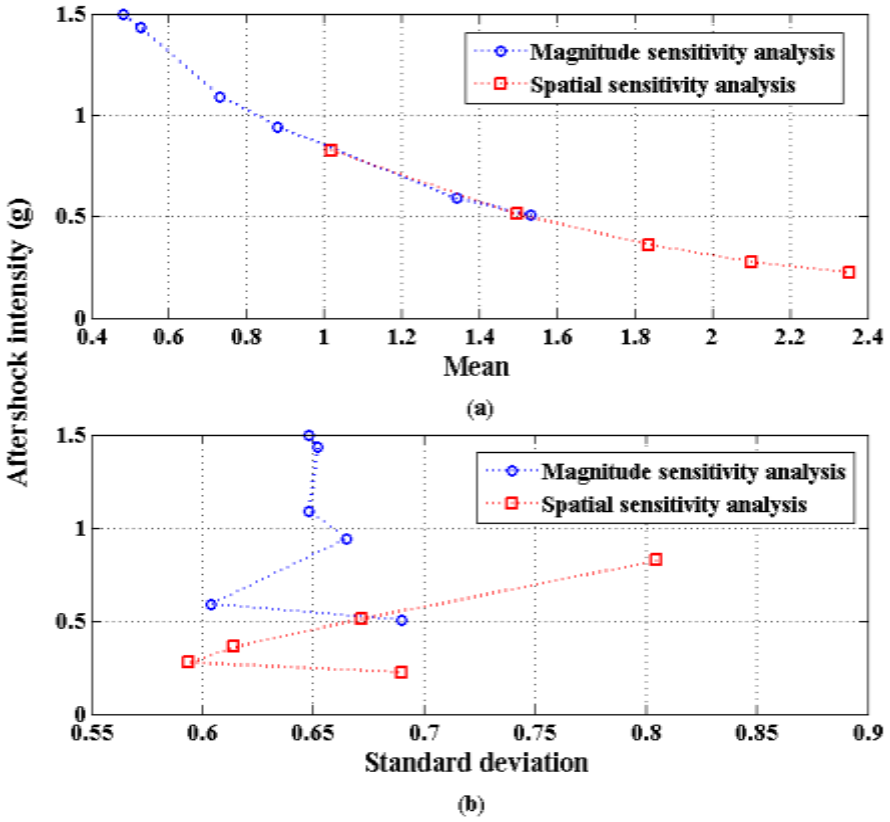

Figure 5.6 Fitted lognormal curve parameters to the MS+AS fragility curves in each scenario (a) Mean, (b) Standard deviation

The conditional probability of collapse (the fragility) determined using nonlinear time history analysis (NLTHA) can then be convolved with the site-specific seismic hazard curve to determine the unconditional probability of collapse when the structure is subjected to a MS at the prescribed magnitude as explained in section 2.5 of this dissertation. The probability of exceedance of different scenarios can be computed using Eq. 1.8. The MS and MS+AS fragility

curves were convolved with the associated MS and AS hazard curves, respectively to compute the MS collapse probability (P(MS)) and AS collapse probability (P(AS)). The MS hazard curve for Los Angeles, CA which was presented earlier in Fig. 3.7 was used to compute the MS collapse probability. The AS hazard curve for the same location was generated based on the procedure presented by Yeo and Cornell (2005). Eq. 1.8 was used to calculate the mean aftershock rates. The developed AS hazard curve in Fig. 3.7 was then used to calculate the AS collapse probability. Note that the MS+AS collapse probability is similar to the AS collapse probability since the occurrence of an AS is dependent on the occurrence of the previous MS.

Figures 5.7 and 5.8 show the calculation of the MS and AS collapse probabilities for scenario no. 1 and 2 in case no. 1. The first subplot presented in Fig. 5.7 is the MS hazard curve which is convolved with the PDF form of the MS fragility curve. The area under the third subplot in Fig. 5.7 is 0.002307 which is equal to the MS collapse probability. The AS collapse probability for scenario no. 2 in case 1 was computed with a similar procedure except that the AS hazard curve (see the first subplot in Fig. 5.8) was used in the AS probability calculation.

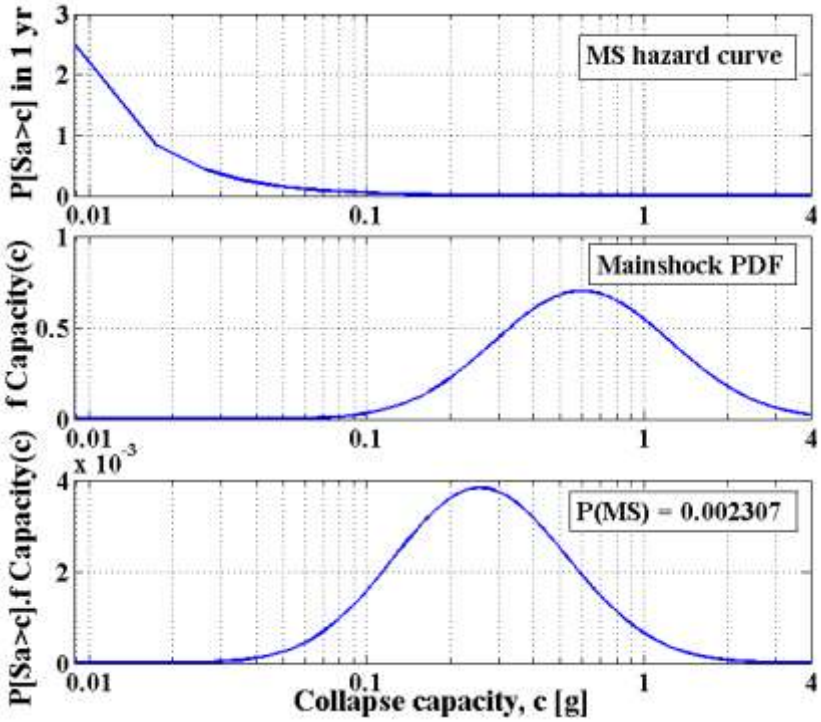

Figure 5.7 Calculation of the risk integral of the probability of collapse in 1 year for the two-story model for MS

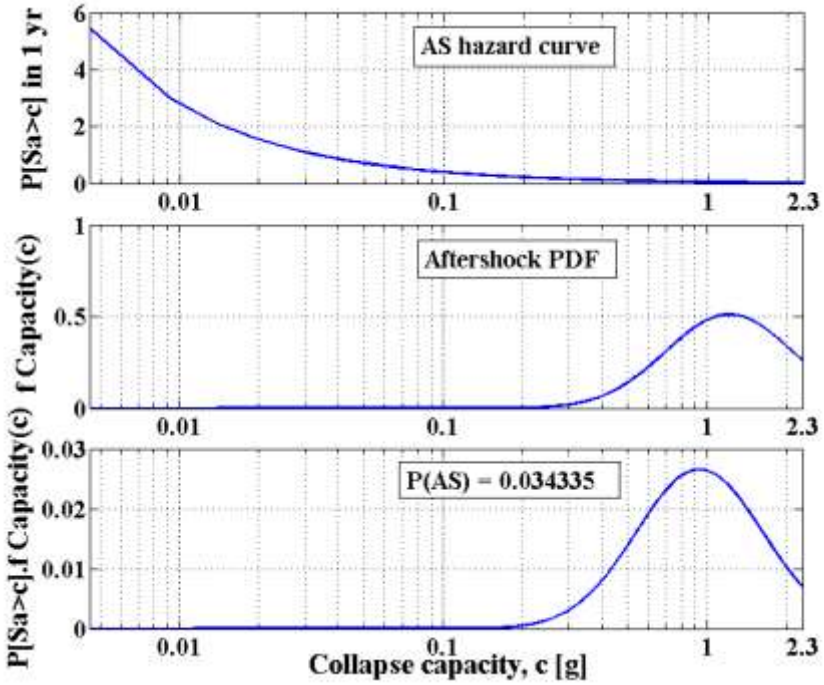

Figure 5.8 Calculation of the risk integral of the probability of collapse in 1 year for the two-story model for AS

Tables 5.5 and 5.6 present the total MS and AS collapse probabilities for different scenarios in two cases of magnitude and spatial distribution of aftershocks. The total probability theorem presented in Eq. 1.8 was used to calculate the total collapse probabilities in 1 year. Eq. 1.9 was used to compute the associated 50 years collapse probabilities of each scenario.

Table 5.5. Total collapse probabilities for case no. 1

Case No. 1	variable: Magnitude	P(AS)	1 yr collapse probability	50 yrs collapse probability (%)
Scenario No. 1	**MS(M7.3)**	**-**	**P(MS)=0.002307**	**10.91**
Scenario No. 2	**MS+AS(M7.2)**	**0.034335**	**0.002386**	**11.26**
Scenario No. 3	MS+AS(M7)	0.034104	0.002385	11.26
Scenario No. 4	MS+AS(M6.8)	0.030244	0.002377	11.22
Scenario No. 5	MS+AS(M6.7)	0.027041	0.002369	11.18
Scenario No. 6	MS+AS(M6.4)	0.017643	0.002348	11.09
Scenario No. 7	MS+AS(M6.3)	0.015510	0.002343	11.07

Table 5.6. Total collapse probabilities for case no. 2

Case No. 2	variable: Magnitude	P(AS)	1 yr collapse probability	50 yrs collapse probability (%)
Scenario No. 1	MS(R10)	-	P(MS)=0.002307	**10.91**
Scenario No. 2	MS+AS(R5)	0.023295	0.002361	11.15
Scenario No. 3	MS+AS(R10)	0.015476	0.002343	11.06
Scenario No. 4	MS+AS(R15)	0.011579	0.002334	11.02
Scenario No. 5	MS+AS(R20)	0.009156	0.002328	11.00
Scenario No. 6	MS+AS(R25)	0.007648	0.002324	10.98

The variation of 50 years collapse probabilities with respect to the AS moment and site-to-distance are presented in Fig. 5.9(a) and Fig. 5.9(b), respectively. The collapse probability for MS-only scenario in both cases is less than the collapse probability values for MS+AS scenarios as it was expected. The 50 years collapse probability for both cases is 10.91% which is shown in bold in Tables 5.5 and 5.6. The total collapse probabilities calculated for different scenarios in case no. 1 show a reasonable trend. These values increase with increase in the AS intensity due to the increase in the AS magnitude (see Table 5.5 and Fig. 5.9(a)). However, the total collapse

probabilities computed for case no. 2 show a decreasing trend with increasing the site-to-source distance of aftershocks which results in decreasing the AS intensities.

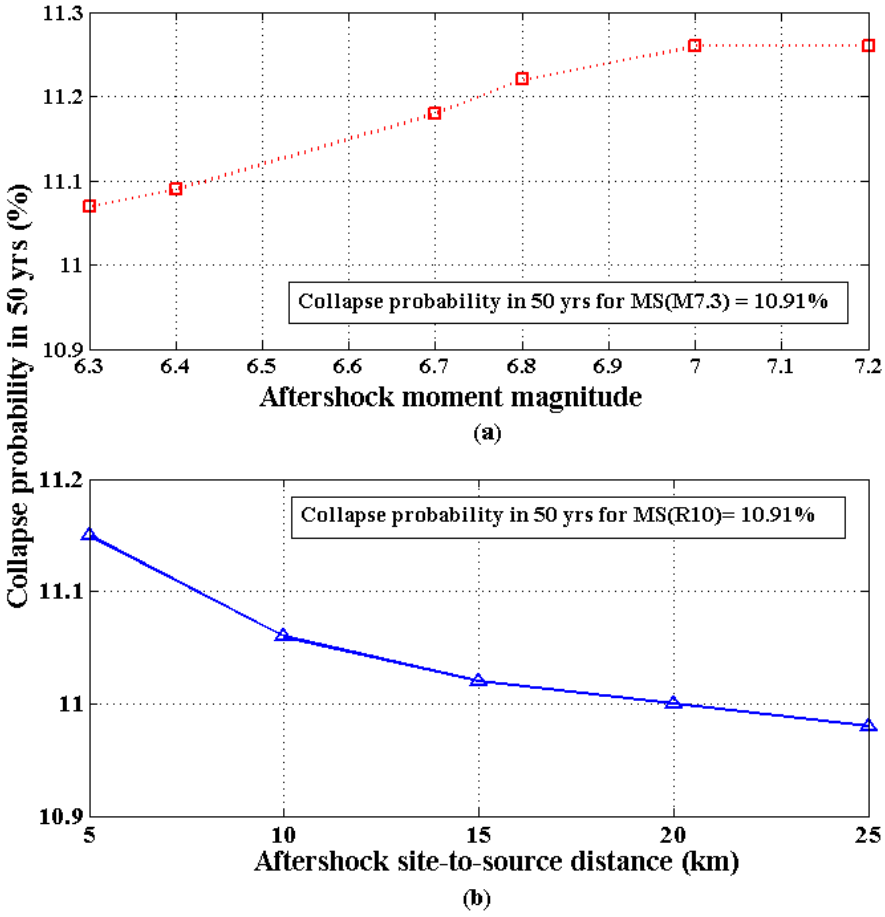

Figure 5.9 Collapse probabilities in 50 years (a) Magnitude sensitivity analysis, case no. 1, (b) Spatial sensitivity analysis, case no. 2

CHAPTER SIX: SUMMARY, CONCLUSIONS AND RECOMMENDATIONS

6.1. Summary

Based on the evidence and observations in previous earthquakes it is becoming increasingly evident that considering the aftershocks is necessary to ensure safe structures. Although, the importance of multiple earthquakes in the progressive damage to the structures has been observed, current design codes for buildings do not take into account multiple earthquakes in the assessment and design of structures. To date, the probability of aftershocks has not been included in Performance-Based Engineering (PBE) and this dissertation develops and explains a new methodology to include aftershock hazard in PBE. The key finding in this dissertation is the development of a methodology to integrate the aftershock hazard into Direct Displacement Design (DDD) by quantifying the changes needed in design due to the aftershock effects. The developed methodology can be applied to any structure provided that a simplified global level model of the structure with strength and stiffness degradation accurately represented, is available. Each structure was modeled as an n-Degree of Freedom (DOF) model with lumped masses at each story. The spring model used to represent each story of the building should have the capability to account for the degradation of the model during the mainshock earthquake. This degraded model can be used in the subsequent nonlinear time-history analysis (NLTHA) for the aftershock. In this study, the well-known 10-parameter CUREE model was used to model the behavior and include the stiffness and strength degradation of the woodframe building model during the mainshock earthquake. The major contributions to the field of this dissertation are summarized as follows:

1) The total collapse probabilities for the MS-only case and MS+AS case were computed for a building portfolio by convolving the collapse fragilities with the hazard curves. The building should then be modified to account for the aftershock effects such that the MS+AS collapse probability is equal to the MS-only collapse probability for the original building. This was the key concept used throughout this dissertation in order to quantify the needed change in performance-based design due to the aftershock hazard effects.
2) The needed change in the two parameters of the CUREE model due to the aftershock effects was investigated for the two-, four- and six-story buildings in the portfolio.
3) A comprehensive sensitivity analysis was performed in this study to examine the effect of different parameters such as the number of stories and the location of the building on the needed change in design due to aftershock effects.
4) A methodology was developed that can serve as a model for application to all types of buildings and other structures to incorporate the effect of aftershock hazard into performance-based earthquake engineering.

6.2. Conclusions

The main conclusions of the research study are summarized as follows:

1) Using the methodology developed in this study, the needed changes in the stiffness and strength parameters of the CUREE model was quantified for the two-, four- and six-story buildings introduced in the portfolio. This could be extended to other model types.
2) The effect of the number of stories in the building was investigated through application of the methodology developed in this study on three buildings. These buildings include a two-, four- and six-story buildings designed using DDD approach for 4% design drift and

50% probability of non-exceedance (P_{NE}). It was observed the needed change in design is very small for the two-story low-rise buildings compared to that of the four- and six-story buildings. The calculated X_v calculated for Los Angeles, CA with a MS(M8)+AS(M7) scenario are 1.05, 1.24 and 1.35 for the two-, four and six-story buildings with the assumption that the design drift of the buildings is 4% and a non-exceedance probability is 50% using the DDD approach.

3) The needed change in design for the two-, four- and six-story buildings are investigated once for a high seismic hazard zone such as Los Angeles, CA and once for a low seismic hazard zone such as Sacramento, CA. It was observed that the needed change in design is negligible for both low-rise and mid-rise woodframe buildings in the low seismic hazard zone of Sacramento, CA. For example the base shear adjustment factor, X_v calculated for Los Angeles, CA with a MS(M8)+AS(M7) scenario are 1.05, 1.24 and 1.35 for the two-, four and six-story buildings designed for 4% design drift and P_{NE}=50 using the DDD approach. However, the X_v values are 1.004, 1.008, 1.022 for the two-, four and six-story buildings, respectively.
4) The effect of the design drift for the original building was also investigated through analysis of a four- and six-story building to P_{NE} of 50% and design drifts of 4%, 3% and 2% using DDD approach. As expected, the needed change in design is less for the stronger building which was designed originally for a smaller design drift using the DDD approach.
5) The effect of magnitude of the mainshock and aftershock was examined by using different MS+AS scenarios. The effect of mainshock and aftershock magnitude was also included in the generation of the aftershock hazard curves and, it was observed that the

mainshock magnitude has a considerable effect on the mean aftershock rates. This results in a considerable effect of mainshock magnitude on the needed change in design due to the aftershock effects.

6) The needed change in design shows a reasonable trend with the change in the magnitude of the mainshock and aftershock. However, this change in design is very sensitive to the mainshock magnitude.

7) The needed change in design was also computed for different MS+AS scenarios for the two-, four and six-story buildings. It was observed that the needed change in design (or base shear adjustment factor, X_v) calculated for the four- and six-story mid-rise woodframe buildings is more sensitive to the changes in aftershock magnitude compared to the low-rise two-story woodframe building.

8) The elapsed time after the mainshock, denoted as t and the duration after time t, denoted as T have a considerable effect on the computed mean rate of aftershocks, μ^*. The mean aftershock rate μ^* is used in generating the aftershock hazard curve which is convolved with the MS+AS collapse fragilities. Therefore, scenarios with different time intervals of (t, t+T) will result in different changes in design due to the aftershock effects (or different base shear adjustment factors, X_v). It was observed that the base shear adjustment factors for different time intervals, (t, t+T) follow a similar trend to that of the mean aftershock rate, μ^*. The base shear adjustment factors have a decreasing trend with increasing the elapsed time from the mainshock, t. Also, the base shear adjustment factor follows an increasing trend with increasing the duration being considered after the elapsed time from the mainshock (T). The base shear adjustment factors is no longer sensitive to the duration of T after T=1000 days. It was observed that the effect of aftershock hazard

becomes negligible after 1000 days from the initial mainshock (see Yeo and Cornell, 2005). The effect of aftershock hazard was also investigated on collapse probabilities for different damage states.

6.3. Recommendations

The methodology to integrate the aftershock hazard in PBE has been demonstrated in this study, but future research work needs to be oriented towards application of this methodology to other types of structures such as steel and concrete buildings. This will require some modifications in the spring model used to represent each story of the building at the global level. Since, the stiffness and strength degradation of a building is also dependent on the type of the material used, improvement in nonlinear numerical modeling such as detailed Finite Element Models (FEM) is also desired, provided the computational needs do not become intractable.

The aftershock hazard curves used in this study are generated using the generic California model parameters. Therefore, the needed change in design due to aftershock effects were calculated only for the buildings located in California. However, the needed change in design can be investigated for other locations by extrapolation of the results computed for California. This can be achieved by generating the aftershock hazards for other locations using the associated model parameters. The collapse fragilities for the buildings designed for each location should be convolved with the aftershock hazard curve for each location.

In this dissertation a procedure proposed by Yeo and Cornell (2005) was used to generate the aftershock hazard curves. But, their procedure was only applicable when the intensity measure (IM) used in the horizontal axis of the aftershock hazard curve is Peak Ground Motion

(PGA). However, the intensity measure is more useful in terms of Spectral acceleration (S_a) for the purpose of convolution with the collapse fragility curves. An approximate approach was used for conversion of the intensity measure from PGA to S_a in this study. A more accurate procedure is desirable for this conversion to generate more precise aftershock hazard curves.

The probabilities of occurrence for aftershocks of different magnitudes are different after the initial mainshock (Reasenberg, 1994). For example, the probability is higher for a M5.5 aftershock compared to a M7 aftershock assuming that a M8 mainshock has already occurred. Therefore, it is conservative if the change needed in design is calculated by considering the worst case scenario of MS(M8)+AS(M7) for the initial mainshock of M8. In this dissertation, the probabilities of occurrence for aftershocks of different magnitudes were used as weights in order to adjust the conservative base shear adjustment factor, X_v computed for the MS(M8)+AS(M7). Although, Reasenberg (1994) generated the probabilities of occurrence of aftershocks of different magnitudes for the Loma Prieta earthquake using Bayesian model parameters, it was assumed that these probabilities can be used in this study. Probabilities of occurrence should be revised based from the parameters taken from the generic California model used in this study.

The needed change due to the aftershock effects was examined on only two parameters of the CUREE model. These parameters are the stiffness and strength in this study. More investigation is required to find the needed changes in other parameters of the CUREE model especially the parameters that account for the degradation of the model such as α and β.

REFERENCES

Abrahamson, N. A., Silva, W. J. (1997) "Empirical Response Spectral Attenuation Relations for Shallow Crustal Earthquakes", *Seismological Research Letters*, 68(1).

Abrahamson, N. A., Silva, W. J. (2008) "Summary of the Abrahamson and Silva NGA ground-motion relations," Earthquake Spectra 24, 67-97.

Abdelnaby, A., (2012) "Multiple Earthquake Effects on Degrading Reinforced Concrete Structures," (Doctoral Dissertation), University of Illinois at Urbana-Champaign, http://hdl.handle.net/2142/34345, Retrieved March 15 2014.

Allameh Zadeh, M. (2004) "Prediction of aftershocks pattern distribution using self-organising feature maps," In 13th World Conference on Earthquake Engineering, August 2004. paper no. 198, Vancouver, B.C., Canada.

Al-Hajjar, J., Blanpain, O. (1997) "Semi-Markovian approach for modeling seismic aftershocks," Engineering Structures 19(12), 969-976.

Alessandri, S. et al. (2014) "Assessment of the Seismic Response of a Base Isolated HV Circuit Breaker with Steel Cabled Dampers," Second European Conference on Earthquake Engineering and Seismology, Istanbul, August 25-29, 2014.

Alliard, P.M., Léger, P. (2008) "Earthquake Safety Evaluation of Gravity Dams Considering Aftershocks and Reduced Drainage Efficiency," Journal of Engineering Mechanics Asce, 134(1), p. 12-22.

ASCE (2005) "Minimum Design Loads for Buildings and Other Structures," (ASCE Standard 7 05, Including Supplement No. 1). American Society of Civil Engineers, Reston, VA.

ATC-63. (2009) "Quantification of building seismic performance factors," FEMA P695, Redwood City, CA.

Bachman R.E., Hamburger R.O., Comartin C.D., Rojahn C., Whittaker A.S. "ATC-58 Framework for Performance-Based Design of Nonstructural Components," ATC-29-2 Seminar on Seismic Design, Performance, and Retrofit of Nonstructural Components in Critical Facilities. 2003: Applied Technology Council. 49-61.

Bahmani, P., van de Lindt, J., and Dao, T. (2013) "Displacement-based design of buildings with torsion: Theory and verification," J. Struct. Eng., 10.1061/(ASCE)ST.1943-541X.0000896, 04014020.

Baker, J. W., and Cornell, C. A. (2005) “A vector-valued ground motion intensity measure consisting of spectral acceleration and epsilon,” Earthquake Eng. Struct. Dyn., 34(10), 1193–1217.

Båth, Markus (1965) "Lateral inhomogeneities in the upper mantle," Tectonophysics 2: 483–514. Bibcode:1965Tectp.2.483B. doi:10.1016/0040-1951(65)90003-X.

Bazzurro, P., Cornell, C.A., Menun, C. and Motahari, M. (2004) “Guidelines for seismic assessment of damaged buildings,” In: Proceedings of the 13th World Conference on Earthquake Engineering, Vancouver, Canada.

Benavent-Climent, A. (2007) “An Energy-Based Damage Model for Seismic Response of Steel Structures,” Earthquake Engng. Struct. Dyn., 36;1049-1064.

Benjamin, J.R., and Cornell, C.A. (1970) “Probability, statistics, and decision for civil engineers,” New York, McGraw-Hill

Bernal, D., (1992) “Instability of buildings subjected to earthquakes,” Journal of Structural Engineering 118(8): 2239–2260.

Bradley, B., Cubrinovski M., (2011) “Near-source strong ground motions observed in the 22 February 2011 Christchurch earthquake,” *Bulletin of the New Zealand Society of Earthquake Engineering*, Special Issue on the 22 February 2011 Christchurch earthquake, 2011, 44(4), 205-226.

Chai, Y.H., Romstad, K.M, Bird, S.M. (1995) “Energy-Based Linear Damage Model for High Intensity Seismic Loading,” J. of Struct. Eng., ASCE 1995; 121(5):857-864.

Christovasilis, I., Filliatrault, A., Wanitkorkul, A. (2010) “NW-01: Seismic Testing of a Full-scale Two-story Light-Frame Wood Building: NEESWood Benchmark Test,” http://nees.org/resources/551.

Christophersen, A., Smith, E. “ A Global Model for Aftershock Behaviour,” Paper presented 12th World Conference on Earthquake Engineering, Auckland, New Zealand, January-February 2000.

Christophersen, A., Gerstenberger, M., Rhoades, D., Stirling, M. (2011) “Quantifying the effect of declustering on probabilistic seismic hazard,” Ninth Pacific Conference on Earthquake Engineering. Auckland, New Zealand.

Christophersen, A., Rhoades, D., Hainzl, S. (2013) “Sensitivity study of aftershock occurrence for a Wellington Fault earthquake,” *Paper presented at the New Zealand Society for Earthquake Engineering Technical Conference*, Wellington, New Zealand.

Cornell, C. A. (1968). Engineering seismic risk analysis. Bulletin of the Seismological Society of America, 58, 1503–1606.

Cornell, C.A., Krawinkler, H. (2000) “Progress and challenges in seismic performance assessment,” PEER Center News 3, No. 2.

Cosenza E, Manfredi G. (2000) “Damage indices and damage measures,” Progress in Structural Engineering and Materials 2000;2(1):50–9.

Deam, B.L. (2005) “A displacement-focused, force-based structural design procedure,” Wairakei: NZSEE Annual Technical Conference and AGM, 11-13 Mar, 2005. 8.

Deierlein, G. (2004) “Overview of a Comprehensive Framework for Earthquake Performance Assessment,” Proceedings of the International Workshop on performance-based seismic design concepts and implementation, Bled, Slovenia, *Pacific Earthquake Engineering Research Center,* PEER Report 2004/05: 15-26, Berkley, CA.

Douglas Zechar, J., Schorlemmer, D., Werner, M.J., Gerstenberger, M.C., Rhoades, D.A., Jordan, T.H. (2007) “Regional Earthquake Likelihood Models I: First-order results,” *Bulletin of the Seismological Society of America,* 103(2a).

Dreger, D. and B. Savage (1998) “Aftershocks of the 1952 Kern County, California, Earthquake Sequence,” Bull. Seism. Soc. Am., 89 , 1094–1108.

Ellingwood, B. R. (1998) “Reliability-based performance concept for building construction,” Structural engineering world wide 1998 paper T178-4 (CD-ROM), Elsevier.

Ellingwood, B. (2000) “Performance-based design: Structural reliability considerations,” Proc., Structures Congress 2000: Advanced technology in civil engineering, SEI/ASCE, New York.

Ellingwood, B.R., D.V. Rosowsky, Y. Li and J.H. Kim (2004), “Fragility assessment of light-frame wood construction subjected to wind and earthquake hazards,” J. Struct. Engrg. ASCE 130(12):1921-1930.

Federal Emergency Management Agency (FEMA), (2009) “Quantification of Building Seismic Performance Factors,” *FEMA Report P695,* Washington, D.C.

Federal Emergency Management Agency (FEMA), (2004a), “NEHRP Recommended Provisions for Seismic Regulations for New Buildings and Other Structures,” FEMA 450-1/2003 Edition, Part 1: Provisions, Federal Emergency Management Agency, Washington, DC.

Federal Emergency Management Agency (FEMA), (2004b) “NEHRP Recommended Provisions for Seismic Regulations for New Buildings and Other Structures, FEMA 450-2/2003 Edition, Part 2: Commentary, Federal Emergency Management Agency, Washington, DC.

Folz, B., and Filiatrault, A. (2004a) “Seismic analysis of woodframe structures I: model formulation,” J. Struct. Eng., 10.1061/(ASCE)0733-9445 (2004)130:9(1353), 1353–1360.

Folz, B., and Filiatrault, A. (2004b). “Seismic analysis of woodframe structures. II: Model implementation and verification,” J. Struct. Eng., 130(9), 1426–1434.

Gerstenberger, M. C., Jones, L. M., Wiemier, S. (2007) “Short-term Aftershock Probabilities: Case Studies in California,” Seismol. Res. Lett. 78, 66-77, doi:10.1785/gssrl.78.1.66.

Gutenberg, B. and Richter, C.F. (1949) “Seismieity of the Earth and Associated Phenomena,” Princeton Univ.Press, Princeton, NJ., l-273.

Haselton, C., Baker, J., Liel, A., Dierlin, G., (2011) “Accounting for ground motion spectral shape characteristics in structural collapse assessment through an adjustment for epsilon”, Journal of Structural Engineering, 137(3), 332-334.

Hauksson, E., Jones, L.M., Hutton, K. and Eberhart-Phillips, D. (1993) “The 1992 Landers earthquake sequence: Seismological observations,” Journal of Geophysical Research 98: doi: 10.1029/93JB02384. issn: 0148-0227.

Ibarra , L. (2003) “Global Collapse of Frame Structures under Seismic Excitations,” PhD Dissertation of CEE, Stanford University, 2003.

Ibarra, L.F., Medina, R.A., and Krawinkler, H. (2005) “Hysteretic models that incorporate strength and stiffness deterioration,” Earthquake Engineering and Structural Dynamics, Vol. 34, pp. 1489-1511.

Jennings, E., van de Lindt,J.W. (2014) “Numerical retrofit study of light-frame wood buildings using shape memory alloy devices as seismic response modification devices,” J. Struct. Eng. 2014;140(7):04014041.

Kagan, Y. and, Huston, H. (2005) “Relation between mainsock rupture process and Omori’s law for aftershock moment release rate,” Geophys. J. Int., 163(3), 1039-1048.

Khashaee, P. (2005) “Damage-Based Seismic Design of Structures” Earthquake Spectra, Vol. 21,No. 2, pp. 459-468.

Krawinkler, H., and Zhorei, M. (1983) "Cumulative damage in steel structures subjected to earthquake ground motions,” Camp. and Struct., 16(1-4),531-541.

Krawinkler, H. and Zareian F., Lignos D. and Ibarra L., CA (2009) “Prediction of Collapse of Structures under Earthquake Excitations,” *Computational Methods in Structural Dynamics and Earthquake Engineering*, 22-24.

Lew M. et al., (2000) "The significance of the 21 September 1999 Chi-Chi earthquake, Taiwan, for tall buildings," STRUC DES T, 9(2), pp. 67-72.

Li, Q., Ellingwood, B. (2007) “Performance evaluation and damage assessment of steel frame buildings under mainshock-aftershock sequences,” Earthquake Engineering and Structural Dynamics **26**, 405-427.

Li, Y. and Ellingwood, B.R. (2007b) “Reliability of Wood-Frame Residential Construction Subjected to Earthquakes,” Structural Safety, 29(4), 294-307.

Li, Y., Song, R., and van de Lindt, J.W. (2014) “Collapse Fragility of Steel Structures Subjected to Earthquake Mainshock-Aftershock Sequences,” Journal of Structural Engineering, (In press).

Li, Y., Yin, Y., Ellingwood, B. R., and Bulleit, W. M. (2010) “Uniform Hazard Versus Uniform Risk Bases for Performance-Based Earthquake Engineering of Light-Frame Wood Construction,” Earthquake Engineering and Structural Dynamics 39, 1199-1217.

Liang, H., Wen, Y. K., and Foliente, G. (2011) “Damage modeling and damage limit state criterion for wood-frame buildings subjected to seismic loads,” J. Struct. Eng., 137(1), 41–48.

Liel, A.B., Haselton, C.B., Dierlein, GG, Baker, J.W. (2009) “Incorporating Modeling Uncertainties in the Assessment of Seismic Collapse Risk of Buildings,” Structural Safety 2009; 31(2):197-211.

Luco, N. Bazzurro, P., Cornell, C.A. (2004) “Dynamic versus static computation of the residual capacity of a mainshock-damaged building to withstand an aftershock,” 13th World Conference on Earthquake Engineering, Vancouver, Canada, No. 2405, New Zealand Society of Earthquake Engineers.

Luco, N., Ellingwood B. R., Ronald O. H., et al. (2007) “Risk-targeted versus current seismic design maps for the conterminous United States” In: SEAOC 2007 Convention Proceedings.

Luco N, Gerstenberger MC, Uma SR, et al. (2011) “A Methodology for Post-Mainshock Probabilistic Assessment of Building Collapse Risk,” Proceedings of the 9th Pacific Conference on Earthquake Engineering.

Malekpour, S. and Dashti, F. (2012) “Application of the Direct Displacement Based Design Methodology for Different Types of RC Structural Systems,” Int. J. of Concrete Structures and Materials, Vol.7, No.2, pp.135-153, June 2013.

McGuire, R.K., Cornell, C.A., Toro, G.R. (2005) “The Case of Using Mean Seismic Hazard,” Earthquake Spectra, 23(3), 879-886.

Moehle, J. P., “A Framework for Performance-Based Earthquake Engineering,” Proceedings, Tenth U.S.-Japan Workshop on Improvement of Building Seismic Design and Construction Practices, 2003, ATC-15-9 Report, Applied Technology Council, Redwood City, CA.

Nakashima, M., Chusilp, P. (2003) “A partial view of Japanese post-Kobe seismic design and construction practices. Earthquake Engineering and Engineering Seismology, 4(1)3–13.

Nazari, N., van de Lindt, J.W., Li, Y. (2014) “Effect of Mainshock-Aftershock Sequences on Woodframe Building Damage Fragilities”, Accepted for publication in the ASCE Journal of Performance of Constructed Facilities, March, 2013.

Omori, F., Rigakushi (1894) “On the After-shocks of Earthquakes”, The Journal of College of Science, Imperial University, Japan, Vol. 7, part 2. Published by The University, Tokyo, Japan.

Park, S. and, Lindt, J. W. (2009) “ Formulation of Seismic Fragilities for a Wood-Frame Building Based on Visually Determined Damage Indexes,” Journal of Performance of Constructed Facilities, 346-352. 2009.

Parsons T. (2002) “Global Omori law decay of triggered earthquakes: Large aftershocks outside the classical aftershock zone,” J. Geophys. Res. 107:10.1029/2001JB000646.

Pei, S., van de Lindt, J. (2010) “User’s manual for SAPWood for windows seismic analysis package for woodframe structures,” NEEShub (nees.org); 2010.

Pei, S., and van de Lindt, J. W. (2009) “Coupled shear-bending formulation for seismic analysis of stacked shear wall systems,” Earthquake Eng. Struct. Dyn., 38(14), 1631–1647.

Pang, W., Rosowsky, D.V., Pei, S., van de Lindt., J.W. (2010) “Simplified Direct Displacement Design of a Six-Story Woodframe Building and Pre-Test Performance Assessment,” Journal of Structural Engineering 136 (7), 813-825.

Pang, W., Rosowsky, D., van de Lindt, J., Pei, S. (2009) “Simplified Direct Displacement Design of Six-story NEESWood Capstone Building and Pre-Test Seismic Performance Assessment,” NEESWood Report No. 5.

Pang, W. and Ziaei, E. (2012) “Nonlinear Dynamic Analysis of Soft-Story Light-Frame Wood Buildings,” Structures Congress 2012, 1767-1777.

Pang, W., Shirazi, S. (2013) “Corotational Model for Cyclic Analysis of Light-Frame Wood Shear Walls and Diaphragms,” ASCE Journal of Structural Engineering 139, SPECIAL ISSUE: NEES 2: Advances in Earthquake Engineering, 1303-1317.

Park, Y-J., and Ang, A. H-S. (1985) "Mechanistic seismic damage model for reinforced concrete," J. Struct. Engrg., ASCE, 111(4), 722-739.

Pei, S., van de Lindt, J.W. (2010) “User’s Manual for SAPWood for Windows: Seismic Analysis Package for Woodframe Structures,” Colorado State University, download available at: http://www.engr.colostate.edu/NEESWood/SAPWood.htm.

Pei, S., van de Lindt, J.W. (2010) "Methodology for Long-Term Seismic Loss Estimation: An Application to Woodframe Buildings," Structural Safety 31, 31-42.

Poljansek, K., Perus, I., Fajfar, P. (2009) "Hysteretic energy dissipation capacity and the cyclic to monotonic drift ratio for rectangular RC columns in flexure," Earthquake Engineering and Structural Dynamics, 38, 907-928.

Priestley, M.J.N. and Kowalski, M.J. (1998) "Aspects of Drift and Ductility Capacity of Cantilever Structural Walls," Bulletin, NZNSEE 31, 2.

Ramanathan, K., DesRoches, R., Padgett, J.E. (2010) "Analytical Fragility Curves for Seismically and Non-Seismically Designed Multi-Span Continuous Concrete Girder Bridges in Moderate Seismic Zones," Transportation Research Record: Journal of the Transportation Research Board , No. 2202, 173-182.

Reasenberg, P. A. and L. M. Jones (1989) "Earthquake hazard after a mainshock in California," Science, 243, 1173-1176, 1989.

Reasenberg, P. A. and L. M. Jones (1994) "Earthquake aftershocks: update," Science, 265, 1251-1252, 1994.

Rosowsky, D. V. (2002) "Reliability-based seismic design of wood shear walls," J. Struct. Eng., 128(11), 1439–1453.

Rosowsky, D. V., and Ellingwood, B. R. (2002) "Performance-based engineering of wood frame housing: Fragility analysis methodology," J. Struct. Eng., 128(1), 32–38.

Ryu, H., Luco, N., Uma S.R., Liel ,A.B. (2011) "Developing Fragilities for Mainshock-Damaged Structures through Incremental Dynamic Analysis," Proceedings of the Ninth pacific Conference on Earthquake Engineering, Auckland, New Zealand, New Zealand Society of Earthquake Engineers.

Scholz, C. H. (2002) "The mechanics of earthquakes and faulting, Cambridge University Press," Cambridge, U.K, 2nd Edition, ISBN: 9780521655408.

Shi, W., Lu, X.Z., Ye I.P., (2012) "Uniform-Risk-Targeted Seismic Design for Collapse Safety of Building Structures," Sci China Tech Sci, 55:1481-1488, doi: 10.1007/s11431-012-4808-7.

Shinozuka, M. and, Tan, R.Y. (1983) "Seismic Reliability of Damaged Concrete Beams," ASCE, J. of Str. Engr., July, 1983.

Shinozuka M, Feng MQ, Lee J, Naganuma T. (2000) "Statistical analysis of fragility curves," Journal of Engineering Mechanics, ASCE 2000;126(12):1224–31.

Smith, E., Christophersen, A. (2005) “A time of recurrence model for large earthquakes”, Paper presented at the New Zealand Society for Earthquake Engineering Technical Conference, Wellington, New Zealand.

Sucuoglu H, Erberik MA. (2004) “Energy based hysteresis and damage models for ˘ deteriorating systems,” Earthquake Engineering and Structural Dynamics 2004;33:69–88.

Tsai, Y., Huang, M. (2000) “Strong Ground Motion Characteristics of the Chi-Chi Taiwan Earthquake of September 21, 1999”, Earthquake Engineering and Engineering Seismology, 2(1) 1-21.

USGS (2013). http://earthquake.usgs.gov/hazards/designmaps/grdmotiondoc.php, access date: December 2013.

Utsu, T. (1969) “Aftershocks and earthquake statistics (I) Source parameters which characterize an aftershock sequence and their interrelations,” J.Fac. Sci., Hokkaido Univ., Ser., VII(3), 129-195.

Utsu, T., (1995), “The centenary of the Omori Formula for a decay law of aftershock activity”, Journal of the Physics of the Earth, 43:1-33.

Vamvatsikos, D., Cornell, C.A. (2002) “Incremental Dynamic Analysis,” Earthquake Engineering and Structural Dynamics 31, 491-514.

van de Lindt JW, Walz MA (2003) “Development and application of wood shear wall reliability model,” J Struct Eng 129:405–413.

van de Lindt and Gup van de Lindt, J. W. (2005). “Damage-based seismic reliability concept for woodframe structures,” J. Struct. Eng., 131(4), 668–675.

van de Lindt, J. W., and Gupta, R. (2006). “Damage and damage prediction for wood shearwalls subjected to simulated earthquake loads,” J. Perform. Constr. Facil., 20(2), 176–184.

van de Lindt, J.W. (2008) “Experimental Investigation of the Effect of Multiple Earthquakes on Woodframe Structural Integrity,” ASCE Practice Periodical on Structural Design and Construction, 13(3), 111-117.

van de Lindt, J.W., Pei, S., Liu, H., Filiatrault, A. (2010) “Seismic Response of a Full-Scale Light-Frame Wood Building: A Numerical Study,” ASCE Journal of Structural Engineering 136(1), 56-65.

van de Lindt, J.W., Pei, S., Pang, W., Shirazi, S. (2012) “Collapse Testing and Analysis of a Light-Frame Wood Garage Wall,” ASCE Journal of Structural Engineering 138 (4), 492-501.

van de Lindt, J.W., Nazari, N., Li, Y. (2013) "Effect of Seismic Aftershock Uncertainty on Mainshock Collapse Probabilities for Woodframe Buildings," 11th International Conference on Structural Safety and Reliability, June 16-20, 2013, Colombia University, New York, NY.

van de Lindt, J.W., Pei, S., Liu, H., Filiatrault, A. (2010) "Three-Dimensional Seismic Response of a Full-Scale Light-Frame Wood Building: Numerical Study," Journal of Structural Engineering 136(1), 56-65..

Wen X., Zhang P., Du F., Long F. (2009) "The background of historical and modern seismic activities of the occurrence of the 2008 Ms 8.0 Wenchuan, Sichuan, earthquake," Chin J Geophys 52:444–454 (in Chinese with English abstract).

Whitman, R.V. et al (1975) "Sismic Design Decision Analysis," ASCE, J. of Str. Div., May, 1975.

Whittaker, Bertero, Wight, Higashino, et. al. (1997) "Seismic Engineering Codes for Japan," Available from http://nisee.berkeley.edu/kobe/codes.html, cited December 2014.

Yamanaka, Y. (1990) "Configuration of the High-Velocity Slab Beneath the Kuril Arc.," Thesis, Univ. Tokyo, Tokyo, 24 pp.

Yeo, G., Cornell, C. (2005) "Stochastic Characterization and Decision Bases under Time-Dependent Aftershock Risk in Performance-Based Earthquake Engineering," PEER Report 2005/13, Pacific Earthquake Engineering Research Center, University of California, Berkley, http://peer.berkeley.edu/publications/peer_reports/reports_2005/reports_2005.html, 9/10/2012.

Yeo, G., Cornell, A (2009) "A Probabilistic Framework for Quantification of Aftershock Ground-Motion Hazard in California: Methodology and Parametric Study," Earthquake Engineering and Structural Dynamics; 38(1):45-60.

Yin, Y.J. and Li, Y. (2010) "Seismic Collapse Risk of Light-Frame Wood Construction Considering Aleatoric and Epistemic Uncertainties," Structural Safety, 32(4), 250–261.

Yin, Y.J., Li, Y. (2011) "Loss Estimation of Light-Frame Wood Construction Subjected to Mainshock-Aftershock Sequences," Journal of Performance of Constructed Facilities 25(6), 504-513.

Zareian, F., Krawinkler, H. (2007) "Assessment of Probability of Collapse and Design for Collapse Safety," Earthquake Engineering and Structural Dynamics; 36:1901-1914.

APPENDIX A

Seismic hazard for Los Angeles, CA and Sacramento, CA

Seismic Hazard for Los Angeles, CA:

Location: Longitude = 34.0537°, Latitude = -118.2427°

Seismic Design Category: D

Site Class: D (stiff soil)

Note that the spectral acceleration values determined following the requirements of ASCE 7-10 Standard using the USGS website (http://earthquake.usgs.gov/designmaps/us/application.php).

Mapped values for short and one-second spectral accelerations:

$S_s = 2.448$ g

$S_1 = 0.858$ g

Site Coefficients:

$F_a = 1$ [From ASCE 7-10, Table 11.4-1]

$F_v = 1.5$ [From ASCE 7-10, Table 11.4-1]

Maximum Credible Earthquake (MCE) [ASCE 7-10 Section 11.4]

$S_{Ms} = F_a \times S_s = 1 \times 2.448 = 2.448$ g

$S_{M1} = F_v \times S_1 = 1.5 \times 0.858 = 1.288$ g

Seismic Hazard for Sacramento, CA:

Location: Longitude = 38.5816°, Latitude = -121.4944°

Seismic Design Category: D

Site Class: D (stiff soil)

Mapped values for short and one-second spectral accelerations:

$S_s = 0.294$ g

$S_1 = 0.675$ g

Site Coefficients:

$F_a = 1.8$ [From ASCE 7-10, Table 11.4-1]

$F_v = 1.26$ [From ASCE 7-10, Table 11.4-1]

Maximum Credible Earthquake (MCE) [ASCE 7-10 Section 11.4]

$S_{Ms} = F_a \times S_s = 1.8 \times 0.294 = 0.532$ g

$S_{M1} = F_v \times S_1 = 1.5 \times 0.675 = 0.851$ g

APPENDIX B

Direct Displacement Design (DDD) design base shears for the buildings in the portfolio

Note that the displacement-based shear wall design database and the procedure provided by Pang et al. (2010) were used in this section. See Pang et al. (2010) for description of the parameters. The buildings are designed for MCE level spectral acceleration values.

Table B.1. Design base shears for the two-story building located in Los Angeles, CA

Story	Design Drift (%)	Vs(KN)	Design Drift (%)	Vs(KN)
2	4	307	0.5	369
1		423		512

Table B.2. Design base shears for the two-story building located in Sacramento, CA

Story	Design Drift (%)	Vs(KN)	Design Drift (%)	Vs(KN)
2	4	133	0.5	160
1		182		222

Table B.3. Design base shears for the four-story building located in Los Angeles, CA

Story	Design Drift (%)	Vs(KN)	Design Drift (%)	Vs(KN)	Design Drift (%)	Vs(KN)	Design Drift (%)	Vs(KN)
4	4	512	3	747	2	1219	1	1824
3		894		1308		2135		3194
2		1152		1681		2749		4106
1		1277		1868		3051		4559

Table B.4. Design base shears for the four-story building located in Sacramento, CA

Story	Design Drift (%)	Vs(KN)	Design Drift (%)	Vs(KN)	Design Drift (%)	Vs(KN)	Design Drift (%)	Vs(KN)
4	4	222	3	325	2	534	1	636
3		391		569		934		1112
2		503		734		1201		1428
1		556		814		1334		1584

Table B.5. Design base shears for the six-story building located in Los Angeles, CA

Story	Design Drift (%)	Vs(KN)	Design Drift (%)	Vs(KN)	Design Drift (%)	Vs(KN)	Design Drift (%)	Vs(KN)
6	4	191	3	276	2	454	1	1094
5		360		525		859		2073
4		489		712		1165		2811
3		583		854		1397		3367
2		649		952		1552		3750
1		685		1005		1641		3959

Table B.6. Design base shears for the six-story building located in Sacramento, CA

Story	Design Drift (%)	Vs(KN)	Design Drift (%)	Vs(KN)	Design Drift (%)	Vs(KN)	Design Drift (%)	Vs(KN)
6	4	85	3	120	2	200	1	391
5		156		231		374		738
4		214		311		507		1001
3		254		374		609		1201
2		285		414		676		1339
1		298		440		716		1410

APPENDIX C

Backbones for the buildings of the portfolio designed using the DDD approach

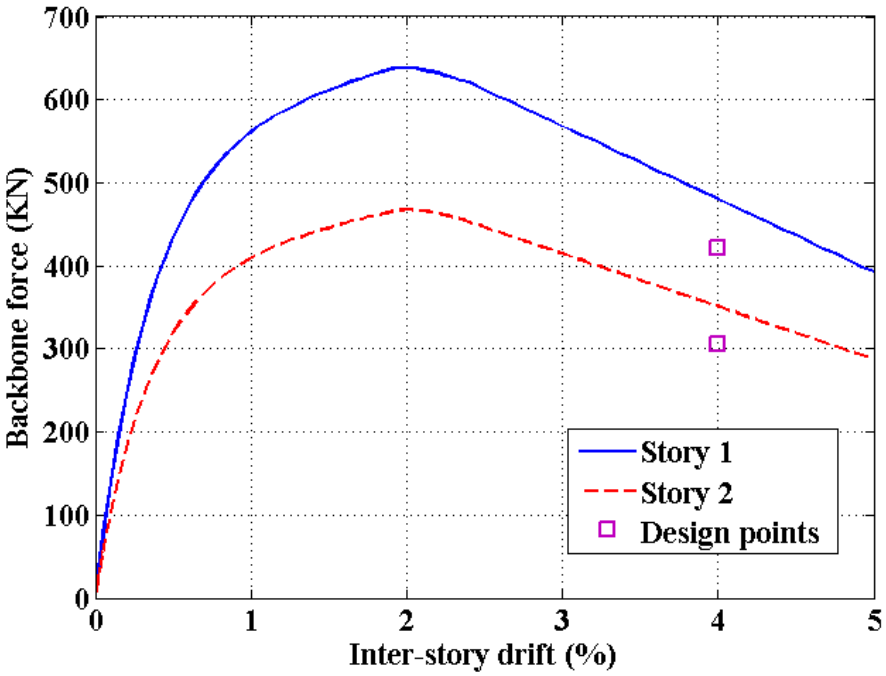

Figure C.1 Design points and inter-story backbone curves for the two-story building with 4% design drift, Location: Los Angeles, CA

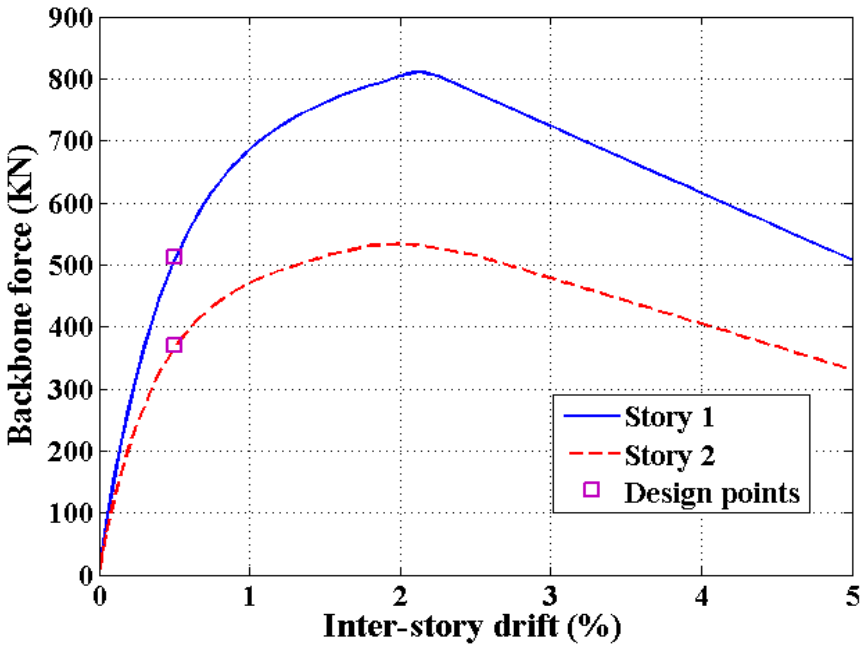

Figure C.2 Design points and inter-story backbone curves for the two-story building with 0.5% design drift, Location: Los Angeles, CA

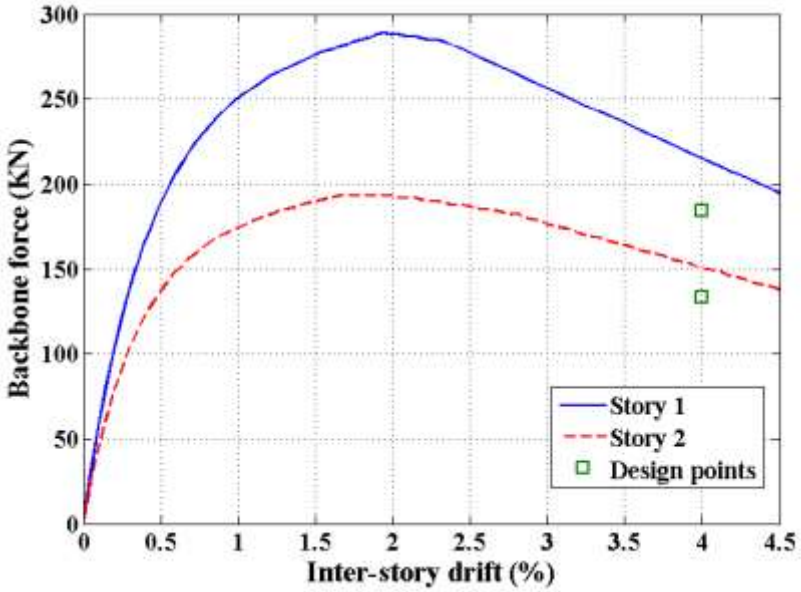

Figure C.3 Design points and inter-story backbone curves for the two-story building with 4% design drift, Location: Sacramento, CA

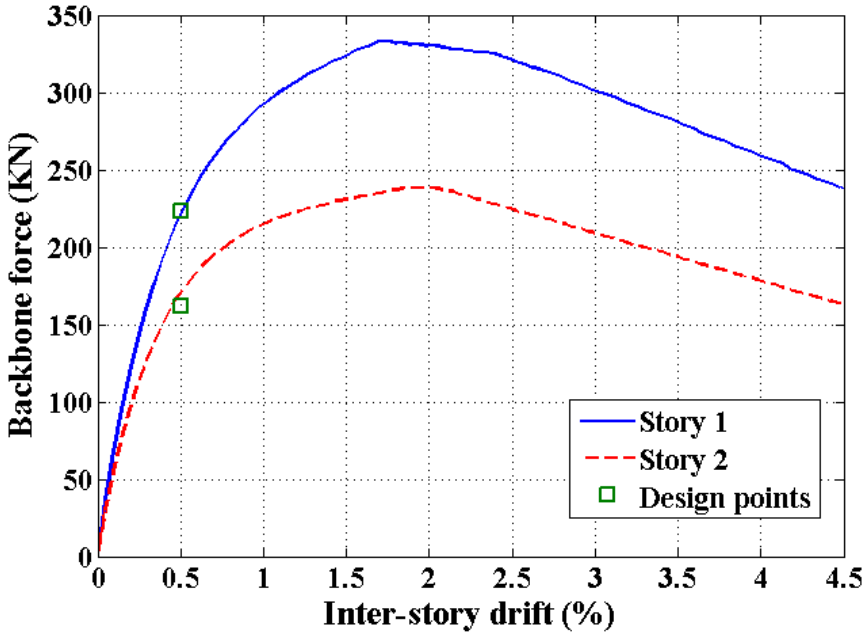

Figure C.4 Design points and inter-story backbone curves for the two-story building with 0.5% design drift, Location: Sacramento, CA

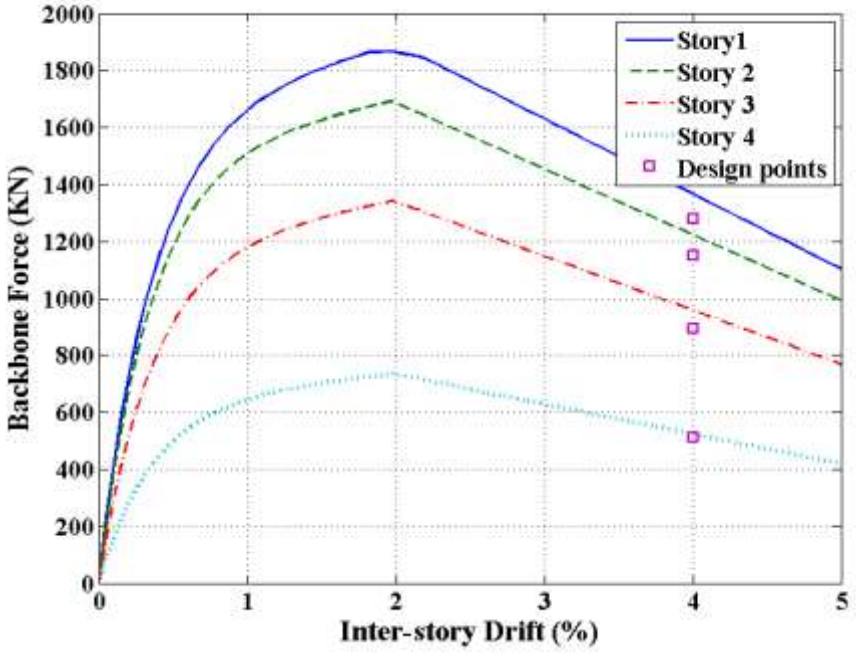

Figure C.5 Design points and inter-story backbone curves for the four-story building with 4% design drift, Location: Los Angeles, CA

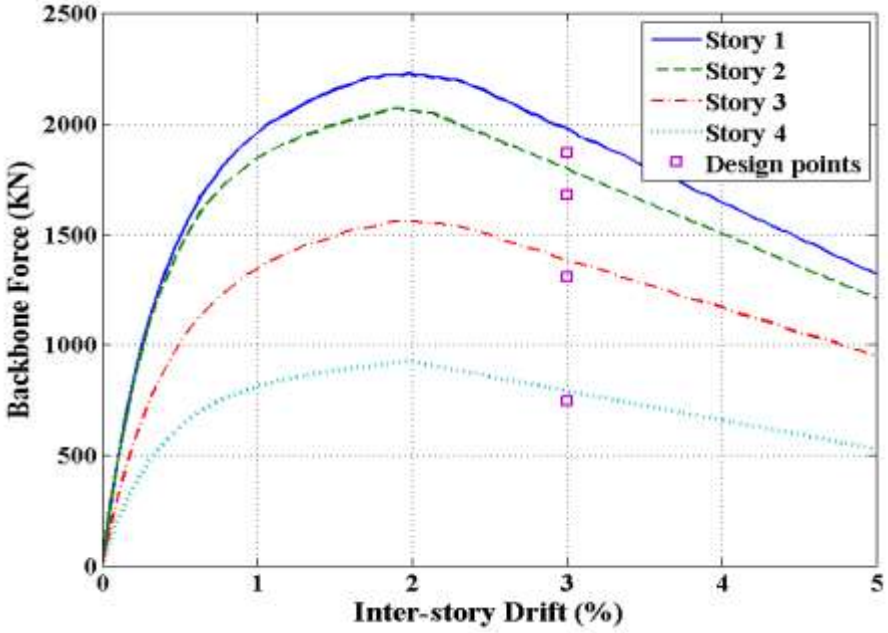

Figure C.6 Design points and inter-story backbone curves for the four-story building with 3% design drift, Location: Los Angeles, CA

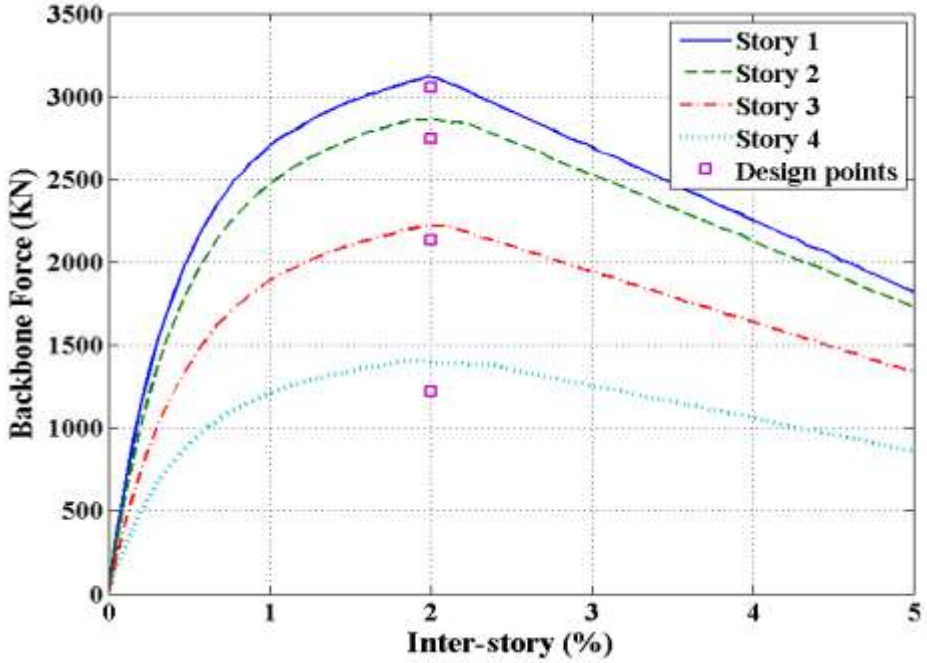

Figure C.7 Design points and inter-story backbone curves for the four-story building with 2% design drift, Location: Los Angeles, CA

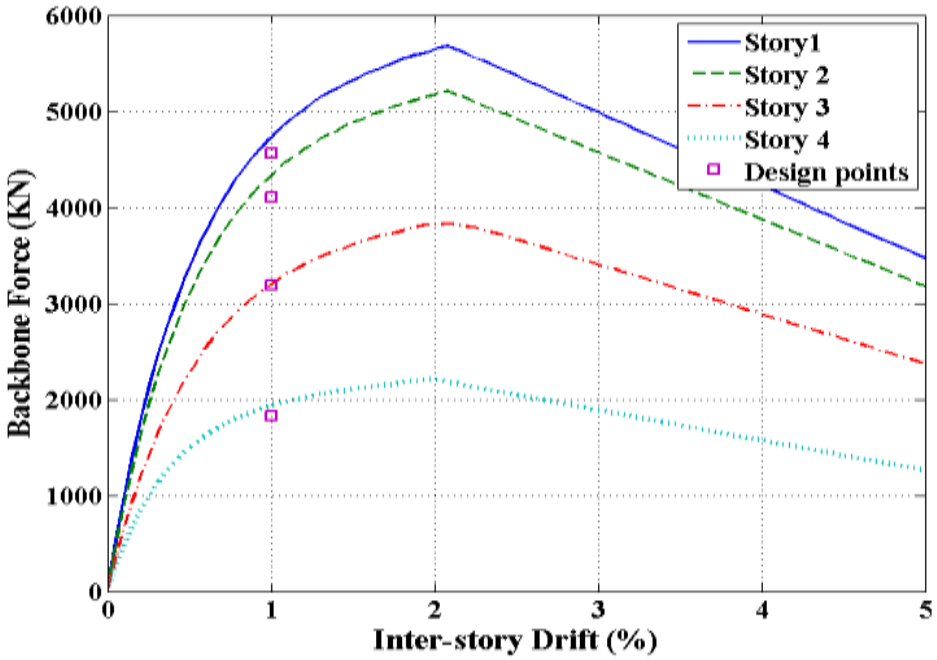

Figure C.8 Design points and inter-story backbone curves for the four-story building with 1% design drift, Location: Los Angeles, CA

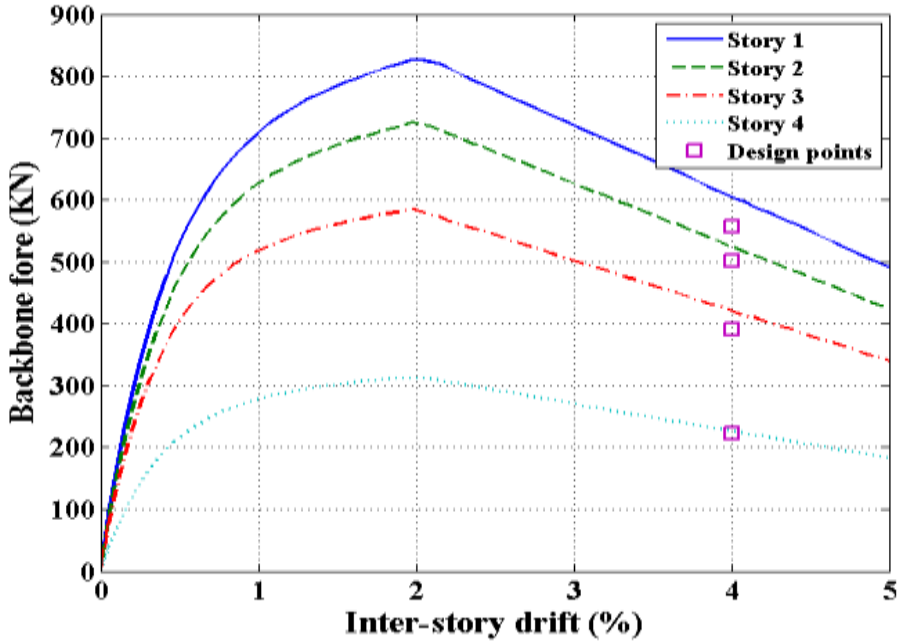

Figure C.9 Design points and inter-story backbone curves for the four-story building with 4% design drift, Location: Sacramento, CA

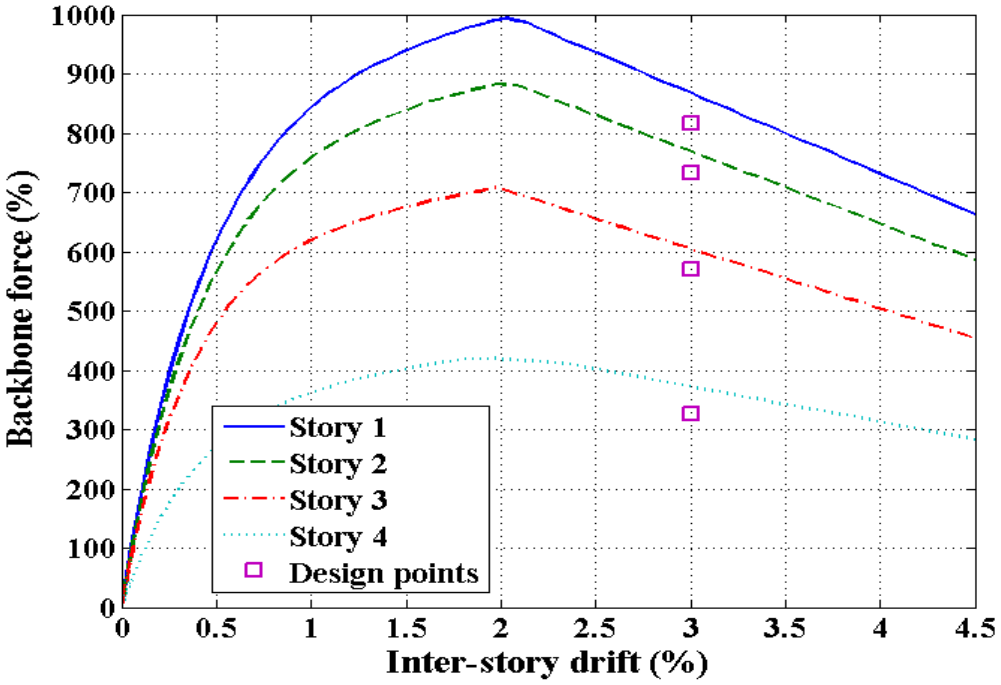

Figure C.10 Design points and inter-story backbone curves for the four-story building with 3% design drift, Location: Sacramento, CA

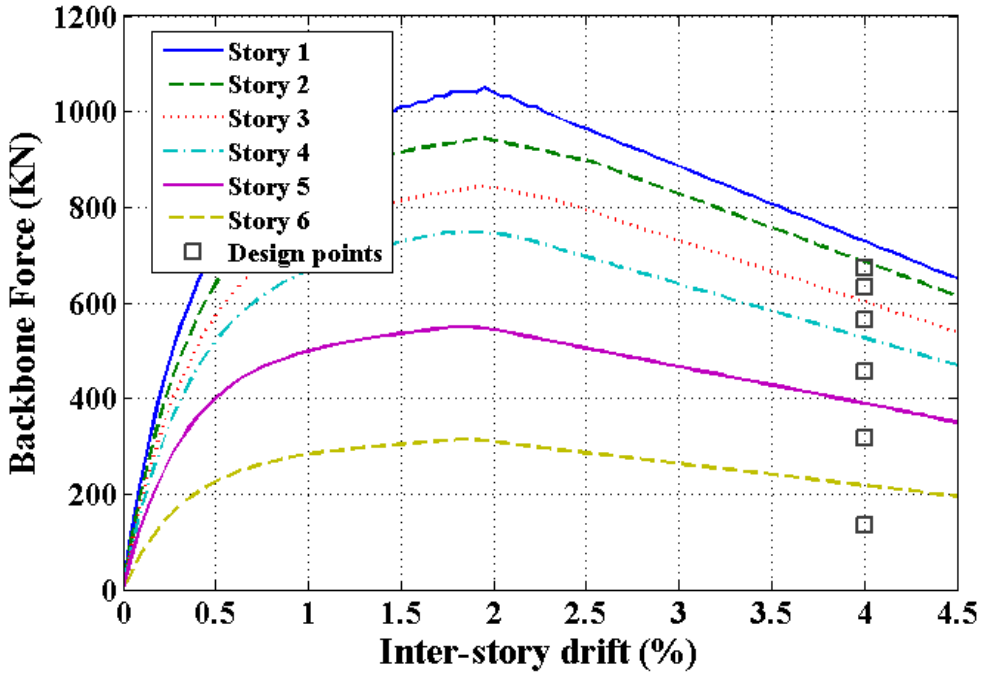

Figure C.11 Design points and inter-story backbone curves for the six-story building with 4% design drift, Location: Los Angeles, CA

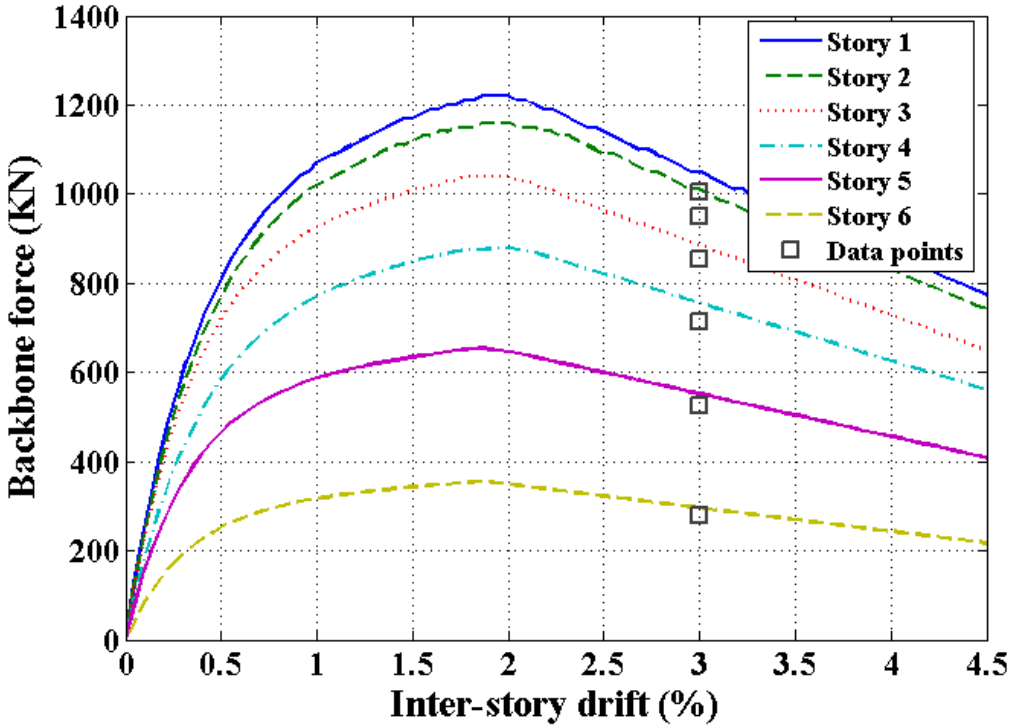

Figure C.12 Design points and inter-story backbone curves for the six-story building with 3% design drift, Location: Los Angeles, CA

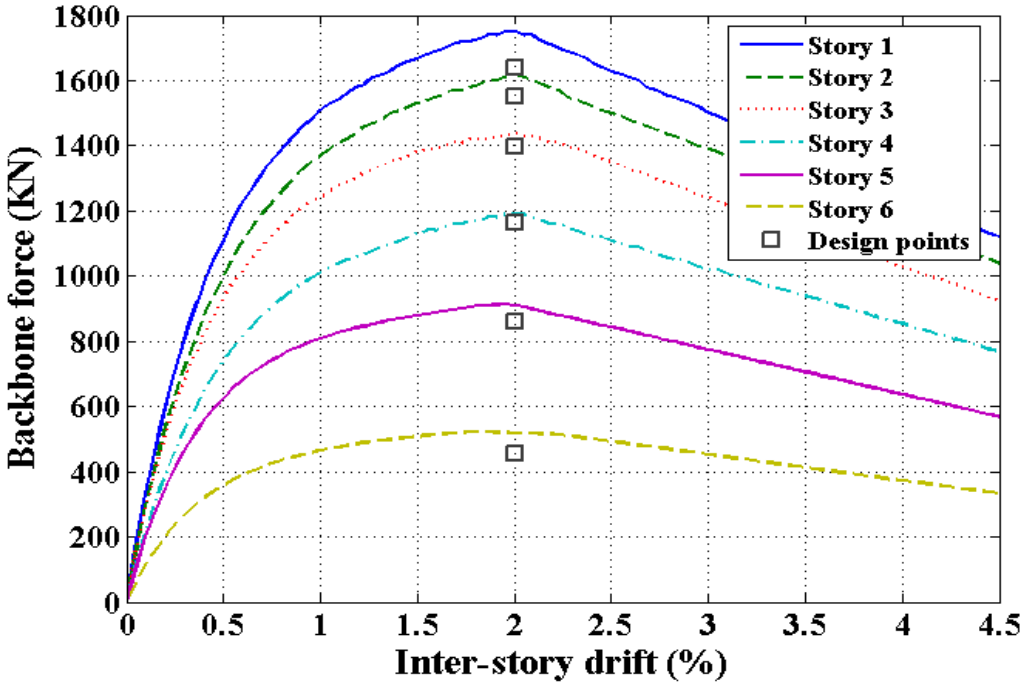

Figure C.13 Design points and inter-story backbone curves for the six-story building with 2% design drift, Location: Los Angeles, CA

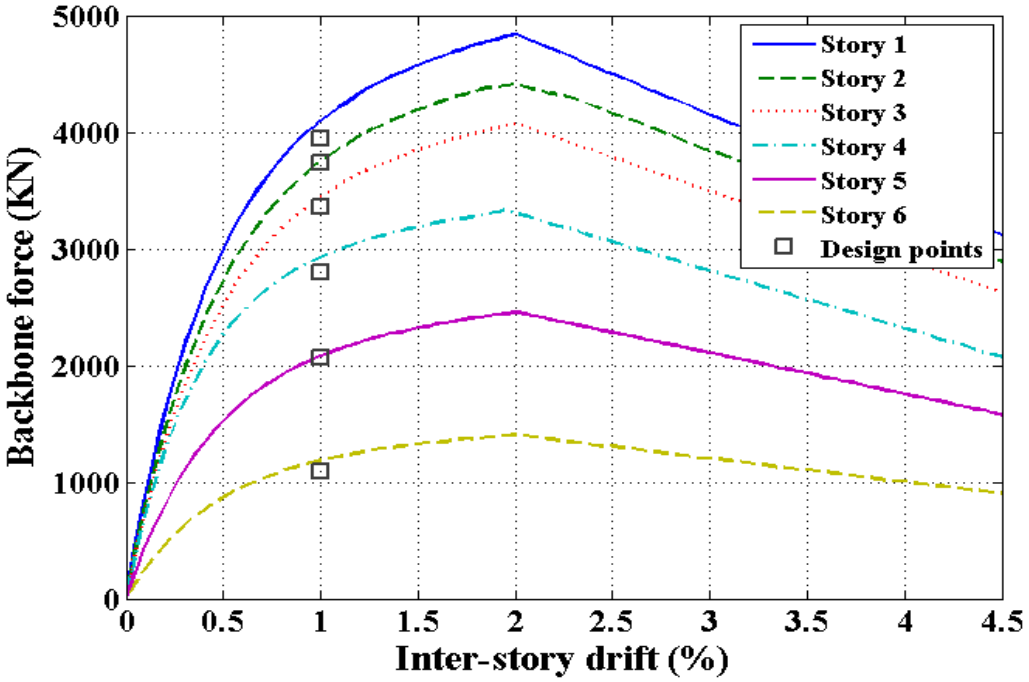

Figure C.14 Design points and inter-story backbone curves for the six-story building with 1% design drift, Location: Los Angeles, CA

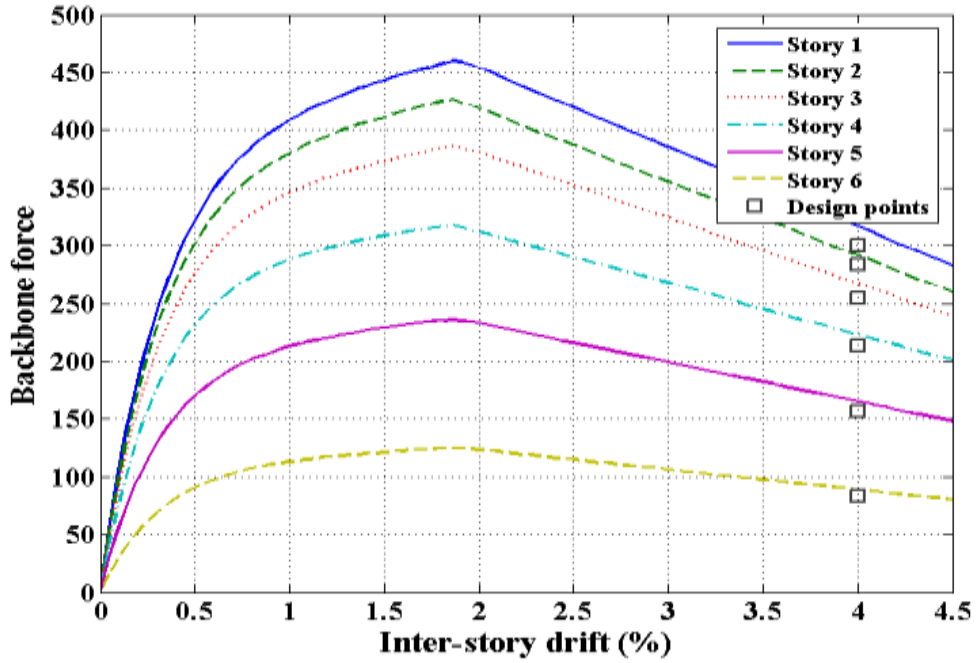

Figure C.15 Design points and inter-story backbone curves for the six-story building with 4% design drift, Location: Sacramento, CA

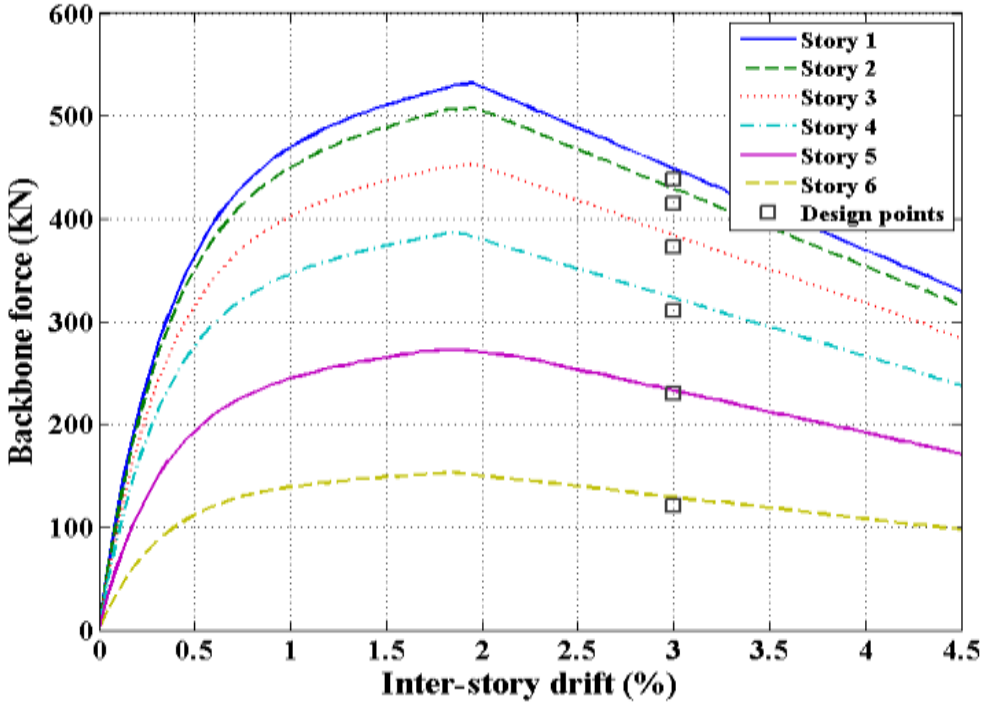

Figure C.16 Design points and inter-story backbone curves for the six-story building with 3% design drift, Location: Sacramento, CA

APPENDIX D

Parameters of the fitted CUREE model for the buildings of the portfolio designed using the DDD approach

Table D.1. Fitted CUREE model parameters for the 4% DDD two-story building located in Los Angeles, CA

Parameters (KN, mm)	First story	Second story
K_0	61.43	43.97
F_0	547.58	393.80
F_1	95.73	70.06
R_1	0.03	0.03
R_2	-0.06	-0.06
R_3	1.00	1.00
R_4	0.02	0.02
X_u	52.07	51.44
α	0.75	0.75
β	1.1	1.1

Table D.2. Fitted CUREE model parameters for the 0.5% DDD two-story building located in Los Angeles, CA

Parameters (KN, mm)	First story	Second story
K_0	72.05	51.19
F_0	684.14	451.49
F_1	121.04	80.16
R_1	0.03	0.03
R_2	-0.06	-0.06
R_3	1.00	1.00
R_4	0.02	0.02
X_u	52.07	52.07
α	0.75	0.75
β	1.1	1.1

Table D.3. Fitted CUREE model parameters for the 4% DDD two-story building located in Sacramento, CA

Parameters (KN, mm)	First story	Second story
K_0	25.45	19.00
F_0	250.57	168.90
F_1	43.32	28.96
R_1	0.03	0.03
R_2	-0.06	-0.05
R_3	1.00	1.00
R_4	0.02	0.02
X_u	53.34	53.34
α	0.75	0.75
β	1.1	1.1

Table D.4. Fitted CUREE model parameters for the 0.5% DDD two-story building located in Sacramento, CA

Parameters (KN, mm)	First story	Second story
K_0	30.47	24.08
F_0	290.02	204.40
F_1	49.95	35.77
R_1	0.30	0.03
R_2	-0.05	-0.05
R_3	1.00	1.00
R_4	0.02	0.02
X_u	53.34	50.80
α	0.75	0.75
β	1.1	1.1

Table D.5. Fitted CUREE model parameters for the 4 % DDD four-story building located in Los Angeles, CA

Parameters (KN, mm)	First story	Second story	Third story	Fourth story
K_0	188.09	175.30	139.09	76.18
F_0	1617.37	1447.01	1136.97	612.96
F_1	277.70	253.73	201.37	110.72
R_1	0.03	0.02	0.03	0.03
R_2	-0.06	-0.05	-0.06	-0.06
R_3	1.00	1.00	1.00	1.00
R_4	0.02	0.02	0.02	0.02
X_u	46.99	46.99	46.99	46.99
α	0.75	0.75	0.75	0.75
β	1.10	1.10	1.10	1.10

Table D.6. Fitted CUREE model parameters for the 3 % DDD four-story building located in Los Angeles, CA

Parameters (KN, mm)	First story	Second story	Third story	Fourth story
K_0	230.82	215.58	159.89	94.69
F_0	1871.37	1758.38	1270.86	784.22
F_1	334.11	310.13	234.02	138.87
R_1	0.04	0.03	0.04	0.03
R_2	-0.06	-0.05	-0.05	-0.06
R_3	1.00	1.00	1.00	1.00
R_4	0.02	0.02	0.02	0.02
X_u	46.99	46.99	48.26	47.24
α	0.75	0.75	0.75	0.75
β	1.10	1.10	1.10	1.10

Table D.7. Fitted CUREE model parameters for the 2 % DDD four-story building located in Los Angeles, CA

Parameters (KN, mm)	First story	Second story	Third story	Fourth story
K_0	301.92	282.30	210.15	131.08
F_0	2667.60	2405.60	1853.57	1214.36
F_1	467.51	429.12	333.39	209.82
R_1	0.03	0.04	0.04	0.04
R_2	-0.06	-0.06	-0.06	-0.06
R_3	1.00	1.00	1.00	1.00
R_4	0.02	0.02	0.02	0.02
X_u	47.75	46.99	48.26	46.99
α	0.75	0.75	0.75	0.75
β	1.10	1.10	1.10	1.10

Table D.8. Fitted CUREE model parameters for the 1 % DDD four-story building located in Los Angeles, CA

Parameters (KN, mm)	First story	Second story	Third story	Fourth story
K_0	524.33	474.24	341.85	211.03
F_0	4537.19	4249.83	3224.07	1914.07
F_1	852.72	790.45	574.27	330.86
R_1	0.04	0.04	0.04	0.03
R_2	-0.06	-0.06	-0.06	-0.06
R_3	1.00	1.00	1.00	1.00
R_4	0.02	0.02	0.02	0.02
X_u	49.53	49.53	48.26	46.99
α	0.75	0.75	0.75	0.75
β	1.10	1.10	1.10	1.10

Table D.9. Fitted CUREE model parameters for the 4 % DDD four-story building located in Sacramento, CA

Parameters (KN, mm)	First story	Second story	Third story	Fourth story
K_0	83.34	74.04	60.63	31.84
F_0	672.57	594.73	504.43	271.83
F_1	0.16	0.15	0.09	0.10
R_1	0.04	0.03	0.02	0.02
R_2	-0.06	-0.06	-0.06	-0.06
R_3	1.00	1.00	1.00	1.00
R_4	0.02	0.02	0.02	0.02
X_u	48.26	47.50	46.99	46.99
α	0.75	0.75	0.75	0.75
β	1.10	1.10	1.10	1.10

Table D.10. Fitted CUREE model parameters for the 3 % DDD four-story building located in Sacramento, CA

Parameters (KN, mm)	First story	Second story	Third story	Fourth story
K_0	95.08	86.36	72.48	35.87
F_0	818.92	736.63	597.40	291.94
F_1	0.16	0.15	0.12	0.12
R_1	0.04	0.03	0.03	0.03
R_2	-0.06	-0.06	-0.06	-0.06
R_3	1.00	1.00	1.00	1.00
R_4	0.02	0.02	0.02	0.02
X_u	48.26	48.26	46.99	46.99
α	0.75	0.75	0.75	0.75
β	1.10	1.10	1.10	1.10

Table D.11. Fitted CUREE model parameters for the 4 % DDD four-story building located in Los Angeles, CA

Parameters (KN, mm)	First story	Second story	Third story	Fourth story	Fifth story	Sixth story
K_0	95.81	86.43	77.32	68.47	52.84	30.24
F_0	897.21	809.58	715.72	646.33	481.74	270.14
F_1	156.98	141.59	126.69	112.18	82.51	47.24
R_1	0.03	0.03	0.03	0.03	0.02	0.03
R_2	-0.06	-0.06	-0.06	-0.06	-0.05	-0.06
R_3	1.00	1.00	1.00	1.00	1.00	1.00
R_4	0.02	0.02	0.02	0.02	0.02	0.02
X_u	53.34	53.34	53.34	53.34	50.80	50.80
α	0.75	0.75	0.75	0.75	0.75	0.75
β	1.10	1.10	1.10	1.10	1.10	1.10

Table D.12. Fitted CUREE model parameters for the 3 % DDD four-story building located in Los Angeles, CA

Parameters (KN, mm)	First story	Second story	Third story	Fourth story	Fifth story	Sixth story
K_0	111.77	106.35	95.55	78.68	62.91	34.85
F_0	1023.09	983.06	894.98	746.86	559.59	298.03
F_1	183.09	174.24	156.53	131.89	98.26	53.11
R_1	0.03	0.03	0.03	0.03	0.03	0.03
R_2	-0.06	-0.06	-0.06	-0.06	-0.06	-0.06
R_3	1.00	1.00	1.00	1.00	1.00	1.00
R_4	0.02	0.02	0.02	0.02	0.02	0.02
X_u	53.34	53.34	53.34	54.61	50.80	50.80
α	0.75	0.75	0.75	0.75	0.75	0.75
β	1.10	1.10	1.10	1.10	1.10	1.10

Table D.13. Fitted CUREE model parameters for the 2 % DDD four-story building located in Los Angeles, CA

Parameters (KN, mm)	First story	Second story	Third story	Fourth story	Fifth story	Sixth story
K_0	152.90	137.74	126.76	102.61	83.80	49.67
F_0	1422.10	1318.01	1203.69	967.49	765.98	438.46
F_1	262.22	242.65	215.43	179.09	137.32	78.33
R_1	0.04	0.04	0.03	0.04	0.03	0.03
R_2	-0.06	-0.06	-0.06	-0.06	-0.06	-0.05
R_3	1.00	1.00	1.00	1.00	1.00	1.00
R_4	0.02	0.02	0.02	0.02	0.02	0.02
X_u	54.61	54.61	54.61	54.61	53.34	50.80
α	0.75	0.75	0.75	0.75	0.75	0.75
β	1.10	1.10	1.10	1.10	1.10	1.10

Table D.14. Fitted CUREE model parameters for the 1 % DDD four-story building located in Los Angeles, CA

Parameters (KN, mm)	First story	Second story	Third story	Fourth story	Fifth story	Sixth story
K_0	423.81	377.75	349.55	298.42	211.73	125.23
F_0	3848.16	3557.24	3314.81	2869.10	2026.16	1104.94
F_1	728.17	662.34	612.52	500.42	369.56	0.20
R_1	0.05	0.04	0.04	0.03	0.04	0.05
R_2	-0.06	-0.06	-0.06	-0.06	-0.06	-0.06
R_3	1.00	1.00	1.00	1.00	1.00	1.00
R_4	0.02	0.02	0.02	0.02	0.02	0.02
X_u	54.61	54.61	54.61	53.34	54.61	54.61
α	0.75	0.75	0.75	0.75	0.75	0.75
β	1.10	1.10	1.10	1.10	1.10	1.10

Table D.15. Fitted CUREE model parameters for the 4 % DDD four-story building located in Sacramento, CA

Parameters (KN, mm)	First story	Second story	Third story	Fourth story	Fifth story	Sixth story
K_0	42.08	40.33	37.02	30.51	22.63	12.50
F_0	398.52	364.98	334.06	278.37	204.93	107.47
F_1	0.11	0.12	0.10	0.09	0.10	0.09
R_1	0.03	0.03	0.02	0.02	0.02	0.02
R_2	-0.06	-0.06	-0.06	-0.05	-0.05	-0.05
R_3	1.00	1.00	1.00	1.00	1.00	1.00
R_4	0.02	0.02	0.02	0.02	0.02	0.02
X_u	50.80	50.80	50.80	50.80	50.80	50.80
α	0.75	0.75	0.75	0.75	0.75	0.75
β	1.10	1.10	1.10	1.10	1.10	1.10

Table D.16. Fitted CUREE model parameters for the 3 % DDD four-story building located in Sacramento, CA

Parameters (KN, mm)	First story	Second story	Third story	Fourth story	Fifth story	Sixth story
K_0	49.37	46.51	41.49	37.11	26.15	14.71
F_0	444.82	436.37	393.67	331.17	234.02	133.85
F_1	0.12	0.12	0.10	0.11	0.12	0.09
R_1	0.03	0.03	0.02	0.03	0.03	0.02
R_2	-0.06	-0.06	-0.06	-0.05	-0.05	-0.05
R_3	1.00	1.00	1.00	1.00	1.00	1.00
R_4	0.02	0.02	0.02	0.02	0.02	0.02
X_u	53.34	52.83	53.34	50.80	50.80	50.80
α	0.75	0.75	0.75	0.75	0.75	0.75
β	1.10	1.10	1.10	1.10	1.10	1.10